universität wien

MASTERARBEIT / MASTER'S THESIS

Titel der Masterarbeit / Title of the Master's Thesis

„Immunometabolism in *Salmonella* infected macrophages and their modulation by iron availability "

verfasst von / submitted by

Julia Telser BSc

angestrebter akademischer Grad / in partial fulfilment of the requirements for the degree of

Master of Science (MSc)

Wien, 2017 / Vienna 2017

Studienkennzahl lt. Studienblatt / degree programme code as it appears on the student record sheet:	A 066 830
Studienrichtung lt. Studienblatt / degree programme as it appears on the student record sheet:	Masterstudium Molekulare Mikrobiologie, Mikrobielle Ökologie und Immunbiologie
Betreut von / Supervisor:	Univ.-Prof. Dr. Günter Weiss

Declaration of Originality

I hereby confirm truthfully that I completed the master thesis on my own with the assistance of the respective supervisor. All direct or indirect sources used are acknowledged as references.

Text and figures that were adopted unchanged or with alteration, from the work of others have been marked with the corresponding reference. Objects that are not marked with references are my own work. This thesis was compiled to the best of my knowledge.

Acknowledgement

First and foremost, I would like to give my appreciation to my supervisor Univ.-Prof. Dr. Günter Weiss who gave me the possibility to have an insight in the laboratory of infectious diseases and immunotherapy of the medical university of Innsbruck and gave me the opportunity to write my master thesis at this department. I am thankful for the support throughout my scientific work and for the help at any time point.

Furthermore, I would like to thank Univ.-Prof. Dr. Thomas Decker how make it possible to perform my scientific work at an external university.

My special thank also go to Chiara Volani, PhD for her advices and support. Thank you for helping me out and assisting me with the metabolite measurements.

I would also like to thank Verena Ploner, PhD and Richard Hilbert for their friendly and helpful suggestions. Thank you for motivating me throughout the hole project and for always having an open ear.

I am also grateful to Markus Seifert and Silvia Berger for passing their knowledge about Western blotting and ELISA.

Additionally, I would like to thank everyone of the institute, who welcomed me friendly, gave me support and make my stay pleasurable.

Finally, I would like to thank my family for their support and encouragement throughout my biology studies.

Table of contents

3. Materials and methods

3.1 Materials

3.1.1 Preparation of ferric chloride

3.1.2 Preparation of LB-broth agar plates

3.2 RAW264.7 cell culture

3.2.1 Cultivation of RAW264.7 cells

3.2.2 Counting of RAW264.7 cells

3.2.3 Freezing of RAW274.7 cells

3.3 Treatment of RAW264.7 cells

3.3.1 Treatment with LPS and IFN-gamma

3.3.2 Treatment with rapamycin

3.3.3 Treatment with gentamycin

3.3.4 Treatment with iron and iron chelators

3.4 Stimulation of RAW264.7 cells

3.4.1 Stimulation with $FeCl_3$/DFP and *S*. Tm:

3.4.2 Stimulation with rapamycin and *S*. Tm:

3.4.3 Stimulation with $FeCl_3$/DFP, rapamycin and *S*. Tm:

3.5 Storage of supernatant

3.6 Handling of *Salmonella enterica* serovar Typhimurium

3.6.1 Preparation of LB-broth agar plates:

3.6.2 Storage of *S*. Typhimurium

3.6.3 Heat inactivating of *S*. Typhimurium

3.6.4 *S*. Typhimurium infection in vitro

3.6.5 Determination of CFU/ml

3.7 RNA

3.7.1 RNA isolation

3.7.2 cDNA

3.7.3 qRT-PCR

3.7.4 Primer and Probes for qRT-PCR

3.8 Proteins

1. Introduction

1.1. Macrophages

Macrophages are important cells of the innate immune system, since they exhibit a first line of defense against numerous microorganisms and are thus essential for controlling infections (Janeway et al., 2001; Ginhoux and Jung, 2014; Elhelu, 1983).

Macrophages are derived from bone marrow precursor cells. These precursor cells develop into monocytes from stem cells of the granulocytic-monocytic lineage that are submitted to cytokines such as the granulocyte macrophage colony stimulating factor (GM-CSF) (Duque et al., 2014). Monocytes migrate into the bloodstream and circulate through the body, having a half-life of 70 hours. After they migrate into connective tissue, they develop into macrophages (Duque et al., 2014).

1.1.1. The role of macrophages in innate immunity

Macrophages are important phagocytic cells and play a critical role in controlling microorganism during the early period of an infection (Janeway et al., 2001).

If pathogens permeate the epithelial surface, they encounter cells and molecules that can induce an immune response. Such cells of the innate immune system are macrophages, which can recognize common compositions of the bacterial surface, such as lipoproteins, polysaccharides or oligonucleotides. This recognition of such pathogen associated molecular patterns (PAMPs) by macrophage pattern recognition receptors (PRR) triggers the macrophage to engulf the pathogen (Janeway et al., 2001; Duque et al., 2014).

Next to PRR, macrophages also express major histocompatibility complex class I and II (MHC-I and MHC-II) molecules on their surface. This is important for activation of the adaptive immune response, since after engulfment of the bacterium, it gets processed and antigens get presented to helper T-cells (T_H-cells) through MHC-II (Duque et al., 2014). This results in cytokine release with consequent activation of B-cells that secret antibodies specific to the antigen presented by macrophages. The binding of such antibodies to antigens, present either on the surface of microbes' or on the membrane of invaded cells, results in increased phagocytosis by macrophages (Duque et al., 2014).

1.1.1.1. Cytokine secretion by macrophages

Parallel to phagocytosis of pathogens and induction of the adaptive immune system, macrophages are able to secrete cytokines or chemokines, upon recognition of microbes. These biological active signaling molecules influence other cells, which carry receptors for them and allow therefore intercellular communication.

Cytokines drive many important processes such as cellular proliferation, metabolism, tissue repair or regulating the inflammatory response (Weiss and Schaible, 2015; Duque et al., 2014; Janeway et al., 2001).

If macrophages are extradited to inflammatory stimuli or microbes, they produce pro-inflammatory cytokines such as tumor necrosis factor-α (TNF-α), interleukin-1 (IL-1), IL-6, IL-8, IL-10 and IL-12 **(Fig.1)** (Duque et al., 2014).

TNF-α is thereby one of the first cytokines which gets secreted in reply to microbes and stimulates the acute phase of the immune response. Nonetheless, IL-6 also plays an important role as a pro-inflammatory cytokine and promotes the production of acute phase proteins, similar to TNF-α. Additionally, it promotes the differentiation of B-cells into antibody producing plasma cells and activates cytotoxic T-cells (T_C-cells) (Duque et al., 2014). However, next to its pro-inflammatory characteristics, IL-6 also has anti-inflammatory properties, which results in inhibition of apoptosis and regeneration of epithelial cells (Duque et al., 2014; Scheller, 2011; Gabay, 2006; Xing et al., 1998).

To prevent tissue damage through inflammation, it is crucial to regulate inflammation by inhibitors and antagonists, such as anti-inflammatory cytokines. One of these molecules produced by macrophages is IL-10, which represses the activation of macrophages and thereby the secretion of pro-inflammatory cytokines such as TNF-α and IL-6 and the expression of MHC-II and therefore inhibits antigen presentation. In this way, IL-10 lowers the microbicidal activity of macrophages (Duque et al., 2014).

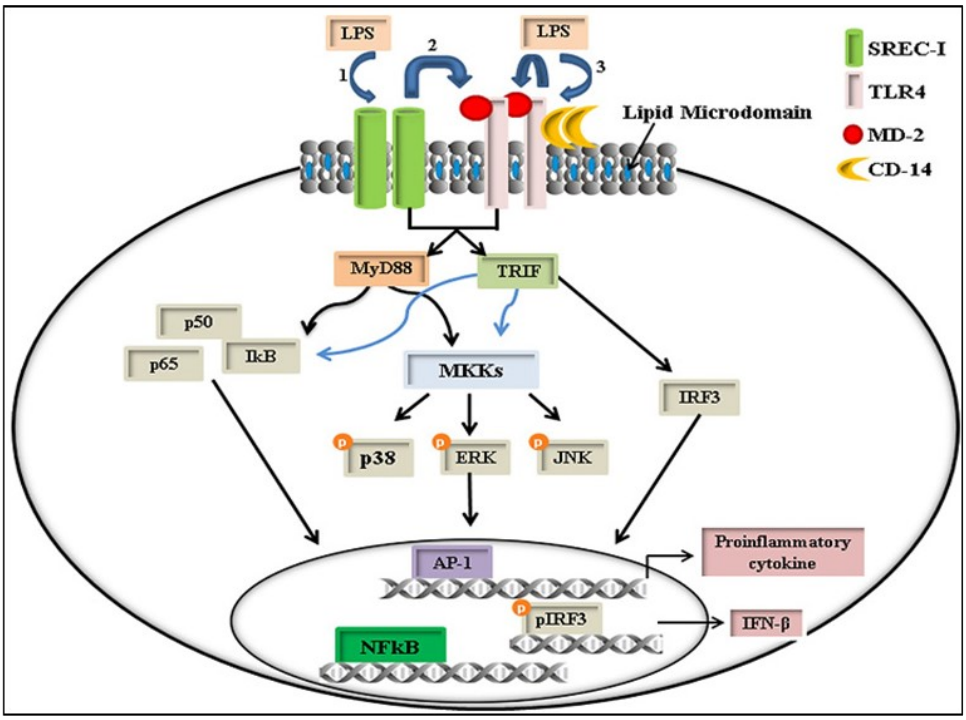

Figure 1 Schematic representation of a signal transduction cascade upon macrophage stimulation (Murshid et al., 2015)

In addition to cytokine production, macrophages produce reactive oxygen species (ROS) and reactive nitrogen species (RNS), which participate in efficient clearance of microbes.

ROS are thereby mainly formed by the NADHP oxidases (NOXs) and the mitochondrial electron transport chain (ETC). During this process, the generated superoxide anion ($O_2^{\circ-}$) is converted to hydrogen peroxide (H_2O_2) by the hyperoxide dismutase. Via the Fenton reaction, H_2O_2 can then react with Fe^{2+} to form hydroxyl radical (HO) **(Fig.2)** (Spooner and Yilmaz, 2011; Paiva and Bozza, 2014; Mone` et al., 2014).

Additionally, oxygen radicals can combine with nitric oxide (NO) to form RNS. NO is thereby synthesized from arginine by the action of the inducible nitric oxide synthase (iNOS). NO can then react with $O_2^{\circ-}$ to generate peroxy-nitrite ($OONO^-$), which can be protonated to generate OH· and nitrogen dioxide ($\cdot NO_2$), which are known to be more reactive products **(Fig.2)** (Mone` et al., 2014; Paiva and Bozza, 2014).

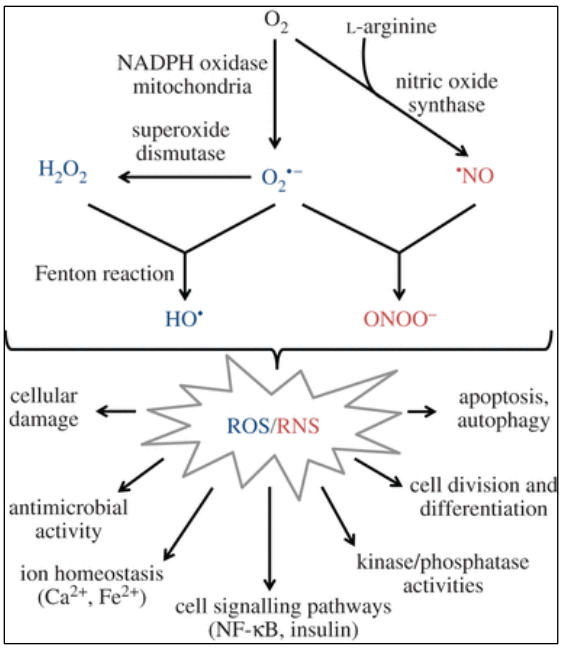

Figure 2 ROS/RNS generation and their effects on cellular functions

Together, all these strategies allow macrophages to suppress bacterial expansion and proliferation and promote elimination of the microbes and control of infections.

However, another grave innate immune mechanism used by macrophages against invading microbes used is the control of iron homeostasis, as both, mammalian cell and microbes have a substantial need for the metal (Cassat et al., 2012; Soares and Weiss, 2015).

1.2. Iron trafficking within macrophages

Iron is a crucial element for many organisms because it is a co-factor for enzymes involved in the mitochondrial electron transport system, the citric acid cycle, the oxygen transport as well as the electron transport (Nairz et al., 2015; Muckenthaler et al., 2017).

The average adult human contains 3-4 g iron of which about 2-3 g are present in hemoglobin of circulating red blood cells. 25% is present in the liver and spleen, where iron is stored in macrophages and hepatocytes and the remaining 15% is bound to myoglobin in muscles (Abbaspour et al., 2014).

Smaller amounts of iron are found in iron-containing proteins of all other cells. These proteins execute essential functions since they are important for energy metabolism, signaling pathways and host defense mechanisms (Ganz, 2013).

Iron absorption, in humans, takes place in the duodenum and jejunum. Daily absorption of iron (2mg) is enough to counter physiological iron loss, but it is not adequate to provide sufficient iron for all cellular requirements (Gammella et al., 2014).

Hence, macrophages of the red pulp in the spleen and liver developed mechanisms to recycle iron from damaged or aged red blood cells, which contain about 60-70% of human iron,

complexed to heme moieties in hemoglobin (Theurl et al, 2016; Knutson et al., 2005).

This recycling process of iron from red blood cells is known as erythrophagocytosis.

1.2.1. Erythrophagocytosis

During this process, aging related alterations of erythrocytes must accomplish a threshold that is detected by macrophages (Ganz, 2012; Gammella et al., 2014).

After red blood cells get recognized by macrophages, they become engulfed into the phagolysosome where they are exposed to reactive oxygen species (ROS) and hydrolytic enzymes, which results in the release of hemoglobin and then heme into the vacuolar fluid (Ganz, 2012; Gammella et al., 2014).

There, heme is further degraded by heme oxogenase-1 (HO-1), to release ferrous iron into the cytoplasm. Therefore, HO-1 required molecular oxygen and NADPH-reducing equivalents to cleave heme into iron, carbon monoxide and biliverdin, which is further converted by the biliverdin reductase to bilirubin **(Fig.3)** (Ganz et al., 2012).

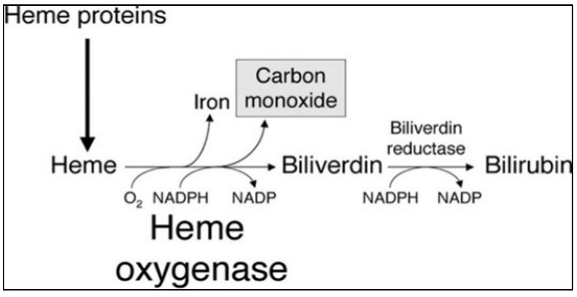

Figure 3 HO-1 enzymatic reaction (Dulak et al., 2008)

1.2.2. Alternative iron recycling pathways

Another fundamental process for recovering iron from damaged cells is intravascular hemolysis. Damaged erythrocytes release hemoglobin into the plasma, where it binds to the carrier protein haptoglobin. This hemoglobin-haptoglobin complex is sensed and taken up by macrophages via the CD163 receptor and the iron is recycled by mechanisms like those that follow erythrophagocytosis (Schaer et al., 2014).

Additionally, hemoglobin can be oxidized which results in the oxidation of ferrous iron into ferric iron, which is present in heme. This results in the release of hemin, which binds to hemopexin. The complex is further taken up by macrophages via the CD91 receptor and iron is ruptured by HO-1 (Hvidberg, 2005).

By the divalent metal transporter (DMT1) or the natural resistance associated protein 1 (Nramp1), iron is then transported across the phagosomal membrane (Soares and Weiss, 2015; Abbaspour et al., 2014; Soe-Lin et al., 2009).

The cytosolic iron can then be used by phagocytic cells to be integrated into proteins and enzymes, be stored or exported out of the cells (Gammella et al., 2014).

The transport of iron through the cytoplasm to the storage protein ferritin, is carried out by chaperons, called poly(rC) binding proteins 1-4 (PCBP), that neutralize the chemical reactivity and toxicity of iron (Shi et al., 2008).

For this transport mechanisms, the ferric reductase and ferroxidase play important roles, as they facilitate the interchange of ferrous and ferric iron to match the demands of iron transporters and storage processes (Ganz et al., 2012; Abbaspour et al., 2014).

Ferrous iron is exported across the plasma membrane of macrophages by ferroportin (Fpn), which is so far, the only known export protein for iron. Iron is then subsequently loaded onto its carrier transferrin, which liberates iron for erythropoiesis and for other cells, which require iron to carry out essential functions such as mitochondrial energy production (Gammella et al., 2014; Muckenthaler et al., 2017).

The binding of iron to transferrin is important to reduce the free radical production, catalyzed by iron and to promote the transport of iron to target cells, where it is delivered by receptor mediated endocytosis (Muckenthaler et al., 2017).

However, transferrin binds only ferric iron and therefore, iron must be re-oxidation to Fe^{3+} by the membrane bound ferroxidase hephaestin when it gets released form

macrophages. Hephaestin thereby interacts with ferroportin. Additionally, also the plasma homologue enzyme ceruloplasmin is needed (Ganz, 2012; Abbaspour et al., 2014).

At the systemic level iron homeostasis is regulated by the liver derived peptide hepcidin (Ganz, 2012, Nairz et al., 2015). Hepcidin is a 25-amino acid peptide and controls the release of iron from macrophages by causing the endocytosis and proteolysis of the exporter ferroportin (Ganz et al., 2012).

The production of hepcidin is regulated by iron levels in plasma and tissue but also by inflammatory signals, hormones and erythropoietic and hypoxia signals. Therefore, hepcidin regulated iron export is the most important control point for the regulation of iron concentrations in plasma (Ganz, 2012).

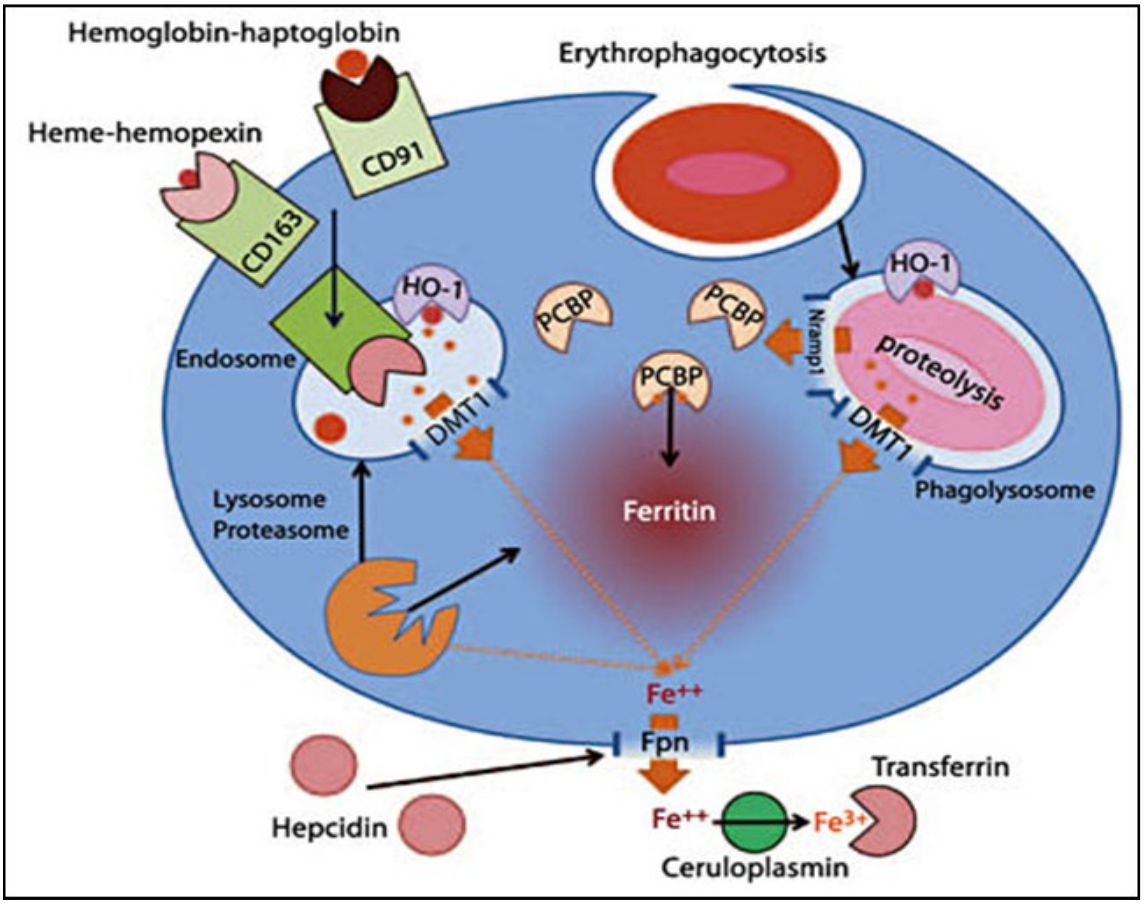

Figure 4 Flow of iron within macrophages (Ganz, 2012)

1.2.3. Regulation of iron homeostasis

To prevent cellular damage through iron overload or anemia through iron deficiency, the metabolism of iron is strictly regulated. On one hand, lack of iron can result in cellular growth arrest and death. On the other hand, iron excess can result in the formation of hydroxyl or lipid radicals and is therefore extremely toxic for cells. However, the difference between iron deficiency and overload is a question of some milligrams of iron and therefore, the concentrations of iron must be tightly regulated (Guan et al., 2014).

This regulation of iron homeostasis is controlled by at least two mechanisms.

1.2.3.1. Iron regulatory protein 1 and 2

On one hand, intracellular iron concentrations are controlled post-transcriptionally and translationally by iron regulatory proteins 1 and 2 (IRP1 and IRP2), located in the cytoplasm. These proteins interact with iron responsive elements (IREs) which are found within the messenger RNA (mRNA)-encoding genes linked to iron metabolism.

IREs have been found within the 5' untranslated region of the mRNA coding for ferritin, the central protein for iron storage. Additionally, five IREs have been identified within the 3' untranslated region of the mRNA coding for transferrin receptor (TfR) (Muckenthaler et al., 2017; Ronault and Maio, 2017).

The binding of IRPs to IREs results under iron-deficient states and functions to re-establish iron levels through stabilization and prolonging the half-life of transferrin receptor-1 (TfR1) mRNA and consequently enhance the expression of the protein and iron uptake. Additionally, ferritin expression is blocked by impacting the building of the translation initiation complex and cellular iron export is lowered through the suppression of ferroportin-1 (Fpn1) (Bayeva et al.,2013; Muckenthaler et al., 2017).

If iron is abundant, the activity of IPRs binding to IREs is lowered which results in increased translation of ferritin, while the contrary effect results with TfR mRNA (Weiss, 2002).

Additionally, IRP1 binds to iron-sulfur clusters (ISC) and thereby functions as a cytosolic aconitase. In contrast, IRP2 does not show aconitase activity, despite the

60% sequence identity to IRP1. Iron controls the binding affinity of IRP2 to the mRNA by mediating its ubiquitination and degradation in the proteasome (Guan et al., 2014).

1.2.3.2. Hepcidin

Next to the control of iron homeostasis through IRPs, iron homeostasis is also regulated through the liver peptide hepcidin. This hormone is produced by hepatocytes and is the most important regulator of systemic iron homeostasis, due to the property to regulate iron entry into plasma. (Abbaspour et al., 2014). Enhanced levels of the metal in iron stores, such as ferritin, induces the production of hepcidin, which results in a post-translationally control of iron export by binding of hepcidin to ferroportin, leading to its internalization and degradation and thus avoids iron entry into plasma. Conversely, suppressed expression of hepcidin leads to enhanced cell surface ferroportin expression and increased iron release (Nemeth et al., 2004).

Hepcidin levels in the plasma are regulated by diverse stimuli such as cytokines or plasma iron concentrations. It is not surprising that dysregulation of hepcidin expression leads to iron disorders. On one hand, an enhanced expression of hepcidin and therefore low plasma iron concentrations results in anemia of chronic diseases. On the other hand, under-expression of hepcidin results in an overload of plasma iron levels which leads to hereditary hemochromatosis (HFE) with followed iron accumulation in organs (Fleming and Ponka, 2012; Weiss and Goodnough, 2005; Pietrangelo, 2004).

Iron overload not only results in cellular damage due to the adverse redox chemistry of free iron, individuals additionally suffer from a higher risk of certain infections, since the disposability of iron to microbes is increased (Cassat et al., 2012).

1.2.4. Iron metabolism under inflammatory conditions

Iron is an important metal for both, humans and pathogens because both have an essential need for iron to fulfill many important metabolic processes (Nairz et al., 2010). Therefore, regulation of iron homeostasis by the host is inevitable in host-pathogen interactions and acts as a control mechanism against invading pathogens (Cassat et al., 2012; Soares and Weiss, 2015).

Macrophages developed diverse strategies against invading microbes, including the property to modify the expression and regulation of proteins participating in iron metabolism (Gammella et al., 2014).

Interactions between cellular iron homeostasis and immune functions are well established. On one hand, iron affects the production of cytokines and the action of transcriptions factors involved in the immune response, since it is a co-factor for the formation of antimicrobial oxygen radicals by macrophages. On the other hand, immune cell mediators and acute phase proteins influence iron homeostasis (Nairz et al., 2010, Weiss, 2002). Iron overload of mononuclear cells correlates with diminished cell-mediated function and reduced control of intracellular pathogens since their proliferation and radical detoxification are dependent on iron (Weiss, 2002).

A defense strategy used by macrophages is the deprivation of iron from invading microbes and therefore iron-withholding, also known as hypoferremia. This is a major strategy used by mammalian as an antimicrobial defense that attend inflammatory conditions (Cherayil, 2011; Gammella et al., 2014; Nairz et al., 2013).

Inflammatory signaling cascades during an infection results in a reduction of free iron availability and sequestration of the metal in the reticuloendothelial system (RES), which results in lower availability of iron to pathogens in the circulation and therefore reduced possibility of microbes to achieve full virulence (Nairz et al., 2010). In addition, the binding of free extracellular iron by transferrin conduce as host defense strategy to limit the existence of iron to microorganisms (Nairz et al., 2010). In healthy organisms, transferrin is saturated less than 50% with iron. If the capacity of iron-binding by transferrin exceeds, iron can also be bound with diminished affinity by diverse molecules in the plasma, for example albumin, citrate and amino acids. Additionally, other plasma proteins such as haptoglobin, haemopexin, lactoferrin, lipocalin-1 and lipocalin-2 are also common for binding of iron with high affinity to make it unavailable for pathogens (Nairz et al., 2010).

The uptake of such proteins by the mononuclear phagocyte system (MPS) and the storage of iron into ferritin results in lower iron concentrations in the circulating blood, also known as hypoferremia and diminished iron availability to extracellular pathogens (Nairz et al., 2010).

However, as a side action, iron accumulation in the reticuloendothelial cells, results in an anemia associated with chronic inflammation, also known as anemia of chronic disease or ACD (Weiss and Goodnough, 2005). The mechanism of this response involves inflammatory stimulus-mediated regulation of iron homeostasis genes at different level. This results in enhanced ferritin expression and down-regulation of ferroportin in macrophages (Gammella et al., 2014)

Additionally, also hepcidin mediates the hypoferremic response and therefore reduces iron concentrations in the serum in response to infection. Hepcidin secretion from the liver is stimulated by pro-inflammatory cytokines such as IL-6, TNF-α and Toll-like receptor 4 (TLR4)/MyD88 pathway activation. However, also macrophages are able to produce hepcidin in response to infection and hence modulating the iron availability at the site of infections (Weiss, 2005; Theurl et al., 2008; Gammella et al., 2014).

However, these iron-withholding strategies are disadvantageous if microbes have an intracellular life cycle such as *Salmonella enterica* serovar Typhimurium, since it would spur intracellular pathogen growth (Nairz et al., 2013; Kim et al., 2014).

1.2.4.1. *Salmonella enterica* serovar Typhimurium (*S*. Typhimurium; *S*. Tm)

Salmonella Typhimurium is a murine gastrointestinal pathogen. It is a Gram-negative, rod-shaped, flagellated, aerobic bacterium that has a facultative intracellular lifestyle (Arsenault et al., 2013). *Salmonella* can colonize different habitats, however, the adaption to life within the host cell is crucial for systemic infections (Dandekar et al., 2012).

Like other intracellular bacteria, *Salmonella* can grow inside a membrane-bound vacuole within host cells, which is called *Salmonella*-containing vacuole or SCV (Leung et al., 1991). This SCV arrests the endosomal pathway of the host at the late endosome stage. It needs some late endosome markers such as vATPases and LAMP1, but loses some of them such as mannose-6-phospate receptor. Since the SCV is a nutrient deprived environment, *Salmonella* evolved strategies to derive nutrition from the Golgi apparatus and thus indicates a successful adaption of *Salmonella* to these unfavorable conditions, since this bacterium is able to replicate within the SCV (Garai et al.,2012; Dandekar et al., 2012). Additionally, *Salmonella* can alter this vacuole and thereby

avoiding the fusion with acidic lysosomes which results in escaping bacterial killing in the endocytic (Pan et al., 2010).

1.2.4.2. Iron metabolism during infections with intracellular pathogens

Host defense mechanisms against intracellular pathogens such as *Salmonella* also include alterations in cellular iron homeostasis, such as down-regulation of iron uptake pathways and contrary, up-regulation of iron export pathways (Nairz et al., 2010).

The produced nitric oxide (NO) during infections thereby stimulates Nrf2-dependent ferroportin expression and iron export from macrophages, which counterbalance the hepcidin mediated ferroportin down-regulation (Nairz et al., 2013).

Since *Salmonella* is deprived from various extracellular iron carries within macrophages, the bacterium has developed several strategies to successful acquire iron from different intracellular and extracellular resources (Nairz et al., 2007). Therefore, like other intracellular pathogens, *Salmonella* utilizes many strategies to acquire iron from the circulation, which include extracellular iron mobilization, uptake of iron and intracellular assimilation (Gammella et al., 2014).

Salmonella is able to secrete small molecules, also known as siderophores which are able to bind ferric iron with high affinity. Iron-siderophore complexes are than taken up by receptors, such as IroN, FepA and Cir, which are located at the outer membrane of *Salmonella*. After binding iron, siderophores are transported over the periplasmatic space and taken up by the cytoplasmic membrane using ABC-transporters such as FepBCDG and iroC. Additionally, *Salmonella* produces Feo for uptake of ferrous iron (Nairz et al., 2007).

In addition, PRR binding and pro-inflammatory cytokines decrease iron uptake, carried out by TfR1, while enhancing the expression of the intracellular iron transporter Nramp1 and the iron exporter Fpn1, leading to a reduced iron level in early endosomes and limited availability for intracellular pathogens (Soares and Weiss 2015; Nairz et al., 2010).

However, TfR1 expression is increased only during the early time period of a *Salmonella* infection. This effect is lost during the later period, showing that *Salmonella*

does not require iron uptake by TfR1 for subsequent growth inside the host cell (Pan et al., 2010). Contrary, Fpn1 levels and therefore iron efflux are increased during an infection. Additionally, a change in cellular iron stores can be observed during *Salmonella* invasion. The increased binding affinity of IRP1 during an infection results in a diminished cytoplasmic labile iron pool and a reduced incorporation of iron into the storage protein ferritin (Nairz et al., 2007).

To counterbalance these strategies used by intracellular pathogens, the host modulates the iron homeostasis pathways through the production of lipocalin 2 (Lcn2) or lactoferrin in response to infections (Pan et al., 2010).

The antimicrobial peptide Lcn2 thereby scavenges iron or withholds it from intracellular bacteria by interaction with bacterial iron-siderophore complexes. Lcn2 transports siderophore-bound iron to mammalian cells, which than import the complex via lipocalin 2 receptor (LcnR). Studies show that upon bacterial recognition through TLR4 pathways, such as *Salmonella* lipopolysaccharide (LPS), Lcn2 expression is increased and provides a major component of the innate immune response (Pan et al., 2010; Nairz et al., 2007).

In response to environmental changes, such as iron deprived stages or infections, a reprogramming of the metabolism of immune cells can be observed. Since the 1960, the relationship between energy metabolism and functions of immune cells has been studied. In the past few years, a novel research field developed, aimed at studying the requirement of metabolic processes for a strong immune response. Upon activation, immune cells underlie robust metabolic alterations which are important for determining the functions of immune cells. This novel research field is also defined as immunometabolism (Stienstra et al., 2017).

1.3. Cellular energy metabolism

Mostly all functions that a cell must perform require energy. The most important carbon and nitrogen sources for mammalian cells are glucose and glutamine. However, also other carbohydrates as well as amino acids and fatty acids are needed as energy sources. Under normal circumstances, the major pathways in cellular energy metabolism involve the glucose metabolism, the pentose-phosphate pathway (PPP), the citric acid cycle (TCA) and finally oxidative phosphorylation in mitochondria. Via

glycolysis, glucose is degraded to pyruvate which gets decarboxylated to acetyl-CoA and introduced into the TCA cycle. The citrate cycle supplies NADH for oxidative phosphorylation, which is important to generate the electron gradient for adenosine 5'-triphosphate (ATP) formation (Oexle et al., 1999; Eisenreich et al., 2013). ATP plays an essential role in the energy metabolism of cells, since it can store free energy within cells **(Fig.5)** (Cooper, 2000).

1.3.1. Glycolysis

Glucose is known to be the major energy producing molecule for lots of individuals. During glycolysis, glucose is converted into pyruvate in the cytoplasm of cells. The breakdown of glucose requires ten chemical reactions, with each reaction being catalyzed by a specific enzyme (Li et al., 2014).

The initial reactions in the pathway need ATP to phosphorylate glucose into glucose-6-phosphate by hexokinase and afterwards fructose-6-phosphate to fructose-1,6-bisphospate by phosphofructokinase. The major control enzyme of the glycolytic pathway is the enzyme phosphofructokinase, which is blocked upon high ATP levels within the cell. This leads to high glucose-6-phospate levels within the cells, which in turn inhibits the hexokinase activity and therefore the breakdown of glucose (Cooper, 2000).

The reactions following the fructose-1,6-bisphospate account the energy-producing section of the pathway. In total, four molecules of ATP are generated from each glucose molecule of which two ATPs are needed for initial reactions. The net gain of ATP is therefore two molecules (Cooper, 2000).

Additionally, two molecules of NADH are formed during glycolysis. However, in anaerobic terms, NADH gets re-oxidized to NAD^+ by the conversion of pyruvate into lactate or ethanol (Cooper, 2000).

Contrary, under aerobic conditions, NADH is used as an additional source of energy by transporting its electrons to the electron transport chain (Cooper, 2000).

1.3.2. Citric acid cycle

The product of the glycolytic pathway, pyruvate gets decarboxylated and forms with coenzyme A (CoA) the molecule acetyl-CoA, which is than able to enter the citric acid cycle within the mitochondria. The citric acid also known as TCA cycle or Krebs cycle was discovered in 1937 by Hans A. Krebs (Dean et al., 2013). This cycle is the most important pathway in oxidative metabolism, since it finishes the oxidation of glucose to six CO_2 molecules (Cooper, 2000). Additionally, two molecules of ATP, six molecules of NADH and two molecules of $FADH_2$, which is another carrier of electrons, are formed during the citric acid cycle (Cooper, 2000).

In the first reaction, acetyl-CoA gets connected with oxaloacetate to produce citrate by the enzyme citrate synthase. Thereafter, citrate undergoes isomerization to form cis-aconitic acid and further isocitrate. This reaction is catalyzed by the enzyme aconitase (Dean et al., 2013).

Isocitrate is further oxidized by a NAD molecule, forming α-ketoglutarate. The enzyme involved in this process is called isocitrate-dehydrogenase (IDH).

In the next step, coenzyme A oxidizes α-ketoglutarate. A molecule of NAD is thereby reduced to NADH, which leaves the citric acid cycle. Succinyl-CoA is formed by the enzyme α-ketoglutarate-dehydrogenase.

A water molecule loses its hydrogen atoms to coenzyme A. A free phosphate group replaces coenzyme A and binds to the succinyl complex. Thereafter, the phosphate is displaced to an ADP molecule to produce a molecule of ATP. A molecule of succinate remains behind. This reaction is catalyzed by the enzyme succinate thiokinase (Dean et al., 2013; Cooper, 2000).

Next, succinate-dehydrogenase converts succinate into fumarate. This step requires the oxidation of succinate by FAD. Thereafter, a water molecule is added to fumarate and malate is formed by the enzyme fumarase (Dean et al., 2013).

In the last step of the citric acid cycle, malate gets oxidized by NAD, which results in the formation of oxaloacetate which can then combine again with acetyl-CoA and the citric acid cycle starts again (Dean et al., 2013).

1.3.3. Oxidative phosphorylation

During oxidative phosphorylation (OXPHOS), electrons donated by NADH and $FADH_2$ flow through the electron transport chain and are finally combined with oxygen (O_2), allowing the generation of large quantities of energy.

The elements of the electron transport transfer chain or OXPHOS for oxidative phosphorylation complexes (I-IV) are located in the inner mitochondrial membrane of cells, also called cristae. Together with ATP synthase (complex V), they form the components for producing ATP. Thereby, 38 molecules of ATP are generated from breakdown of one molecule glucose. (Cooper, 2000; Chaban et al., 2013).

The complexes I-IV are enzymes, composed of many subunits and create an electrochemical proton gradient across the mitochondrial membrane that is utilized by the ATP synthase for ATP formation via oxidative phosphorylation (Chaban et al., 2013).

For understanding OXPHOS at molecular level, it is essential for a more detailed look at the functions of the complexes.

The largest enzyme of the electron transport chain (ETC) is complex I or NADH dehydrogenase. This complex binds NADH and transports two electrons via flavine mononucleatide (FMN) and seven iron-sulphur clusters to a ubiquinone, which gets reduced. This leads to the translocation of four protons across the mitochondrial membrane via four channels (Chaban et al., 2013).

Complex II of succinate dehydrogenase oxidizes succinate which is generated during glycolysis, and transfers thereby electrons through three iron-sulphur clusters to ubiquinone. It is therefore not directly involved in the formation of the proton gradient, since it is not a proton pump (Chaban et al., 2013).

Cytochrome c oxidoreductase or complex III converts ubiquinone into ubiquinol and translocate two protons into the intermembrane space. The electrons from ubiquinol are passed to the carrier cytochrome c (Chaban et al., 2013).

Complex IV or cytochrome c oxidase gets electrons form cytochrome c and locates them to an oxygen molecule to convert it into two water molecules. Thereby, it pumps four protons to the intermembrane space (Chaban et al., 2013).

Lastly, complex V or ATP synthase uses the energy stored in the proton gradient to convert ADP into ATP (Chaban et al., 2013).

1.3.4. Pentose phosphate pathway

The pentose phosphate pathway (PPP) diverges from glycolysis at the first step, which is catalyzed by hexokinase.

This pathway is composed on one hand of an oxidative branch and on the other hand of a non-oxidative branch. Thereby, the oxidative branch produces NADPH, that is needed to keep the cellular redox balance and for the formation of fatty acids. This branch consists of three irreversible reactions (Patra et al., 2014; Geeraerts et al., 2017).

The first reaction involves the activity of glucose-6-phosphate dehydrogenase (G6PDH), which converts G6P into 6-phosphogluconlactone. Thereby, NADPH is produced. 6-phosphogluconlactone is hydrolyzed by phosphogluconolactonase (6PGL) into 6-phosphogluconate. Lastly, 6-phosphogluconate is decarboxylated by 6-phosphogluconate dehydrogenase (6PGDH), to produce another NADPH and ribulose-5-phosphate (Ru5P). Ru5P is then transformed into ribose-5-phospahte (R5P) (Geeraerts et al., 2017).

The non-oxidative branch consists of reversible reactions that need additional glycolytic molecules such as fructose-6-phosphate (F6P) and glyceraldehyde-3-phosphate (G3P), which can be transformed into pentose phosphate. This branch provides molecules that are used for nucleotide and amino acid synthesis (Geeraerts et al., 2017).

Through the reversibility of reaction of the non-oxidative branch of the PPP, the pathway can adapt to metabolic requirements of the cell. If for example maintaining the redox properties of cells is more important than nucleic acid synthesis, the PPP can shift the non-oxidative branch towards re-synthesizing F6P from pentose phosphate, which is then formed back to G6P that can be used by the oxidative branch (Geeraerts et al., 2017; Patra et al., 2014).

On the other hand, if for example cells must divide rapidly, most of the pentose phosphates that are needed for DNA synthesis are produced during the PPP.

Therefore, pentose phosphates are generated from both, the oxidative- and non-oxidative branch. Thus, the different ways of the PPP influence the glucose flux in glycolysis (Patra et al., 2014).

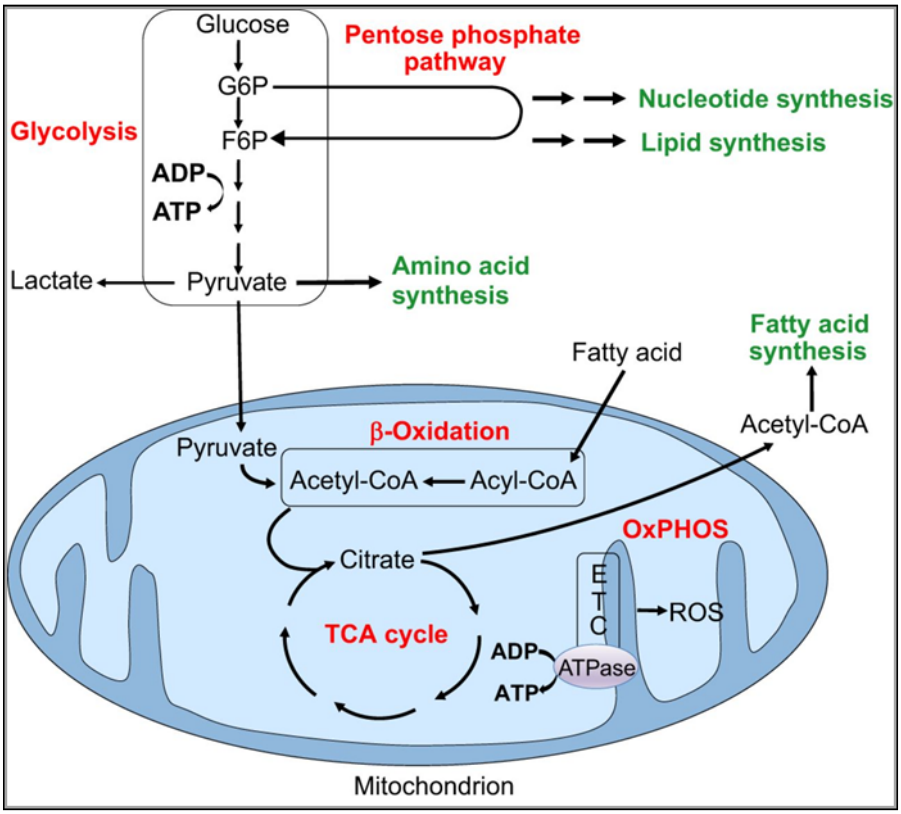

Figure 5 Overview of cellular metabolism (Mathieu, 2017)

1.3.5. Gluthatione (GSH)

The PPP is a major source of NADPH, which is needed for the formation of reduced glutathione (GSH), an important scavenger of reactive oxygen species (ROS) (Patra et al., 2014).

In addition, GSH is involved in many vital functions, such as detoxifying electrophiles, scavenging free radicals, providing cysteines and regulating cellular processes such as DNA synthesis or immune functions.

This tripeptide consists of γ-l-glutamyl-l-cysteinyl-glycine and is found in all tissues. GSH is found mostly in the cytosol and mitochondria of eukaryotic cells. However, at low concentration it is also found in the endoplasmic reticulum (Lu, 2009).

GSH is generated in the cytosol through two ATP-requiring enzymatic steps. The first step requires L-glutamate, L-cysteine and ATP to generate γ-glutamyl-L-cysteine, ADP and Pi. Thereafter, in the second step, γ-glutamyl-L-cysteine, L-glycine and ATP are converted to GSH, ADP and Pi **(Fig.6).**

The first step is catalyzed by glutamate cysteine ligase (GCL or γ-glytamylcysteine synthase). GCL is feedback regulated by GSH. This needs the binding of GSH to glutamate and additionally the availability of its precursor L-cysteine (Lu, 2009).

The second step in GSH synthesis is catalyzed by GSH synthase (GS or GSH synthetase). Reduced GS levels in organisms results in lower GSH concentrations, which leads to accumulation of γ-glutamylcysteine that is than converted to 5-oxoproline. 5-oxoproline can cause metabolic acidosis, hemolytic anemia and additionally damage of the central nervous system (Lu, 2009).

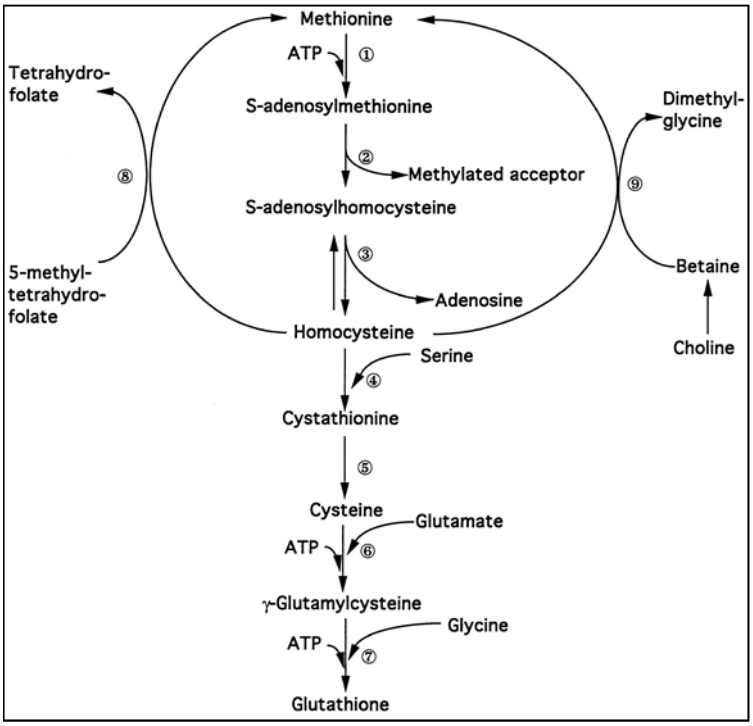

Figure 6 Glutathione production (Lu SC. 1999)

1.4. Reprogramming of cellular energy metabolism during infections

Like mentioned above, under normal conditions and the presence of oxygen, most cells metabolize glucose to carbon dioxide by oxidation of pyruvate in the mitochondrial

TCA cycle. This leads to the production of NADH which is used for OXPHOS to produce ATP. Under such conditions, the production of lactate is minimalized **(Fig.7)** (Vander Heiden et al., 2009).

However, in the 1920s, the German scientist, Otto Heinrich Warburg found alterations in the glycolytic pathway during environmental changes such as they occur during infections or tumor growth. This metabolic reprogramming implies the shifting from oxidative phosphorylation towards aerobic glycolysis, which is also known as Warburg effect or aerobic glycolysis **(Fig.7)** (Vander Heiden et al., 2009).

Energy is thereby mainly produced by a high level of glycolysis continued by lactic acid fermentation in the cytosol, even when enough oxygen is present. Under normal circumstances, glucose is transformed into pyruvate via glycolysis, which results in the production of four ATPs, with 2 ATP molecules being consumed during the glycolytic pathway. The product of the glycolysis, pyruvate, enters the citric acid cycle within mitochondria, which leads to production of high energy levels (Vander Heiden et al., 2009; Li et al., 2014).

However, during infections, the normal metabolic pathway alters, which results in the production of lactate by the enzyme lactate dehydrogenase (LDH) with no ATP producing, instead of pyruvate oxidation. Under such conditions, only 2 ATPs were produced by one glucose molecule (Li et al., 2014).

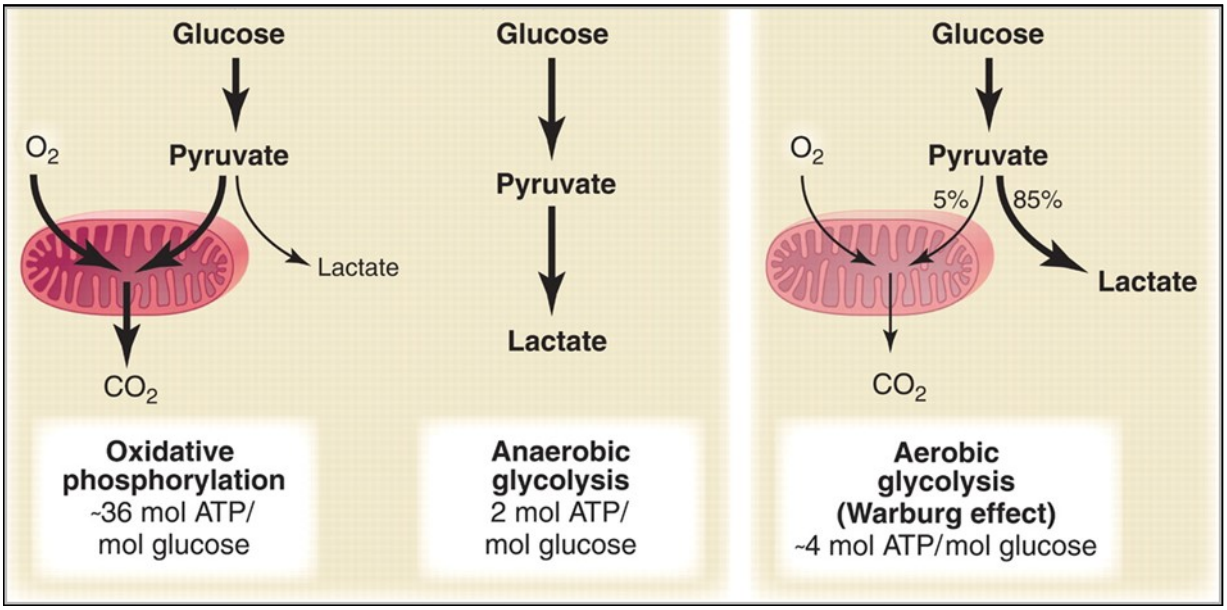

Figure 7 Warburg effect (Vander Heiden et al., 2009)

This leads to the question of why a lower energy producing metabolism is used for proliferating cells.

For many mammalian cells, the only molecules generated in high quantities are glucose and glutamine, which provide carbon, nitrogen and free energy, required for cell growth and division. Therefore, transforming all the glucose to CO_2 via OXPHOS to enhance ATP production is not meaningful. Some glucose has to be converted to macromolecular precursors, like acetyl-CoA for fatty acid production, glycolytic molecules for generating of non-essential amino acids and ribose for nucleotide production. This explains the advantage of the aerobic glycolysis which allows rapid cell division (Vander Heiden et al., 2009).

Additionally, immune response is subjected on the rate of the proliferative expansion of effector immune cells. Thereby, cells must maximize their speed of anabolic growth by transforming glucose into biomass and hence proliferate faster (Vander Heiden et al., 2009).

LPS of bacteria gets recognized by TLR4 and was shown to stimulate metabolic changes resembling the Warburg effect. After infection of macrophages, lactate generated by the glycolytic pathway is immediately transported out of the cell. Immune cells need this metabolic alteration to produce both, ATP and building blocks needed for their activation. Furthermore, the citric acid cycle gets truncated at the steps requiring the enzymes isocitrate dehydrogenase (IDH) and succinate dehydrogenase (SDH), which results in the accumulation of citrate and succinate molecules (Geeraerts et al., 2017).

The high concentrations of citrate are due to the transcriptional down-regulation of IDH1, the enzyme needed for the conversion of isocitrate into α-ketoglutarate. After an infection, mitochondrial citrate is transported out from the TCA cycle into the cytosol and thus drives fatty acid biosynthesis needed for the increment of the endoplasmic reticulum and Golgi apparatus to facilitate cytokine release by macrophages **(Fig.8)** (Stienstra et al., 2017; Kim et al., 2015; Geeraerts et al., 2017).

In addition, the citrate is needed as a precursor to produce the specific molecule itaconic acid within macrophages. The immunoresponsive gene 1 (irg1) plays an important role, since it is coding for the enzyme cis-aconitate decarboxylase, that transforms aconitate to itaconic acid which is enhanced during infections. Itaconic acid

has antimicrobial characteristics against the bacterium *Salmonella enterica*, since it blocks the bacterial enzyme isocitrate lyase, needed for the conversion of isocitrate into succinate and glyoxylate during the glyoxylate shunt pathway (Geeraerts et al., 2017; Cordes et al., 2016).

Moreover, itaconic acid is a driver for the succinate accumulation in macrophages during an infection, since it blocks the enzyme SDH (Geeraerts et al., 2017; Cordes et al., 2016). The enhanced succinate concentrations lead to stabilization of t HIF-1α, a transcription factor which is able to induce the formation of the pro-inflammatory cytokine IL-1β (Ullah et al., 2006) and additionally, increases the glycolytic flux by activating genes involved in the glycolysis, such as glucose transporter 1 (GLUT1), PFKFB3 and monocarboxylate transporter 4 (MCT4) (Stienstra et al., 2017; Geeraerts et al., 2017).

Due to the high glycolytic flux, also the PPP is enhanced in macrophages during infections. The formed NADPH during this pathway is needed as a co-factor to produce the inducible nitric oxide synthase (iNOS) that converts arginine into nitric oxide (NO) and l-citrulline. To maintain antimicrobial nitric oxide (NO) formation, l-citrulline is recycled to arginine. NO can nitrosylate the iron-sulfur-containing complexes of the electron transport chain and therefore blocks mitochondrial respiration and OXPHOS (Geeraerts et al., 2017).

Furthermore, the formed NADPH during PPP can be used as a co-factor for the enzyme NADPH oxidase, which is required to produce ROS and additionally, the anti-oxidant glutathione, which is essential to maintain the redox balance within cells and prohibit cellular damage by ROS (Geeraerts et al., 2017).

Next to production of NADPH by the PPP, NADPH can also be produced during infections by the enhanced citrate concentrations in the cytosol. Thereby, the citrate carrier (CIC) located in the mitochondria, transports citrate into the cytosol, where it is converted back to acetyl-CoA and oxaloacetate (OAA) by the enzyme ATP-citrate lyase (ACLY). OAA is thereafter reduced to malate, which is transformed into pyruvate by the malic enzyme. This results in the production of NADPH **(Fig.8)** (Geeraerts et al., 2017). The formed acetyl-CoA is used to produce fatty acids. Activation of macrophages by TLR4 is associated with lipid accumulation because of fatty acid uptake by CD36, enhanced triglyceride synthesis and reduced triglyceride lipolysis.

The increase in the lipid synthesis results from the up-regulation of the transcription factor sterol regulatory element-binding protein-1c, which enhances the expression of genes involved in the fatty acid synthesis, such as fatty acid synthase (Geeraerts et al., 2017).

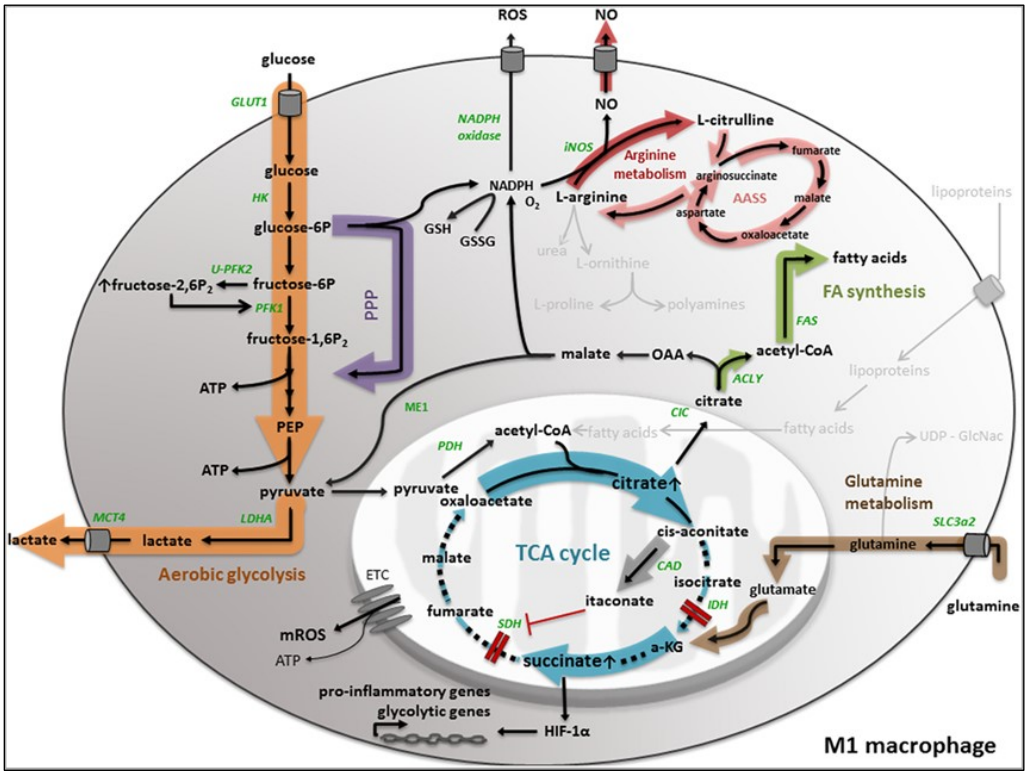

Figure 8 Reprogramming of cellular energy metabolism during infections (Stienstra et al., 2017)

1.5. The role of iron during metabolic reprogramming

Interestingly, reports show that there is a connection between the metabolic reprogramming within macrophages and iron homeostasis due to the fact, that perturbations within the iron metabolism alter the expression of enzymes involved in the citric acid cycle, such as aconitase **(Fig.9)** (Oexle et al., 1999; Volani et al., 2017).

This change in the function of aconitase is shown to be a result of the interaction between iron regulatory proteins (IRPs) and a RNA stem loop structure, iron responsive elements (IRE) within the 5`untranslated region (UTR) of mitochondrial aconitase mRNA (Oexle et al., 1999).

Binding of such IRPs to IREs occurs under iron limited states, oxidative stress or in presence of NO and inhibits the binding of the small ribosomal subunit to the mRNA, which results in blockage of mitochondrial aconitase expression (Oexle et al., 1999).

Contrary, iron overload within cells decreases binding of IRE to IRPs. Under such circumstances, IRP1 can form an iron sulfur-cluster and acting as a cytoplasmic aconitase, whereas IRP2 gets degraded which leads to enhanced aconitase translation and expression (Oexle et al., 1999). Moreover, also the expression of the enzyme succinate dehydrogenase (SDH) is regulated by iron concentrations within the cell, since the subunit d of SDH carry an IRE within its 5' UTR (Muckenthaler et al., 2017).

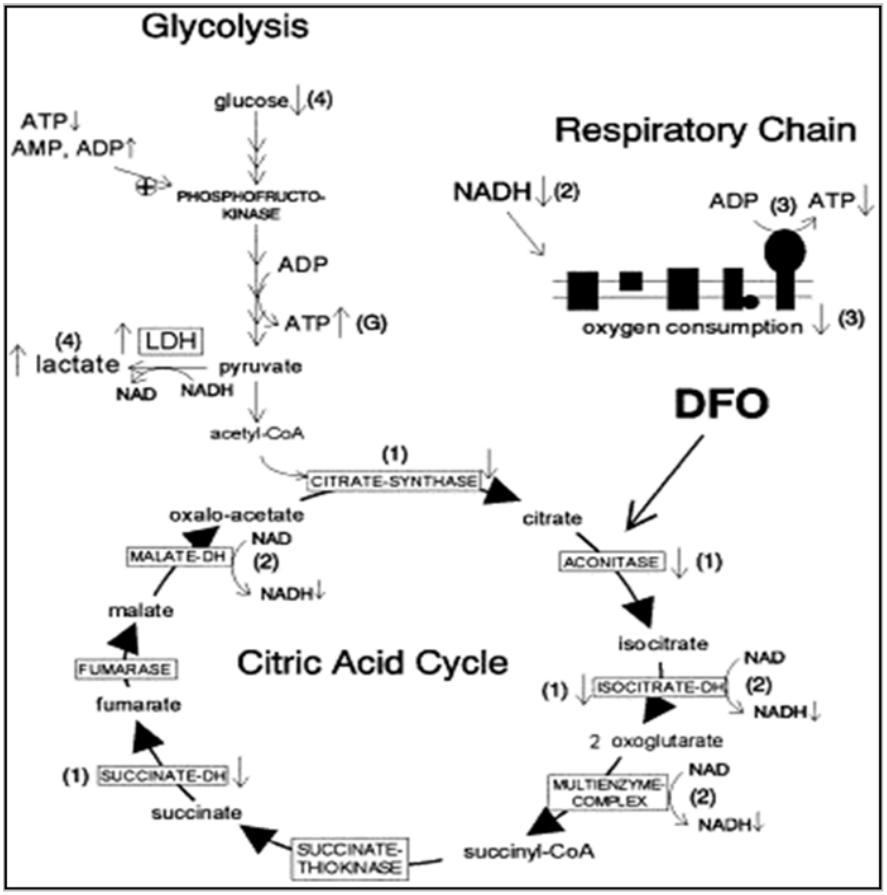

Figure 9 Influence of DFO on cellular energy metabolism (Oexle et al.,1999)

Reports showed that this alterations in the metabolic signaling pathways under abnormal cellular conditions such as infections or iron perturbation states are influenced by the mammalian target of rapamycin (mTOR) signaling pathway (Arsenault et al., 2013).

1.6. mTOR signaling pathway

The mammalian target of rapamycin (mTOR) signaling pathway recognizes a multiplicity of environmental terms, since it is responsive to growth factors, oxygen, energy and stress conditions (Eiden et al., 2016). Most individuals developed mechanisms for changing between anabolic and catabolic stages which enables them to survive also in nutrient deprived environments. In mammalians, such a pathway is the signaling network orchestrated by the mTOR protein kinase (Laplente et al., 2012).

mTOR is a phosphatidylinositol 3-kinase (PI3-K)-like serine/threonine protein kinase that is conserved in all eukaryotic cells. It is the target of a molecule named rapamycin, which was first discovered in 1975 from the bacterium *Streptomyces Hygroscopius* and acquired attention due to its immunosuppressive and anti-proliferative activities. Rapamycin thereby forms a complex with the intracellular FK506-binding protein (FKBP12), which can directly interact with and block the mTORC1 but not mTORC2. However, how in detail the binding of FKBP12-rapamycin to mTORC1 results in inhibition of its action is unknown so far (Laplente et al., 2013; Eiden et al., 2016).

In mammals, mTOR is divided into two structurally and functionally distinct complexes (Eiden et al., 2016). Both complexes have in common that they are large, with mTOR complex 1 (mTORC1) having six and mTOR complex 2 (mTORC2) seven established protein components. In addition, they share the sec-13 (mLST8) subunit, DEP domain containing mTOR-interacting protein (DEPTOR) and the Tti1/Tel2 complex **(Fig.10)** (Laplante et al., 2013).

In contrast, mTORC1 has two specific protein elements, known as proline-rich Akt substrate (pras40) and regulatory-associated protein of mammalian target of rapamycin (raptor), while mTORC2 has three specific elements, known as mammalian stress-activated map kinase-interacting protein 1 (mSin1), rapamycin-insensitive companion of mTOR (rictor), and protein observed with rictor 1 and 2 (protor 1/2) **(Fig.10)** (Laplante et al., 2013).

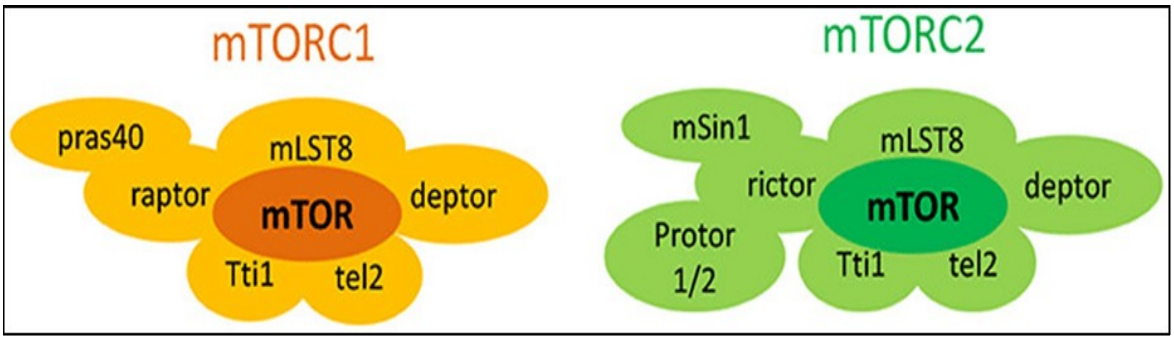

Figure 10 Composition of mTOR complex 1 and mTOR complex 2 (Ong et al., 2016)

1.6.1. mTOR complex 1

mTORC1 is the better characterized complex and receives inputs from five intracellular and extracellular factors, including growth factors, stress, energy status, oxygen and amino acids. This enables the complex to regulate important processes such as protein synthesis, lipid synthesis or autophagy (Laplante et al., 2013).

The major upstream modulator of mTORC1 is a heterodimeric protein, composed of tuberous sclerosis subunit 1 (TSC1) and TSC2 and works as a GTPase-activating protein (GAP) for the Ras homolog (Rheb) GTPase. The GTP bound profile of Rheb interacts with mTORC1 and triggers its kinase activity. TSC1/2 negatively modulate mTORC1 by transforming Rheb into its inactive GDP-binding form (Laplante et al., 2013).

Contrary to energetically beneficial, low stress situations which are known to activate mTORC1 through phosphorylation and therefore inactivation of TSC1/2, high stress-stages such as limitation in energy and oxygen levels leads to blockage of mTORC1 through adenosine monophosphate-activated protein kinase (AMPK) and thereby promote survival through preservation of cellular sources (Bayeva et al., 2012, Laplante et al., 2013).

Cellular processes are controlled by mTORC1 through substrates such as S6 kinase (S6 K) and 4 E binding protein 1 (4E-BP1). So far, protein synthesis is the best characterized process which is controlled by mTORC1. Thereby, mTORC1 phosphorylates the translational mediators of the translation initiation factor 4E (eIF4E) and S6 kinase 1 (S6K1) which trigger protein synthesis. The phosphorylation of 4E-

BP1 inhibits its binding to the cap-binding protein eIF4E, which allows it to form the eIF4F complex, needed for the inition of the cap-dependent translation.

The activation of S6K leads to enhanced mRNA biogenesis, and initiation of translational and elongation (Laplante et al., 2013; Guan et al., 2014; Ramanathan et al., 2009).

Next to controlling the composition of protein complexes, mTORC1 also participates in lipid synthesis which is important for proliferating cells to produce membranes. Thereby, mTOR triggers the synthesis through the transcription factors sterol regulatory element binding protein 1/2 (SREBP1/2) that regulate the expression of genes involved in fatty acid and cholesterol production. Contrary, mTOR blockage leads to limited expression of lipogenic genes (Laplante et al., 2013).

mTORC1 also positively influences cellular metabolism and ATP production, since it enhances the glycolytic flux by activating hypoxia inducible factor-1α (HIF-1α) transcription and translation, which is a positive mediator of many glycolytic genes (Laplante et al., 2013).

Interestingly, mTORC1 also negatively regulates autophagy within cells. This process plays an important role in recycling of damaged substances within cells. Upon inhibition of mTORC1, autophagosomes can be formed which are now able to engulf proteins and organelles and fuse with lysosomes, leading to the destruction of cellular elements (Laplante et al., 2013).

1.6.2. mTOR complex 2

In comparison to mTORC1, mTORC2 signaling is resistant to mitogens, nutrients and rapamycin but is influenced by growth factors and controls downstream targets of the insulin/insulin-like growth factor 1 (IGF-1) receptor via molecules such as Akt and serum/glucocorticoid-regulated kinase (SGK) (Laplante et al., 2013).

Phosphorylation of Akt by mTORC2 results in its activation and thereby enables it to control different cellular tasks such as metabolism, survival, apoptosis, growth and proliferation. Additionally, it regulates cell migration and survival via the activation of Rho GTPases **(Fig.11)** (Guan et al., 2014; Ramanathan et al., 2009; Laplante et al., 2013).

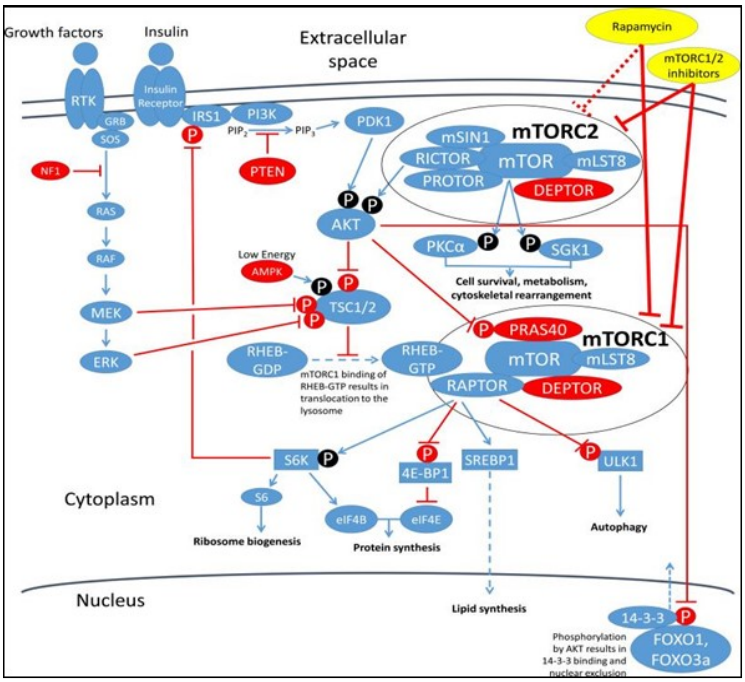

Figure 11 mTOR signaling pathway (Eiden, 2016)

1.7. mTOR orchestrates the metabolic reprogramming

mTOR was shown to act as a metabolic switch, transferring cells from the catabolic state to an anabolic state in response to danger signal, as it occurs during infections.

Together with the phosphatidyl inositol 3'-kinase (PI3K)/Akt route, mTOR and HIF-1α mediate aerobic glycolysis during infections. Thereby, the transcription factor HIF-1α enhances the expression of many enzymes involved in the glycolysis and increases therefore the glycolytic flux to provide all essential resources needed for activated immune cells (Stienstra et al., 2017).

Additionally, the pro-inflammatory activation of HIF-1α leads to induction of pyruvate dehydrogenase kinase, isozyme 1 (PDK1), which is involved in the glycolytic reprogramming by converting pyruvate to lactate (Stienstra et al., 2017). Importantly, such alterations in the glycolytic rate do not affect the production of pro-inflammatory cytokines such as IL-6 or TNF-α (Stienstra et al., 2017).

Additionally, HIF-1α triggers the fatty acid synthesis within macrophages during infections, since it influences the expression of the FASN gene, which is required for the activation of the enzyme fatty acid synthase (FAS) (Stienstra et al., 2017).

However, this process is counteracted by 5'-adenosine monophosphate-activated protein kinase (AMPK), which is a major regulator of the metabolic energy homeostasis. This protein is able to obtain signals of the cellular energy state and can emit corresponding signals through phosphorylation, that affect glycolysis, protein synthesis and fatty acid synthesis. AMPK is activated by enhanced AMP levels, which resembles a low energy state within in the cell (Arsenault et al., 2013). AMPK therefore positively affects oxidative phosphorylation and promotes anti-inflammatory properties (Stienstra et al., 2017).

During infections, mTOR was shown to be essential for an effective immune response since it triggers the migration of immune cells to the site of infections and positively affects the production of pro-inflammatory cytokine as well as the maturation, activation and differentiation of macrophages (Eiden et al., 2016). It is therefore not surprisingly that treatment with rapamycin and therefore inhibition of the mTOR during infections has severe consequences for the host since it results in diminished first line response to pathogens, which in turn provides opportunities for pathogens to proliferate within the body (Eiden et al., 1016).

1.8. The link between mTOR pathway and iron homeostasis

Since many processes which are controlled by mTOR need iron as a co-factor, a steady supply of iron is essential to maintain cellular functions, and limitation of iron within cells decreases the activity of mTOR (Guan et al., 2014). Additionally, blockage of mTOR results in changes of major proteins needed in iron homeostasis, such as TfR1, ferritin, Fpn and hepcidin, which were shown to be up-regulated under such conditions, resulting in iron overload within cells (Bayeva et al., 2012; Silverstri et al., 2016). This provides evidence that there is a connection between the mTOR signaling pathway and cellular iron homeostasis (Bayeva et al, 2012).

1.8.1. Tristetraprolin

Recently, studies described a tandem zinc finger protein, called tristetraprolin (TTP), which is a downstream target of mTOR and mediates iron-regulatory effects of this protein.

TTP is known as an early response gene and contributes to the anti-inflammatory response. Under iron-deficient conditions or in presence of rapamycin, this protein becomes activated which results in destabilization of mRNAs of non-essential iron-containing proteins, thereby liberating iron which can be used in vital processes. Moreover, this protein has the property to interact with TfR1 and alter its stability which results in the degradation of the iron importer and therefore changes in cellular iron flux **(Fig.12)** (Guan et al.,2014; Bayeva et al., 2014). It has been shown that also the expression rate of the two citric acid cycle enzymes, SDH and aconitase is diminished under iron-limited conditions, which correlates with the overexpression of TTP, whereas iron overload results in the opposite effect (Bayeva et al., 2014).

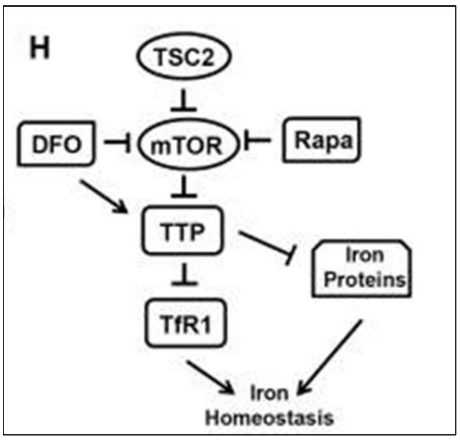

Figure 12 Functions of TTP (Guan et al., 2014)

Taken together, both, the metabolic activity as well as cellular iron homeostasis are able to alter the behavior of immune cells in response to danger signals such as iron-limited states or infections. However, how these two major cellular mechanisms are interconnected it's not fully understood so far and needs further investigations.

2. Purpose of this work

Iron is an essential metal for organisms and of major importance for many metabolic processes as it is part of several enzymes which participate in metabolic tasks. Iron availability within cells affects the energy metabolism, since it controls the activity of the citric acid cycle via regulation of mitochondrial enzymes, such as aconitase expression.

Moreover, iron availability impacts on NADH and lactate formation and thus cellular energy production, since it was shown that under iron-deprived states as well as during infections, macrophages re-program their energy metabolism, shifting from oxidative phosphorylation towards aerobic glycolysis which is demonstrated to be an important mechanism for infection control. Parts of such a shift can been traced back to the mTOR signaling pathway, since it responds to danger signals, via altering the glycolytic flux within immune cells and additionally it regulates major proteins involved in iron homeostasis.

Within the current master thesis, we aim to study if the cellular reprogramming, mediated by mTOR is linked to alterations of cellular iron homeostasis, given the effect of iron in the control of this metabolic process. Furthermore, iron availability is associated with increased pathogen proliferation. We hypothesize that the negative effect of iron on infection control is not only reasoned by the increased availability of the metal for bacteria but also based on changes of the metabolic profile within macrophages which favor pathogen proliferation.

3. Materials and methods

3.1. Materials

Cell culture	Company
Dulbecco's Modified Eagle Medium (DMEM)	Lonza Ldt.
10 % fetal calf serum (FCS) Superior	Biochrome AG
1% Penicillin, Streptomycin, Glutamine (PSG)	PAA Laboratories GmbH, Austria
10 mM MEM non-essential amino acids (NEAA) 100X	Gibco live technologies
1% Sodium pyruvate	Sigma-Aldrich
Dulbecco's phosphate-buffered saline (DPBS)	PAA Laboratories GmbH, Austria
Acridine Orange/ Propidium Iodide stain	Logos Biosystems
RAW264.7 cells	ATCC
Cell culture flask	Falcon
Cell counting slide	Logos Biosystems
Cell scraper	Greiner
Treatment of RAW264.7	
Rapamycin (27,4mM)	Sigma-Aldrich
Gentamycin sulphate solution (50 mg/ml)	Carl Roth
LPS E. coli 005: B5 (5 mg/ml)	Sigma-Aldrich
IFN-γ (100 µg/ml)	R&D systems, USA
Salmonella enterica serovar Typhimurium	ATCC
$FeCl_3$ hexahydrate	Sigma-Aldrich
Deferiprone (DFP)	Cabantic; Israel
ΔentCΔsitΔfeo Salmonella strain	Ferric Fang Seattle, WA
RNA extraction	
peqGOLD Tri-Fast™ reagent	Peqlab, Germany
Chloroform	VWR Chemicals
Isopropanol	Gatt Koller GmbH, Austria
Ethanol	VWR Chemicals
cDNA	
Random Hexamer Primer Mix 5 µM	Roche, Germany
dNTP-Mix 10mM	Roche, Germany
5x First Strand Buffer	Invitrogen, USA
1,4-Dithiothreitol (DTT) 0.1 M	Invitrogen, USA
Moloney Murine Leukemia Virus (M-MLV) RT	Invitrogen, USA
RNAsin 40 U/µl	Promega, USA
qRT-PCR	
SsoFast™ EvaGreen Supermix	BioRad™
SsoFast™ Probes Supermix	BioRad™

Low profile 96well PCR Plate	Peqlab, Germany
Primer (100 µM) and Probes (10 µM)	Microsynth AG, Switzerland
C1000 Thermocycle CFX96 Real-Time system	BioRad
FACS	
DPBS	PAA Laboratories GmbH, Austria
FCS	Biochrome AG
Ethylenediaminetetraacetic acid (EDTA)	Invitrogen, USA
4′,6-Diamidin-2-phenylindol (DAPI)	Thermo Fisher Scientific
FACS-tubes (5 ml)	Greiner Bio One
Fluorescence microscopy	
Bovine serum albumin (BSA)	Sigma-Aldrich
Triton	Carl Roth
Horse serum	Thermo Fisher Scientific
Paraformaldehyde	Carl Roth
Succrose	Carl Roth
Na-phosphate	Carl Roth
DPBS	PAA Laboratories GmbH, Austria
DAPI	Thermo Fisher Scientific
Alexa fluor 594 phalloidin	Life technologies
Immersion oil	Zeiss
Agar-plates	
LB-broth (Lennox)	Sigma-Aldrich
Agar-Agar Kobe 1	Carl Roth
Counting of *S.* Typhimurium	
10% Formalin	Sigma-Aldrich
Trypan blue	Sigma-Aldrich
Western Blot	
Cell scraper	Greiner
Tris base	Bio-Rad
Potassium chloride	Bio-Rad
Triton X 100	Carl Roth
Hydrochloric acid (HCl)	ICN
dH_2O	
Aprotinin	Sigma- Aldrich
Leupeptin	Sigma-Aldrich
BCA protein assay kit Reagent A: Reagent B = 50:1	Pierce, 233225
BSA	Sigma-Aldrich
DPBS	PAA Laboratories GmbH, Austria
96-well microplate	R&D systems
Tris-HCl	ICN

Sodium Dodecyl Sulfate (SDS)	ICN
ß-Mercaptoethanol	Sigma-Aldrich
Glycerol	Merck
Bromphenol blue	Merck
Acrylamide	Bio Rad
Bisacrylamide	Bio Rad
Glycine	ICN
Tetramethylethylendiamin (TEMED)	Sigma-Aldrich
Ammoniumpersulfate (APS)	Bio-Rad
PVDF transfer membrane	GE-Healthcare
Whatmann paper	Amersham
Rainbow protein marker	Amersham
Methanol	Merck
Sodium chloride (NaCl)	Carl Roth
Skim milk powder	ICN
Nitrite measurement	
Griess-Ilosvay's nitirite reagent	Merck-Millipore, Germany
Sodium nitrite ($NaNO_2$)	
DPBS	PAA Laboratories GmbH, Austria
ELISA	
DPBS	PAA Laboratories GmbH, Austria
10% FCS	Biochrome AG
Tween-20	Merck KGaA
1% BSA	Sigma-Aldrich
Capture Antibody (IL-6 and IL-10)	BD Bioscience
Working Detector (IL-6 and IL-10)	BD Bioscience
BM Blue POD substrate (IL-6 and IL-10)	Roche
Stop solution H_2SO_4	Merck
96-well microplate	R&D systems
Capture Antibody (TNF-α)	R&D systems
Working Detector (TNF-α)	R&D systems
Substrate solution (TNF-α)	R&D systems
Freezing medium	
FCS	Biochrome AG
Dimethyl sulfoxide (DMSO)	Carl Roth
Lysis of RAW267.4 cells	
Sodium-deoxicolate	Sigma-Aldrich
DPBS	PAA Laboratories GmbH, Austria

3.1.1. Preparation of ferric chloride $FeCl_3$

67,5 mg of $FeCl_3$ (270,3 g/l) were transferred into a falcon tube and dissolved in 25 ml of dH_2O. After mixing well, the solution was filtrated in a clean falcon tube and $FeCl_3$ was stored at 4°C protected from light.

3.1.2. Preparation of sodium-deoxicolate solution

2,5 g of Sodium-deoxicolate were transferred under sterile conditions into a falcon tube and dissolved in 500 ml of dH_2O. After mixing well, the solution was stored at RT.

3.2 Cell culture techniques

3.2.1 Cultivation of RAW264.7 cells

All experiments were performed with RAW264.7, a mouse leukemic monocyte-macrophage cell line. RAW264.7 murine macrophage like cells were stored in cryotubes in liquid nitrogen at -180°C.

For thawing the cells, they were incubated in a water bath at 37°C. When cells were completely thawed, the were transferred into 75 cm^2 cell culture flask containing 10 ml pre-warmed DMEM supplemented with 10% FCS, 1% penicillin, 1% streptomycin and 1% L-glutamine, 1% minimum essential medium non-essential amino acids (MEM NEAA 100 x) and 2% sodium pyruvate. Cells were grown at 37°C in humidified air containing 5% CO_2 O.N. The next day, the medium was changed.

When approximately 80% of the bottom of the flask were covered with the cells the medium was removed, the cells were washed 3 x with 5 ml sterile DPBS. After the washing step 10 ml of fresh medium was added to the cells and they were scraped from the bottom using a cell scraper and transferred into a 175 cm^2 cell culture flask containing 18 ml of complete DMEM. Thereafter the cells were incubated at 37°C in humidified air containing 5% CO_2 until they were needed for experiments.

3.2.2 Counting of RAW264.7 cells

The medium was removed from the cell culture flask and RAW264.7 cells were washed 3 x with 10 ml DPBS. Thereafter, 10 ml of fresh DMEM was added to the cell culture flask and cells were scraped into a 50 ml falcon. Thereafter, 9 µl of the cells were taken out from the falcon and transferred into a clean 0,5 ml Eppendorf tube. 1 µl of Acridine Orange/ Propidium Iodide stain was supplied (1:10). The suspension was vortexed for 10 sec. and the 10 µl were afterwards transferred into a cell counting slide and cells were count using the cell counter LUNA.

3.2.1 Freezing of RAW264.7 cells

Cells were freeze, when they were growing well, commonly when they reached a confluence of approx. 80%.

The medium was removed from the cells and they were washed 3 x using 10 ml sterile DPBS. Thereafter, 10 ml of sterile DMEM was supplied to the cells and they were scraped into 50 ml falcon tubes using a cell scraper. Cells were centrifuged at 1000 g for 5 min.

The supernatant was discarded and 1 ml freezing medium/vial was added to the pellet.

After resuspending the cells in the solution, 1 ml was transferred into cryotubes and stored at -80°C O.N.

The next day, cells were stored in liquid nitrogen.

Freezing medium (10 ml)	
FCS	9,2 ml
100 % DMSO	0,8 ml
Total Volume	**10 ml**

3.3 Treatment of RAW264.7 cells

3.3.1 Treatment with LPS and IFN-γ

6 x 10^5 cells/ml were transferred into each separate well of a 6-well plate and incubated in 1 ml complete DMEM without antibiotics. Once cells were set on the bottom of the plate, 10 ng/ml of LPS and 10 ng/ml IFN-γ were added directly to the cells. Thereafter

cells were incubated at 37°C humidified air containing 5% CO_2 for 24 hours. After the incubation period of the cells they were processed for further investigations.

3.3.2 Treatment with mTOR inhibitor rapamycin

6 x 10^5 cells/ml were transferred into each separate well of a 6-well plate containing 1 ml of complete DMEM. When the cells were attached on the bottom of the plate, 200 nM of rapamycin were added directly to each well and cells were incubated at 37°C for 1 hour.

Thereafter the medium was removed, and cells were washed 3 x using 1 ml DPBS. After the washing step, 1 ml of fresh medium was added to the cells and 20 nM of rapamycin were supplied for another 23 hours.

3.3.3 Treatment with the antibiotic gentamycin

After infecting RAW 264.7 cells with *S.* Tm (MOI of 10) for 1 hour the medium was removed from the cells and cells were washed 3 x with 1 ml sterile DPBS. 1 ml of fresh DMEM containing 10% FCS, sodium pyruvate and NEAA was added to the cells. To reduce the growth of extracellular bacteria, 50 µM of gentamycin sulphate solution was supplied to the cells. Thereafter, an incubation step for another 23 hours at 37°C in humidified air was performed.

3.3.4 Treatment with iron and iron chelator

6 x 10^5 RAW 264.7 cells were incubated in 1 ml of complete DMEM. 50 µM of $FeCl_3$ or 50 µM of DFP was added directly to the cells for 6 h (37°C). Thereafter, iron or chelator was removed from the cells by washing it 3 x with DPBS. After adding 1 ml of fresh DMEM to the cells, they were infected with *S.* Tm and either incubated in presence (30h of iron treatment) or absence (6 hours of iron treatment) of $FeCl_3$/DFP for another 24 hours at 37°C in humidified air.

3.4 Stimulation of RAW264.7 cells

3.4.1 Stimulation with $FeCl_3$/DFP and *S.* Tm

6 x 10^5 of RAW264.7 cells were seeded into separate wells of a 6-well plate and incubated in complete DMEM at 37°C. When cells were attached to the bottom of the plate, 50 µM of either $FeCl_3$ or DFP were added to each well and incubated for 6 hours at 37°C.

Thereafter, the medium was removed from the cells and they were washed 3 x using DPBS. 1 ml of DMEM without antibiotics was added to the cells and they were infected with *S*. Tm for 1 hour at MOI of 10 in presence (30 h $FeCl_3$/DFP supplementation) or absence (6 h $FeCl_3$/DFP supplementation) of $FeCl_3$/DFP.

After the incubation step, *Salmonella* were removed by washing the cells 3 x using DPBS and incubating the cells again for 24 hours in DMEM containing 50 µM of gentamycin in presence or absence of 50 µM $FeCl_3$ or 50 µM DFP.

3.4.2 Stimulation with rapamycin and *S.* Tm

6 x 10^5 of RAW264.7 cells were seeded into separate wells of a 6-well plate and incubated in complete DMEM at 37°C. When cells were attached to the bottom of the plate, 200 nM of rapamycin was added directly to the cells for 1 hour. Thereafter, cells were washed 3 x using DPBS and infected with *S*. Tm for 1 hour in presence of 20 nM of rapamycin. Thereafter, bacteria were removed and 1 ml of DMEM containing 50 µM of gentamycin was added to the cells. Additionally, 20 nM of rapamycin was supplied directly to the cells prior to incubating it for 24 hours at 37°C.

3.4.3 Stimulation with $FeCl_3$/DFP, rapamycin and *S.* Tm

6 x 10^5 of RAW264.7 cells were seeded into separate wells of a 6-well plate and incubated in complete DMEM at 37°C. When cells were attached to the bottom of the plate, 50 µM of $FeCl_3$ or 50 µM of DFP was added directly to the cells for 5 hours and they were incubated at 37°C. Thereafter, 200 nM of rapamycin was added to the cells for 1 hour.

After the incubation period, the medium was removed and cells were washed 3 x using DPBS. DMEM without antibiotic was added to the cells and they were infected with *S*. Tm for 1 hour at MOI of 10, either in presence of 50 µM $FeCl_3$/DFP (30 h $FeCl_3$/DFP supplementation) and 20 nM of rapamycin or in absence of $FeCl_3$ or DFP (6 h $FeCl_3$/DFP supplementation).

After the incubation step at 37°C, bacteria were removed and DMEM containing 50 µM of gentamycin was added. Additionally, 20 nM of rapamycin was added to the cells and cells were incubated either with or without 50 µM of $FeCl_3$/DFP for 24 hours at 37°C.

3.5 Storage of supernatant

After a desired incubation period of the cells, the supernatant was collected in clean 1,5 ml Eppendorf tubes and centrifuged at 300 g for 5 min. to remove all residual cells. Thereafter, the upper phase was collected and transferred into clean 1,5 ml safe Eppendorf tubes and stored at -80°C until the supernatant was needed for further investigations.

3.6 Handling of *Salmonella enterica* serovar Typhimurium

For all infection assays the bacterium *Salmonella enterica* serovar Typhimurium (*S.* Typhimurium, *S*. Tm wt) strain ATCC14028 was used.

Additionally, a *Salmonella* triple mutant dericative entC::aph sit::bla feo:Tn10 (Kan, Ap, Tet) was used for infections. The mutant strain has a deficiency in enterobactin synthesis, sitABCD- and Feo-mediated iron uptake (ΔentCΔsitΔfeo).

3.6.1 Preparation of LB-broth agar-plates

For the cultivation of *S*. Tm, the nutrient rich LB-broth Lennox microbial growth medium was used.

For preparation of agar plates, 20 tablets of LB-broth Lennox (1 tablet in 50 ml dH2O) and 10 g of Agar-Agar Kobe 1 were dissolved in 1 l of dH_2O and autoclaved.

Thereafter the solution was cooled to 55°C and 13 ml of the solution were poured into Petri dishes. After letting harden the dishes they were stored at 4°C in the dark.

3.6.2 Storage of S. Typhimurium

S. Tm were grown under sterile conditions in 5 ml LB-medium at 37°C on a shaker (200 min^{-1}). After 20 min., the optical density (OD_{600}) was determined using a photometer.

When the bacteria reach the late-logarithmic phase at OD_{600} of 0,5 they were centrifuged at 4700 rpm for 10 min. at 4°C. The LB-medium was removed and 30 ml of DPBS was added to the pellet. The centrifugation step was repeated for another time. After this washing step, the supernatant was poured away and a solution containing 0,180 ml of sterile DPBS and 20 µl of 10% Glycerol was filtrated to the pellet and mixed well. Thereafter, aliquots were made by putting 20 µl of the suspension into sterile 0,5 ml Eppendorf tubes and frozen away at -80°C.

3.6.3 Heat-inactivating of *S*. Typhimurium

S. Tm wt were grown under sterile conditions at 37°C on a shaker in LB-medium to late-logarithmic phase. Thereafter, bacteria were centrifuged at 4600 rpm for 10 min. at 4°C. The supernatant was removed and 30 ml PBS was added to the pellet. The centrifugation step was repeated. The supernatant was removed and 5 ml of sterile DPBS was added directly to the pellet. Thereafter, the number of bacteria was determined using a hemocytometer.

Since in my experiments always 6 x 10^5 of RAW264.7 cells were used, the MOI of 10 was calculated.

After another centrifugation step at 4600 rpm for 10 min. at 4°C, a solution which contains 0,180 ml of sterile DPBS and 20 µl of 10% glycerol was filtered to the pellet and mixed well.

Aliquots were made by putting 15 µl (MOI of 10) of the bacterial suspension into 0,5 ml Eppendorf tubes and the bacterial suspension was incubated in a water bath at 70°C for 35 min. Every 10 min. the Eppendorf tube was vortexed to ensure, that all bacteria get inactivated. Thereafter, the aliquots were frozen away at -80°C.

To ensure the inactivation of the bacteria, three aliquots were plated on agar-plates and incubated for 24 hours at 37°C. If no colonies were formed after the incubation step, the inactivation process was successful.

3.6.4 *S.* Typhimurium infection in vitro

Prior to infection, the deep-frozen wild-type *S.* Tm were defrosted and plated on LB-broth agar plates and incubated at 37°C for 24 hours.

After the bacterial incubation, 6 x 10^5 of RAW264.7 cells/ml were transferred into separate wells of a 6-well plate and incubated in complete DMEM without antibiotics. The macrophages were incubated at 37°C in humidified air containing 5% CO_2 until they were set on the bottom on the plate.

In the meantime, three colonies of *S.* Tm were transferred from the agar plate into 50 ml falcons containing 5 ml of LB-medium and were grown at 37°C on a shaker under sterile conditions to late-logarithmic phase.

When they reached the OD_{600} of 0,5 the bacteria were centrifuged at 4700 rpm for 10 min. at 4°C. The LB-medium was removed and 30 ml of DPBS was added to the pellet. The centrifugation step was repeated for another time. After this washing step, the supernatant was poured away and another 5 ml of DPBS were added to the pellet and mixed well.

To determine the number of the bacteria in the falcon tube, a hemocytometer was used. For this manual counting process, a solution was prepared which makes the bacteria visible.

Therefore, a solution was prepared in a 1 ml sterile Eppendorf tube which contains:

Staining solution	
10% Formalin	0,38 ml
Trypan blue	0,1 ml
Bacterial suspension	20 µl
Total volume	**0,5 ml**

After mixing the solution, 1 µl was transferred into the hemocytometer (depth 0,01 mm) and the number of bacteria within three double-lined squares was counted using a light microscope.

Using the formula (Counted bacteria/3) x 2.5 x 25 x 10^6, the total number of organisms per ml in the sample was determined.

If this was calculated, macrophages were infected with the bacteria at a multiplicity of infection of 10 (MOI 10) for 1 hour. Thereafter cells were washed 3 x with 1 ml sterile

DPBS and incubated afterwards at 37°C in DMEM medium containing the antibiotic gentamycin (50 µM) for another 23 hours.

After the incubation period, cells were prepared for further investigations.

3.6.5 Determination of CFU/ml

For phagocytosis experiments, infections were terminated by washing the cells 3 x with DPBS and subsequent lysis of the cells with 1 ml Na-deoxycholate per each separate well of a 6-well plate.

The solution was transferred into a clean 1,5 ml Eppendorf tube and the number of *Salmonella* colony forming units (CFU) recovered from macrophages after 24 hours of infection was determined by plating serial dilutions of *S.* Tm on agar-plates and incubation for 24 hours at 37°C.

3.7 RNA

3.7.1 RNA isolation

RNA extraction was performed by acid guanidinium thiocyanate-phenol-chloroform extraction.

After the incubation period of the current experiment, medium was removed and 1 ml of peqGOLD Tri-Fast™ reagent was added directly to the cells. The cells were lysed in the culture dish and thereafter transferred in 1,5 ml Eppendorf tubes.

0,2 ml of 100% chloroform was added on top of the cell lysate and the samples were shacked up and down before butting on ice for 5 min.

Thereafter, cells were centrifuged at 14 000 rcf for 10 min. at 4°C and the aqueous upper phase which contains the RNA was collected in clean RNase free 1,5 ml Eppendorf tubes containing 0,5 ml of ice cold 100% isopropanol.

For precipitation, the RNA was incubated at -20°C O.N.

The next day, the samples were centrifuged at 14 000 rcf for 10 min. at 4°C and the supernatant was poured away. To ensure the RNA purity, 1 ml of 75% ethanol was added directly to the pellet and the centrifugation step was repeated for another time.

The ethanol was removed, and the RNA was air-dried at RT for 5 min. Thereafter, the RNA was re-suspended in 7 µl of DEPC H2O and either stored at -20°C or prepared for reverse transcription.

It should be mentioned that the whole process was performed on ice.

3.7.2 Complementary DNA (cDNA)

For making quantitative real-time polymerase chain reaction (qRT-PCR), the RNA is converted into cDNA.

Thereby, 5 µl of the isolated RNA was transferred in clean 0,5 ml Eppendorf tubes and stored on ice.

In the meanwhile, a master mix was prepared which contains:

Master mix	
Random Hexamer Primer Mix	1 µl
dNTP-Mix 10 mM	1 µl
dH_2O	up to total volume of 10 µl
Total volume	**10 µl**

After adding 7 µl of the master mix to each sample containing the RNA (volume in total 12 µl) an incubation step for 5 min. at 65 °C using the 1000 Touch Thermal Cycler was performed. The samples were directly put on ice afterwards.

For reverse transcription, the RNA-dependent DNA polymerase M-MLV RT was used.

For this process, a second master mix was prepared which is composed as follow:

Master mix	
5x First Strand Buffer	4 µl
DTT 0.1 M	2 µl
M-MLV	0,5 µl
RNAsin 40 U/µl	0,5 µl
dH_20	1 µl
Total volume	**8 µl**

8 µl of the second master mix were added to each sample (volume in total 20 µl) and the reverse transcription was performed using the 1000 Touch Thermal Cycler:

Thermal Cycler program	
10 min.	25°C
50 min.	37°C
15 min.	70°C

After the program was finished, 0,18 ml of ddH_2O was added to the cDNA and the samples were either froze away at -20°C or prepared for qRT-PCR.

3.7.3 Quantitative real-time polymerase chain reaction (qRT-PCR):

The quantitative real-time PCR is a method that allows DNA amplification, real-time detection and measurement of the product at the same time in only one single reaction tube and is based on the detection of a fluorescent dye. Thereby, the intensity of the fluorescence emitted during qRT-PCR correlates to the amount of the amplified PCR product. Through detection of the same amount of fluorescence emission at each cycle it is possible to draw inferences about the initial amount of target template afterwards.

For interpretation of the results, the cycle threshold (CT) plays an important role, since it is a real signal that surpasses the threshold level and lies above any background fluorescence.

As fluorescence formats, SYBR-Green and Taqman-probes were used. SYBR-Green dye is a sequence-independent detection assay that emits its fluorescent signal by binding to its corresponding double-stranded DNA. The Taqman-probe is a sequence-specific probe binding assay and is based on the principle of Förster of Fluorescence Resonance Energy Transfer (FRET). Energy is thereby transferred between a fluorescence reporter and a quencher, which are attached to the 5’ end or 3’ end of the probe, respectively. During PCR, Taqman-probes anneal to an integral region of a PCR product. The 5’ exonuclease activity of the Taq-polymerase hydrolyses the probe, the reporter dye gets unquenched and thereby able to emit measurable fluorescent light.

Hence, the increase in fluorescent signal of the reporter dye is directly proportional to the rate of probe cleavage and amount of PCR product. Comparing these two methods, the main advantage of the Taqman-method lies in the higher specific to due detection of only certain PCR products.

Another parameter needed for interpretation is a so-called house-keeping-gene, such as HPRT or Gus-ß, which serves as a normalizer that regulates the variation in the amount and quality of RNA between different samples. This gene is required to maintain basic cellular functions and is expressed at relatively constant levels independent of any other influencing factors. This normalization procedure mainly serves as permission to compare expression of different genes of interest among different samples.

For qRT-PCR a master mix was prepared containing following components:

qPCR reaction mix (2,5 µl cDNA)	**SsoFast Probe**	**SsoFast Eva Green**
2x PCR Mix	6,25 µl	6,25 µl
100 µM fw Primer	0,04 µl	0,06 µl
100 µM rv Primer	0,04 µl	0,06 µl
10 µM Probe	0,25 µl	-
dH_2O	3,43 µl	3,63 µl
Total volume	**10 µl**	**10 µl**

After a centrifugation step, the master mix was transferred into separate wells of a 96-well PCR plate and 2,5 µl of the cDNA was added in duplicates to the wells. Thereafter, the plate was sealed with an optical adhesive film and the plates were briefly centrifuged. The plate was inserted into the PCR machine.

PCR program (40x)	
30 sec.	95 °C
5 sec.	95 °C
10 sec.	60 °C
∞	4 °C

When the run was finished, the data were analyzed using a standard curve as reference. Based on the standard curve it was possible to calculate the relative concentrations of the RNA of the sample.

3.7.4 Primer and Probes for qRT-PCR

All primer and probes were ordered from microsynth. Before storage at -20°C, primers and probes were diluted in buffer containing 1 x TE, 10 mM Tris (pH 8), 1 mM EDTA.

Primer/Probe	Sequence (5'-3')	Annealing Temp. (°C)
mu_Ldha_fw	GCTCCCCAGAACAAGATTACAG	60°C
mu_Ldha_rv	TCGCCCTTGAGTTTGTCTTC	60°C
mu_Aco2_fw	GCCCTTTACCCCTGACTTG	60°C
mu_Aco2_rv	GTCCCATGTCCTCATAGCTTG	60°C
mu_Idh2_fw	GAAGAGGATCAAGGTGGAGAAG	60°C
mu_Idh2_rv	GGAAGCCCAAGGTCAAAATAC	60°C
mu_Sdhd_fw	TCTCTTAAAGCTGGGCGTTC	60°C
mu_Sdhd_rv	AGGTGAATGTGCTGGGTAC	60°C
mu_IL-6_fw	TGTTCTCTGGGAAATCGT	60°C
mu_IL-6_rv	AAGTGCATCATCGTTGTTCATACA	60°C
mu_IL-6_Probe	ATGAGAAAAGAGTTGTGCAATGGCAATTCTG	60°C
mu_IL-10_fw	CCAGAGCCACATGCTCCTAGA	60°C
mu_IL-10_rv	TGGTCCTTTGTTTGAAAGAAAGTCT	60°C
mu_IL-10_Probe	TGCGGACTGCCTTCAGCCAGG	60°C
mu_TNF-α_fw	TTCTATGGCCCAGACCCTCA	60°C
mu_TNF-α_rv	TTGCTACGACGTGGGCTACA	60°C
mu_TNF-α_Probe	CTCAGATCATCTTCTCAAAATTCGAGTGAC	60°C
mu_iNOS_fw	CAGCTGGGCTGTAGAAACCTT	60°C
mu_iNOS_rv	CATTGGAAGTGAAGCGTTTCG	60°C
mu_iNOS_Probe	CGGGCAGCCTGTGAGACCTTTGA	60°C
mu_HPRT_fw	GACCGGTCGCGTCATGC	60°C
mu_HPRT_rv	TCATAACCTCGTTCATCATCGC	60°C
mu_HPRT_Probe	TGCTGGTGAAAAGGACCCCTCGAA	60°C
mu_Gusß_fw	CTCATCTGGAATTTCGCCGA	60°C
mu_Gusß_rv	GGCGAGTGAAGATCCCCTTC	60°C
mu_Gusß_Probe	CGAACCAGTCACCGCTGAGAGTAATCG	60°C

3.8 Proteins

3.8.1 Nitrite measurement by Griess reaction:

The Griess reaction allows determining nitrite concentrations in cellular supernatants photometrically. Nitrite itself is a stable product of nitric oxide and thus a measure of NOS activity. For absolute values, a standard curve of sodium nitrite ($NaNO_2$) solution of known concentration is included.

After the treatment of RAW264.7 cells and the incubation period of the experiment, the supernatant was removed from the cells and collected in separate clean 1,5 ml Eppendorf tubes. To clear the supernatant from residual cells, a centrifugation step at

300 g for 10 min. was performed. The upper phase was transferred in clean 1,5 ml Eppendorf tubes and the rest was discarded.

To determine the nitrite concentration, 50 µl of the supernatant were transferred into separate wells of a 96-well microtiter plate. For determining the nitrite concentration of the test sample, it was compared to a standard curve. The standard was prepared using 1 mM $NaNO_2$ solution and ranged from 0.0 µg/ml to 50 µg/ml:

Standard concentration	$NaNO_2$ solution	DMEM
0 µg/ml	0 µl	1000 µl
1 µg/ml	1 µl	999 µl
5 µg/ml	5 µl	995 µl
10 µg/ml	10 µl	990 µl
25 µg/ml	25 µl	975 µl
50 µg/ml	50 µl	950 µl

50 µl of each standard solution were transferred into separated wells of the 96-well microtiter plate and 100 µl of the Griess-Ilosvay's nitrite reagent were supplied directly to each well, containing the test samples and the standard.

After 15 min. of incubation at RT protected from light, the extinction was measured at OD_{546} nm using a microplate reader (Tecan).

3.8.2 ELISA (IL-6 and IL-10)

For the IL-6 ELISA test, the mouse IL-6 ELISA Set from BD Biosciences was used. Therefore, 0,48 ml of DPBS was transferred into a sterile 1,5 ml Eppendorf tube and 20 µl of the capture antibody was supplied (1:250). After mixing the solution, 50 µl of the diluted capture antibody were added to each well of an ELISA plate and incubated O.N. at 4°C. To avoid contamination, the plate was covered using an adhesive strip.

The test samples which were stored at -80°C were dawn slowly on ice. In the meantime, the Assay Diluent was prepared by mixing 100 ml of DPBS with 10 ml of 10% FCS. Additionally, the Washing Buffer was prepared. Thereby, 500 ml of DBPS were mixed with 0,05 % Tween-20.

After the incubation period, the wells were aspired and washed 3 x with 0,3 ml Wash Buffer/well. After the last wash, the plate was inverted and blotted on absorbent paper

to remove residual buffer. Thereafter, plates were blocked by adding 0,3 ml of the Assay Diluent to each separate well and incubating it for 1 hour at RT.

During this incubation period, the standard was prepared as follow:

A 1000 pg/ml standard was prepared from the stock solution. Thereafter, 0,25 ml of Assay Diluent was added in 6 x 1,5 ml Eppendorf tubes and serial dilutions were performed by adding 0,25 ml of each standard to the next tube. As zero standard (0 pg/ml), Assay Diluent was used.

Standard
1000 pg/ml
500 pg/ml
250 pg/ml
125 pg/ml
62,5 pg/ml
31,3 pg/ml
15,6 pg/ml

Additionally, the test samples were diluted 1:100 using the Assay Diluent.

After the incubation period and the washing step, the samples and standards were pipetted into appropriated wells and another incubation step for 2 hours at RT was performed.

To remove the whole test samples and standard to each plate, the washing step was performed 5 x instead of 3 x.

The Working Detector was prepared as follow:

50 µl of the Working Detector (Detection Ab and SAv-HRP) was added to each well and incubated for another hour at RT.

After the aspiration and washing step with 7 washes in total, 50 µl of the Substrate Solution was added to each well and incubated for 30 min. at RT protected from light.

25 µl of the stop solution (H_2SO_4) was added to each well and the absorbance was red at 450 nm within 30 min. of stopping reaction.

The IL-10 ELISA test was performed using the mouse IL-10 ELISA Set from BD Bioscience. All steps were performed accordingly to the IL-6 ELISA test with the only difference, that the test samples were not diluted.

3.8.3 ELISA (TNF-α)

The TNF-α ELISA test was performed using the mouse TNF-α set from R&D Systems.

The capture antibody was diluted in DPBS (1:125). After mixing well, the 96-well microplate was coated with 50 µl per well of the diluted capture antibody. The plate was incubated overnight at RT.

The test samples which were stored at -80°C, were dawn slowly on ice. In the meantime, the Reagent Diluent was prepared by mixing 100 ml of DPBS with 1 g of 1% BSA. Additionally, the Washing Buffer was prepared. Thereby, 500 ml of DBPS were mixed with 0,05 % Tween-20.

After the incubation period of 24 hours, each well was aspired and washed 3 x using 0,3 ml of the Wash Buffer. After the last wash, the plate was inverted and blotted against a clean paper towel to remove any remaining Wash Buffer.

Thereafter, plates were blocked by adding 0,3 ml of Reagent Diluent to each well and incubating it for 1 hour at RT.

During this incubation period, the standard was prepared as follow:

A 2000 pg/ml standard was prepared from the stock solution. Thereafter, 0,25 ml of Assay Diluent was added in 6 x 1,5 ml Eppendorf tubes and serial dilutions were performed by adding 0,25 ml of each standard to the next tube. As zero standard (0 pg/ml), Assay Diluent was used.

Standard
2000 pg/ml
1000 pg/ml
500 pg/ml
250 pg/ml
125 pg/ml
62,5 pg/ml
31,3 pg/ml

Additionally, the test samples were diluted 1:100 in Reagent Diluent.

After the blocking step, the plates were washed again 3 x like mentioned above and 50 µl of the test samples and standards were added to each appropriate well and incubated for another 2 hours at RT.

To remove the whole test samples and standard to each plate, the washing step was repeated for another 5 x.

Thereafter 50 µl of the Detection Antibody, which was diluted in Reagent Diluent, was added to each well. The plate was covered with a new adhesive strip and incubated at RT for 2 h.

After the washing step, 50 µl of the working dilution of Streptavidin-HRP (1:40) was added to each well and incubated for 20 min. at RT protected from light.

The aspiration and washing step was repeated 5 x and immediately, 50 µl of the Substrate solution (1:1 mixture of Color Reagent A (H_2O_2) and Color Reagent B (Tetramethylbenzidine) was added to each well. The plate was incubated for 20 min. protected from light.

Subsequently, 25 µl of the stop solution (H_2SO_4) were added to each well and mixed well. The optical density was determined immediately using a microplate reader set to 450 nm.

3.8.4 Western Blot

For detecting and analyzing of proteins, western blotting is a well-established method and is based on the interaction of specific antibodies with immobilized proteins on a membrane that are detected using a secondary antibody.

3.8.4.1 Protein extraction

After the incubation period of the experiment, the medium was removed from the cells and they were washed 3 x with 1 ml of DPBS. Thereafter, 1 ml of DPBS was added directly to the cells and they were harvested by scraping it into a 1,5 ml Eppendorf tube using a cell scraper.

A centrifugation step at 200 g for 10 min. at 4°C was performed. Afterwards, the supernatant was removed, and the pellet was processed for cytoplasmic protein extraction.

For this method, cytoplasmic lysis buffer (25 mM Tris–HCl [pH 7.4], 40 mM KCl, and 1% Triton X-100) and protease inhibitor (1 µg/ml aprotinin and 1 µg/ml leupeptin) were mixed (1:100) in a new sterile 1,5 ml Eppendorf tube.

Cytoplasmic lysis buffer	
Tris base	3 g
Potassium chloride	2,98 g
Triton X 100	10 ml
HCl	to pH 7.4
H_2O	1000 ml
aprotinin	1 µg/ml
leupeptin	1 µg/ml

The pellet was thereafter resuspended in 20-40 µl of the solution by pipetting it up and down. Thereafter, the samples war incubated for 40 min. on ice.

The lysis solution was then centrifuged at 13000 rpm for 10 min. at 4°C. Thereafter, the supernatant containing the cytoplasmic protein was collected in a new 1,5 ml Eppendorf tube and stored at -80°C.

3.8.4.2 Protein quantification (BCA measurement)

The protein concentration in solution was measured using the colorimetric BCA protein assay kit.

For the measurement, 0,2 ml of the BCA solution (1:50) was added to each well of a 96-well microplate.

Thereafter, the standard with Bovine Serum Albumin (BSA) protein was prepared by diluting it with DPBS. The standard ranged from 0 µg/ml to 1000 µg/ml. Additionally, the protein samples were diluted 1:40 in DPBS.

Standard
0 µg/ml
31,25 µg/ml
62,5 µg/ml
125 µg/ml
250 µg/ml
500 µg/ml
1000 µg/ml

25 µl of the standards and samples were transferred in duplicates to each appropriate well of the 96-well microplate. The plate was incubated at RT for 30 min. Thereafter, the protein concentration was measured at 562 nm using a microplate reader (Tecan).

3.8.4.3 Sample preparation

20 µl of a 30 µg/ml of total protein were required for the run on a 10% SDS-polyacrylamide gel. Therefore, the proteins were diluted in DPBS to reach the required concentration of 30 µg/ml. Additionally, 5 µl of the 5x protein sample buffer for SDS-PAGE (Laemmli buffer) was added to each sample.

To determine the protein levels of ferritin, samples were afterwards heated at 95°C for 5 min.

5x Protein sample buffer (Laemmli buffer)	
Tris-HCl pH 6.8	1 ml
SDS (15%)	1.5 g
ß-Mercaptoethanol (25%)	2.5 ml
Glycerol (50%)	5 ml
Bromphenol blue (0.025%)	0.0025 g
dH_2O	10 ml

3.8.4.4 Sodium dodecyl sulfate polyacrylamide gel electrophoresis (SDS-PAGE) of proteins

The samples were fractioned by electrophoresis and proteins were separated corresponding to their molecular weight.

In this process, the anionic detergent SDS interacts and denatures the proteins. This leads to a negatively charged protein which will move toward the positive pole when placed in an electric field.

The polyacrylamide gel is responsible for the separation of the proteins in the electric field. Smaller proteins can pass the gel more easily and faster than larger one. The gel is made of acrylamide and N, N-methylene bisacrylamide co-monomers. Ammonium persulfate (APS) is important for the polymerization and tetramethylethylenediamine (TEMED) for the catalysation of a meshwork of pores.

For SDS-PAGE, clean glass plates, plastic backings and spacers were assembled according to the manufactures instructions.

Thereafter, the acrylamide-bisacrylamide-mix as well as the Tris-HCl pH 8.8 must be prepared, since these components are needed for the preparation of the gel:

Acrylamide-Bisacrylamide Mix 30%	
Acrylamide	29.2 g
Bisacrylamide	0.8 g
dH_2O	100 ml

1.5 M Tris-HCl pH 8.8	
Tris	36,4 g
HCl	to pH 8.8
dH_2O	200 ml

Thereafter, the separation gel was performed as followed:

Gel concentration (for 2 gels)	**10% (15-120 kDa)**
30% Acrylamide-Bisacrylamide-Mix	3.3 ml
1.5 M Tris-HCl pH 8.8	2.5 ml
ddH_20	4.2 ml
20% SDS	50 µl
TEMED	5 µl
10% APS	50 µl

TEMED and APS were added at the end of the preparation into the solution to avoid stacking of the gel. Thereafter, the solution was quickly filled into the gaps between the glass plate and the separating gel was covered with isopropanol to remove bubbles and to prevent drying-out. After 20 min. the polymerization was completed, and the isopropanol was removed from the top of the gel using filter papers.

The 4% stacking gel was prepared as followed:

Gel concentration (for 2 gels)	**4%**
30% Acrylamide-Bisacrylamide-Mix	0,65 ml
0.5 M Tris-HCl pH 6.8	1.25 ml
ddH_20	3.05 ml
20% SDS	25 µl
TEMED	5 µl
10% APS	25 µl

The gel was added at the surface of the separation gel and a clean plastic comb was inserted. After another 20 min. the comb was removed, and the gels were assembled into an electrophoresis camber. Its reservoir was filled with 1 x SDS buffer (pH 8.3), which was prepared in advance.

Electrophoresis buffer (SDS buffer)	
Glycine	15 g
Tris	72 g
SDS	5 g
dH2O	1000 ml

The protein samples were briefly centrifuged and 15 µl were loaded into the wells using a micro tip. The outermost slot was loaded with 4 µl of a molecular weight marker.

Thereafter, the electrophoresis apparatus was attached to an electric power and the blot was run for 30 min. at 100 V const.

When the samples reached the separation gel, currency was increased to 180-200 Volt and the gel was run for another 1 ½ hour.

Once the run was finished, the glass plates were taken out and the stacking gel was removed.

3.8.4.5 Protein transfer (Western blotting)

Thereafter, the proteins needed to be blotted from the gel to a transport membrane, for making the detection of the proteins with specific antibodies possible.

For this process, the PVDF transfer membrane was used. One piece of the membrane and 4 pieces of 3 mm Whatman blotting paper were catted in the appropriate size of the gel (9 x 7 cm).

To increase the binding of the separated protein to the membrane, the membrane was wet for 10 sec. in 100% methanol, 10 min. in dH_2O and 10 min. in blotting buffer.

Western transfer buffer (blotting buffer)	
Tris	17,4 g
Glycine	87 g
Methanol	600 ml
SDS	3 g
dH20	3000 ml

Next, the electrophoretic transfer could be started. Therefore, the blotting device was set up according to the manufactures instructions. Onto the black wing of the blotting cassette a pre-wetted sponge (in blotting buffer) was added. This was then layered in the order:

First sponge	1 x
Whatman paper (pre-wet in blotting buffer)	2 x
Gel	1 x
Whatman paper (pre-wet in blotting buffer)	2 x
Second sponge	1 x

Thereafter, the module was put into the western blotting apparatus, where the black side of the apparatus headed to the black wing of the sandwich and the whole sandwich is than submerged in transfer buffer together with a block of ice.

An electric field at 100 V at 4°C for 1 ½ hours was applied so that the negative charged proteins travel towards the positively charged electrode, being stopped and bound to the membrane.

3.8.4.6 Antibody probing

After the blotting process was finished, the membrane was placed in 100 ml of 6% milk containing blocking solution for at least 1 hour on a rocking platform at RT.

The blocking solution was prepared as followed:

10 x TBS	
NaCl 5M	300 ml
Tris/HCl 1M	100 ml
dH_2O	1000 ml

Blocking buffer	
TBS	166 ml
Skim milk powder 3%	5 g

Thereafter, the membrane was rinsed in Tris-buffered saline and 0,1 % Tween-20 (T-TBS) and incubated with the primary antibody O.N. at 4°C under agitation.

After the incubation period, the membrane was washed 3 x with T-TBS to remove residual primary antibody. Subsequently, the secondary antibody, which was carrying a horseradish peroxidase (HRP) was added and incubated for at least 1 hour.

Membranes were thereafter again washed 3 x with T-TBS for 10 min.

3.8.4.7 Antibodies for Western Blot

All antibodies were diluted in T-TBS according to their dilution factor:

Antibody	Dilution	Molecular mass of target protein	Company
Actin mAb	1: 500	~ 42 kDa	Sigma
Ferritin mAb	1:400	~ 22 kDa	Sigma
Transferrin mAb	1:1000	~ 100kDa	Invitrogen
p4E-BP1 Rabbit mAb	1:1000	15-20 kDa	Cellsignal
p70 S6K mAb	1:1000	~ 85 kDa	R&D systems

3.8.4.8 Imaging

During this process, the antibody-protein complex was visualized using the SuperSignal West Dura Extended Duration Substrate which detects the chemiluminescence signal emanated by the HPR of the secondary antibody.

Equal amounts of the Peroxide solution and the Luminol/Enhancer solution were mixed and added to the membrane and incubated for 5 min. Thereafter, a chemiluminescence detection device (BioRad) captured and converted the detected light into an electric signal which was digitalized from image and following analysis.

3.8.5 Metabolite measurement

3.8.5.1 Lactate measurement

The supernatant of treated RAW 264.7 cells was removed after an incubation period for 24 hours at 37°C.

Lactate concentrations were determined using the lactate colorimetric/fluorometric assay kit purchased from Biovision.

Prior to the lactate measurement, all test samples were diluted in DPBS (1:30). 10 µl of the samples were thereafter transferred into separate wells of a 96-well microplate. The volume was adjusted to 50 µl/well with the Lactate Assay Buffer.

The standard curve was prepared by diluting the Lactate Standard to 1 nmol/µl by adding 10 µl of the 100 nmol/µl Standard to 0,99 ml of Lactate Assay Buffer. Thereafter, 0, 2, 4, 6, 8 and 10 µl were added into a series of wells. The volume was adjusted to 50 µl using the Lactate Assay Buffer to generate 0, 2, 4, 6, 8 and 10 nmol/well of the standard.

After preparation of the standard, for each well, a total of 50 µl of Reaction Mix was prepared using the following components:

Reaction mix/well	
Lactate Assay Buffer	46 µl
Lactate Enzyme Mix	2 µl
Probe	2 µl

50 µl of the Reaction mix was added to each well and the plate was incubated for 30 min. at RT protected from light. Absorbance was measured at OD_{570} nm in a microplate reader.

3.8.5.2 Pyruvate measurement

The supernatant of treated RAW 264.7 cells was removed after an incubation period for 24 hours at 37°C.

Pyruvate concentrations were determined using the pyruvate colorimetric/fluorometric assay kit purchased from Biovision.

Therefore, 15 µl of the samples were transferred into separate wells of a 96-well microplate and the volume was adjusted to 50 µl/well with the Pyruvate Assay Buffer.

The standard curve was prepared by diluting the Pyruvate Standard to 1 nmol/µl by adding 10 µl of the 100 nmol/µl Standard to 0,99 ml of Pyruvate Assay Buffer. Thereafter, 0, 2, 4, 6, 8 and 10 µl were added into a series of wells. The volume was adjusted to 50 µl using the Pyruvate Assay Buffer to generate 0, 2, 4, 6, 8 and 10 nmol/well of the standard.

After preparation of the standard, for each well, a total of 50 µl of Reaction Mix was prepared using the following components:

Reaction mix/well	
Pyruvate Assay Buffer	46 µl
Pyruvate Enzyme Mix	2 µl
Enzyme Mix	2 µl

50 µl of the Reaction mix was added to each well and the plate was incubated for 30 min. at RT protected from light. Absorbance was measured at OD_{570} nm in a microplate reader.

3.8.5.3 Isocitrate measurement

The supernatant of treated RAW 264.7 cells was removed after an incubation period for 24 hours at 37°C.

Isocitrate concentrations were determined using the isocitrate colorimetric assay kit purchased from Biovision.

Therefore, 50 µl of the test samples were transferred into separate wells of a 96-well microplate.

The standard curve was prepared by diluting the Isocitrate Standard to 2 nmol/µl by adding 20 µl of the Standard to 0,98 ml of dH_2O. Thereafter, 0, 2, 4, 6, 8 and 10 µl were added into a series of wells. The volume was adjusted to 50 µl using the Isocitrate Assay Buffer to generate 0, 4, 8, 12, 16 and 20 nmol/well of the standard.

After preparation of the standard, for each well, a total of 50 µl of Reaction Mix was prepared using the following components:

Reaction mix/well	
Isocitrate Assay Buffer	46 µl
Isocitrate Enzyme Mix	2 µl
Substrate Mix	2 µl

50 µl of the Reaction mix was added to each well and the plate was incubated for 30 min. at 37°C protected from light. Absorbance was measured at OD_{450} nm in a microplate reader.

3.8.5.4 Free fatty acids measurement

The supernatant of treated RAW 264.7 cells was removed after an incubation period for 24 hours at 37°C.

Free fatty acid concentrations were determined using the free fatty acid quantification colorimetric/fluorometric kit purchased from Biovision.

Therefore, 25 µl of the test samples were transferred into separate wells of a 96-well microplate and the volume was adjusted to 50 µl/well using the Fatty Acid Assay Buffer.

The standard curve was prepared by adding 0, 2, 4, 6, 8 and 10 µl of the Palmitic Standard into a series of wells. The volume was adjusted to 50 µl using the Fatty Acid Assay Buffer to generate 0, 2, 4, 6, 8 and 10 nmol/well of the standard.

After preparation of the standard for each well, 2 µl of Acyl-CoA Synthesis (ACS) Reagent were added into all the standard and sample wells. The reaction was thereafter incubated at 37°C for 30 min.

In the meantime, a total of 50 µl of Reaction Mix was prepared using the following components:

Reaction mix/well	
Fatty Acid Assay Buffer	44 µl
Fatty Acid Probe	2 µl
Enzyme Mix	2 µl
Enhancer	2 µl

50 µl of the Reaction mix was added to each well and the plate was incubated for 30 min. at 37°C protected from light. Absorbance was measured at OD_{570} nm in a microplate reader

3.8.5.5 Metabolomics

All materials were obtained from Sigma–Aldrich (Seelze, Germany) unless stated otherwise. Acetonitrile was purchased from VWR International (Radnor, PE, USA). Water was obtained from a Milli-Q water purification system equipped with LC-pak polisher (Millipore, USA). All chemicals and solvents were of analytical grade or higher

purity. Metabolomics amino acid mix standard containing isotopically labeled amino acids was purchased from Cambridge Isotope Laboratories (Tewksbury, USA).

All samples were extracted using a solution of acetonitrile containing metabolomics amino acid mix standard at a final concentration of 2,6 ug/ml. Next, the supernatant was filtered applying 12 psi pressure (Waters positive pressure-96 processor, Mildford, MA), through a Sirocco protein removal plate (Waters Corporation, Milford, MA).

All samples were analyzed by ultra-high-performance liquid chromatography (UHPLC) (Agilent 1290, Agilent Technologies) coupled to a Q-TOF mass spectrometer (MS) (Triple TOF 5600+, Sciex, Foster City, CA). The chromatographic separation was based on hydrophilic interaction liquid chromatography (HILIC) and performed using an Acquity BEH amide, 100x2.1 mm column (Waters Corporation, Milford, MA).

Separation was achieved using as mobile phase A acetonitrile + 0.1% formic acid and as mobile phase B water + 0.1% formic acid. The injection volume was 5 µL and the flow rate 0.6 ml/min. The following linear gradient was used: 0 min 95% A, 1 min 95% A; 4 min 30% A; 5 min 30% A; 5.1 min 95% A; 8 min 95% A.

The mass spectrometer was operated in full scan mode in the mass range from 50 to1000 m/z and with an accumulation time of 250 ms. In ESI+ mode the source temperature was set at 700°C, the declustering potential at 30 V, the collision energy at 6 V, the ion spray voltage at 5120 V, the curtain gas at 25 psi, the ion source gas 1 and 2 at 60 psi. In ESI- mode the source temperature was set at 650°C, the declustering potential at -45 V, the collision energy at -6 V, the ion spray voltage at -3800 V, the curtain gas 25 psi, the ion source gas 1 and 2 at 30 psi. The instrument was mass calibrated by automatic calibration infusing the Sciex Positive Calibration Solution (part no. 4460131, Sciex, Foster City, CA) for positive mode and Sciex Negative Calibration Solution (part no. 4460134, Sciex, Forster City, Ca) for negative mode after every two sample injections.

Metabolites were identified by verifying retention time, accurate mass, and tandem mass spectrometry against our in-house and/or online databases, including HMDB and METLIN. Only metabolites identified in all technical replicates were considered. The identified metabolites were integrated using MultiQuant 3.0 (Sciex, Foster City, CA). For data anlysis, MetaboAnalyst online tool was used.

3.9 Fluorescence-activated cell sorting (FACS)

After treatment and the current incubation period of RAW264.7 cells, the supernatant was discard from the cells and a washing step with 1 ml DPBS was performed. To remove the whole supernatant from the cells, the washing step was repeated for another 2 x.

1 ml of DPBS was added on top of the cells and they were scraped into 1,5 ml clean Eppendorf tubes. A centrifugation step at 4500 rpm for 10 sec. was performed.

In the meantime, 1 ml of the FACS-Buffer which was already prepared in advance (see table below) was mixed with 1 µl of the fluorescence dye 4',6-Diamidin-2-phenylindol (DAPI, 1:10000).

After the centrifugation, the supernatant was discarded from the samples and 0,3 ml of the FACS-Buffer-DAPI solution was added on top of the pellet.

The cells were resuspended in the solution and filtered into FACS-tubes.

The flow was run on the Gallios™ Flow cytometer. For analysis, FlowJo software was used.

FACS buffer	
DPBS	500 ml
FCS 1%	5 ml
EDTA (0.25M)	5 ml (1M)

3.10 Phagocytose assay staining of RAW264.7

Cover slips were immersed into 100% EtOH and flamed for some sec. Thereafter they were added to separate wells of a 6-well plate.

1 ml of complete DMEM was added into each well of the 6-well plate and 6 x 10^5 RAW264.7 cells were added and incubated at 37°C O.N.

The fixation solution was prepared as follow and dissolved slowly O.N. at RT:

Fixation solution	
Paraformaldehyde	1 g
Sucrose	1 g
H_2O	12,5 ml
Na-phosphate buffer	12,5 ml

The next day, the medium was removed from the cells and they were washed 3 x using DPBS prior to incubating it in DMEM without antibiotics.

The cells were infected with green fluorescent *S*. Tm wt for either 1, 2 3 or 4 hours at 37°C. Thereafter, cells were washed with DPBS containing 50 µM of gentamycin. Subsequently, 1 ml of DPBS was added to the cells to avoid drying it out.

A petri dish was covered with parafilm and the cover slips were transferred from the 6-well plate to the petri dish. Immediately they were covered with DPBS.

The PBS was removed, and the fixation solution was added to the cover slips for 20 min.

In the meantime, the washing solution was prepared as follow:

Washing solution	
0,2% BSA	0,1 g
Triton	0,1 ml
Horse serum	2,5 ml
DPBS	To 50 ml

After removing the fixation solution, the washing solution was added to the cover slips for 30 min.

During this incubation period, phalloidin was diluted in washing solution (1:2000).

After the incubation step, the diluted phalloidin was added to the cover slips and they were incubated for 1 hour at RT protected from light.

Cover slips were washed 3 x with DPBS for 10 min. and afterwards transferred to the microscope slide.

DAPI was directly added to the cover slips and one drop of immersions oil was supplied.

Phagocytosis of RAW264.7 cells was determined using the fluorescence microscope.

3.11 Data analysis

Statistical analysis was carried out using Graph Pad Software. One-way analysis of variance (ANOVA) was used for comparing more groups and Bonferroni's Multiple

Comparison test as correction. The significance level was set at * = p< 0.05; ** = p< 0,01; ***= p< 0,001.

Additionally, Student's t-test was used for comparing two different groups. The significance level was set at * = p< 0.05; ** = p< 0,01; ***= p< 0,001.

4. Results

4.1. Pilot experiment: Toxicity of different components used during experiments on RAW264.7 cells

Since we were interested in the influence of the mTOR inhibitor rapamycin during infections of RAW264.7 cells with *Salmonella enterica* serovar Typhimurium in high- or low iron conditions, we first investigated the influence of the components on the viability of RAW264.7 cells. This is important to ensure that the shown effects during the experiments are not the results of reduced viability of macrophages due to a toxic effect of the indicated dosages of $FeCl_3$, DFP, rapamycin or gentamycin on the cells.

Therefore, we checked the amount of living cells using FACS, after treatment of RAW264.7 cells with either rapamycin (200 nM), different concentrations of $FeCl_3$ or DFP (10 µM, 25 µM, 50 µM) as well as different concentrations of gentamycin (5 µM, 50 µM, 100 µM) prior and after infecting it with *Salmonella enterica* serovar Typhimurium.

The results show, that none of these treatments significantly affects the cell viability and therefore warrant that all shown effects during the following experiments are not influenced due to toxicity of the different components used **(Fig.1A, 1B, 1C, 1D).**

Fig. 1A

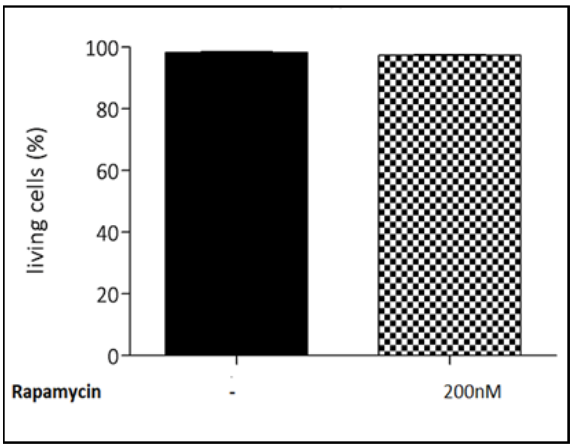

Fig. 1B

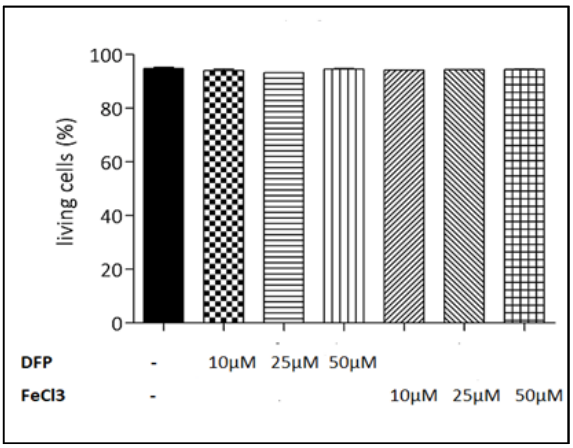

Fig. 1C

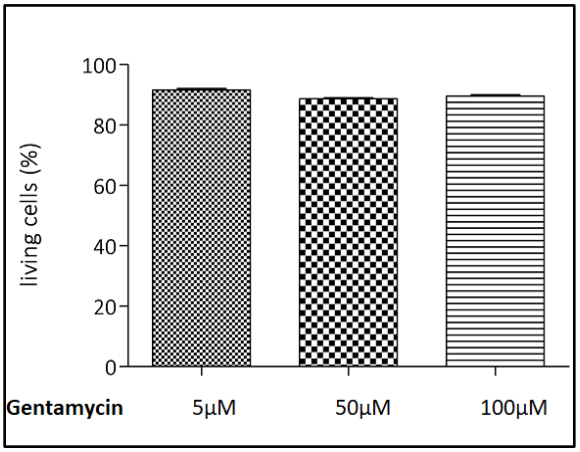

Fig. 1D

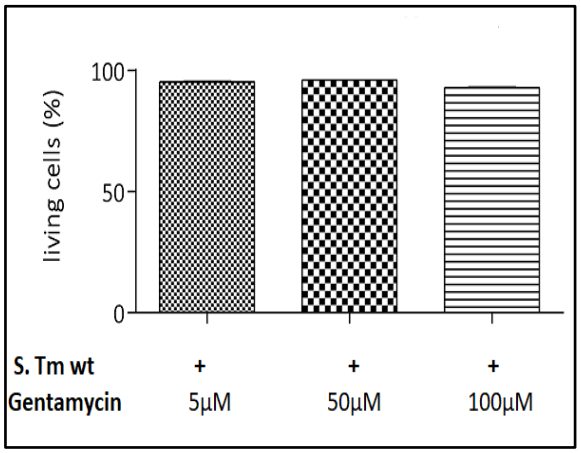

Figure 1 Viability of RAW264.7 cells was determined using FACS after treating cells **(A)** with 200 nM of rapamycin for 1 h and 20 nM for another 23h, **(B)** with different concentrations of the iron chelator DFP or the iron chloride for 24h **(C)** with different concentrations of gentamycin for 24 h **(D)** or after infecting cells with *Salmonella enterica* serovar Typhimurium for 1 h (MOI 10) and incubating it with gentamycin for 24h. Experiments were performed in triplicates. Statistical analysis was performed using the Student's t-test (Fig.1A) and One-way ANOVA with Bonferroni correction (Fig.1B, 1C, 1D). The significance level was set at $p < 0.05$.

4.2 Iron positively affects extra- and intracellular bacterial growth

The first aim was to investigate the influence of exogenous iron on extracellular as well as intracellular pathogen growth and proliferation. Therefore, to see whether the limitation of free exogenous iron as well as the supplementation of exogenous iron alters the growth of *Salmonella*, we supplied either the same concentrations (50 µM) of the iron-chelating agent deferiprone (DFP), able to bind iron with high affinity, or the iron source ferric chloride, to the LB-medium and incubated the samples at 37°C. At the indicated time points, the OD_{600} nm was determined using a photometer. When compared to the control group, we found on one hand an increased growth of *Salmonella* in presence of high iron conditions within the first hour of bacterial growth. However, the increase of bacterial proliferation observed at the beginning, decreases over time.

On the other hand, limitation of free exogenous iron by DFP negatively affects the bacterial growth when compared to the control group. This decrease in bacterial growth can be observed also at later time points of the experiment and indicates the necessity of the metal for bacterial growth **(Fig. 2A).**

Additionally, to see whether intramacrophage iron availability affects the survival of *Salmonella* within macrophages, we tested the impact of either iron supplementation or deprivation on bacterial viability. Therefore, we pre-treated RAW264.7 macrophages with either ferric chloride (50 µM) or deferiprone (50 µM) for 6 hours. Thereafter, the cells were infected for 1 hour with *Salmonella* at a multiplicity of infection of 10 (MOI of 10) and incubated for another 23 hours in the presence of gentamycin (50 µM), as well as $FeCl_3$ and DFP, followed by subsequent washing and lysing of the cells using Na-deoxycolate. The number of *Salmonella* colony forming units (CFU) recovered from macrophages after 24 hours of infection was determined by plating *Salmonella* on agar-plates and incubation for 24 hours at 37 °C.

The results show that the delivery of iron, provided as ferric chloride, resulted in an increase in *Salmonella* numbers within RAW264.7 macrophages. In contrast, deferiprone (DFP), an iron-chelating agent able to scavenge intracellular and extracellular iron, reduced intramacrophage *Salmonella* survival significantly. These results indicate that the intracellular replication of *Salmonella* is strongly dependent on iron **(Fig. 2B).**

Further, we were interested in the bacterial growth using a *Salmonella* mutant strain, deficient in enterobactin synthesis, SitABCD- and Feo-mediated iron uptake. As in the previous experiment, 50 µM of $FeCl_3$ or 50 µM of DFP were added directly to the LB-medium and the OD_{600} nm was determined using a photometer. The results show a decreased bacterial growth in the iron-rich, as well as iron-deprived environments when compared to the control group **(Fig. 2C)**. Additionally, intramacrophage survival of the mutant strain was not influenced by iron availability or limitation **(Fig. 2D**), since no differences in bacterial load can be observed after treatment of macrophages with $FeCl_3$/DFP or in controls. In summary, *Salmonella* uses iron for strong bacterial growth as well as intramacrophage survival.

Fig. 2A

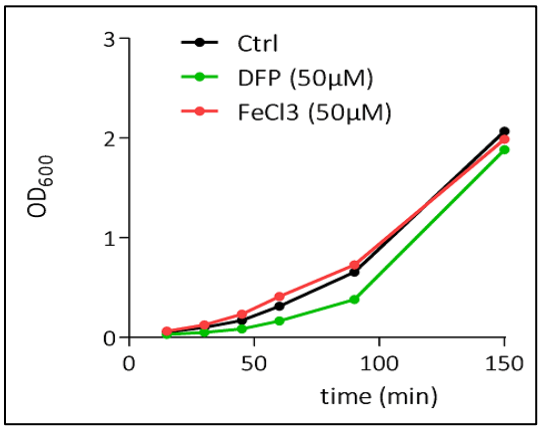

Fig. 2B

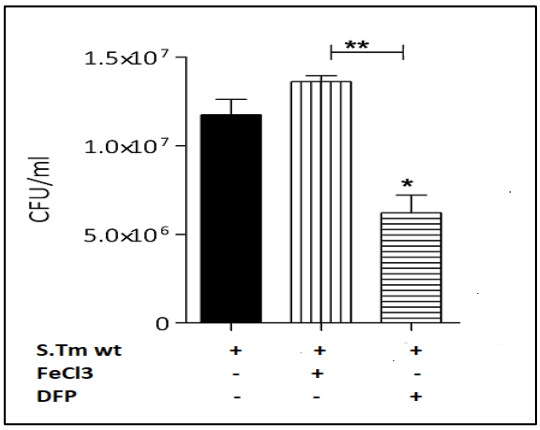

Fig. 2C

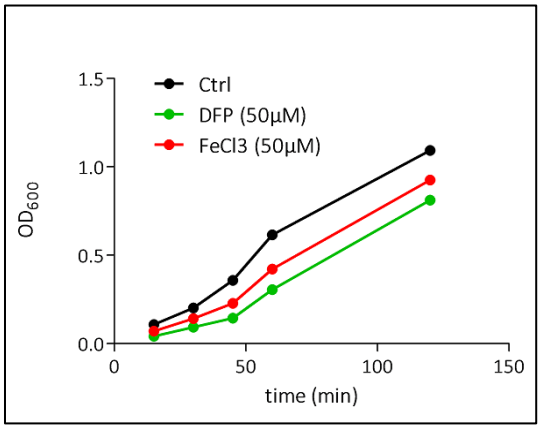

Fig. 2D

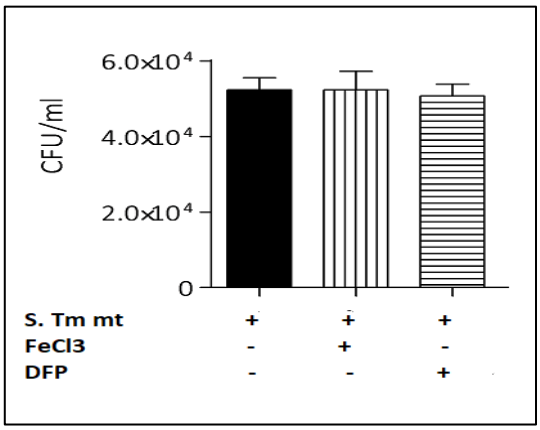

Figure 2 Iron perturbations influence bacterial growth **(A)** Impact of exogenous iron perturbations on bacterial growth was determined by either adding 50 µM of $FeCl_3$ or 50 µM of DFP directly to the nutrient-rich LB-medium. The same amount of *Salmonella* was added to the medium and the OD_{600} was measured at different time points using a photometer. **(B)** Impact of exogenous iron perturbations on intramacrophage survival of *Salmonella* was determined by gentamycin protection assay. Therefore, RAW264.7 macrophages were either treated with 50 µM of $FeCl_3$ or 50 µM of DFP for 6 h. Thereafter, cells were infected with *Salmonella* at a MOI of 10 for 1. After another incubation period for 23 h in presence of gentamycin and $FeCl_3$/DFP, cells were subsequently lysed using natrium-deoxicolate and CFU/ml were determined. **(C)** Impact of exogenous iron perturbations on bacterial growth was determined like explained in A, however, instead of *S*. Tm wt, the *S*. Tm mt strain was used. **(D)** CFU/ml was determined like explained in C, however, instead of *S*. Tm wt, the *S*. Tm mt strain was used. Representative data from three independent experiments performed in triplicates are shown. Statistical analysis was performed using One-way ANOVA with Bonferroni correction. The significance level was set at $p < 0.05$. Unless otherwise noted, * refers to the control group (shown in black).

4.3 Exogenous iron perturbations negatively affect macrophages immune functions:

To study whether the increase in bacterial load after iron supplementation can be referred to modulations of innate immune functions we investigated IL-6, TNF-α, iNOS and IL-10 expression in RAW264.7 macrophages using qRT-PCR as well as the formation of the products in macrophage culture supernatants using the ELISA kits and the Griess test.

Therefore, we pre-treated RAW264.7 macrophages with either ferric chloride (50 µM) or deferiprone (50 µM) for 6 hours and infected the cells afterwards for 1 hour with *Salmonella* wt at a MOI of 10. Extracellular bacteria were removed, and cells were incubated for another 23 hours in the presence of gentamycin (50 µM) as well as $FeCl_3$ and DFP.

As a control, macrophages were also stimulated with heat-inactivated *Salmonella*, added at the same number as viable bacteria. This is important to investigate the influence of bacterial replication on macrophages immune response after an infection.

The results show that the mRNA levels, as well as the protein levels of the pro-inflammatory cytokines IL-6 and TNF-α decreased after stimulating of infected RAW264.7 cells with the iron source $FeCl_3$, whereas the expression- and protein levels of the pro-inflammatory cytokines remained nearly unchanged after DFP treatment **(Fig. 3A, 3B, 3E, 3F).** In addition, the same effects can be observed when we looked at the mRNA level of iNOS and nitrite production **(Fig. 3C, 3G).** Together, these results lead to the assumption that the major effect of iron is to prevent the mRNA expression of these genes, which results in a reduced product and hence impaired control over intramacrophage pathogen proliferation.

When we looked at the effect of iron on the expression of the anti-inflammatory cytokine IL-10, a suppressed formation can be observed in iron loaded macrophages **(Fig. 3D).** Surprisingly, IL-10 protein expression was increased in iron loaded macrophages at the indicated time points **(Fig. 3H).**

When we looked at the effects of the iron-chelator on the expression- and protein production of IL-10, only a little decrease can be observed when compared to macrophages stimulated with bacteria only **(Fig. 3D, 3H).** Hence, iron has suppressive

effects on pro-inflammatory cytokine production as well as iNOS and nitrite formation, but affects positively the production of anti-inflammatory cytokine IL-10.

Fig. 3A

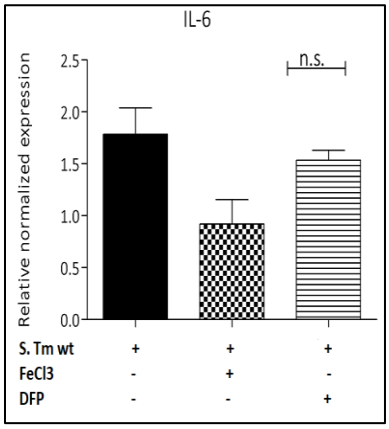

Fig. 3B

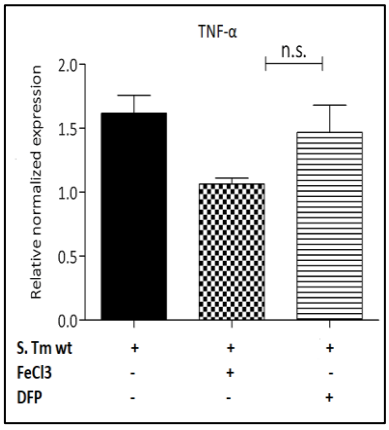

Fig. 3C

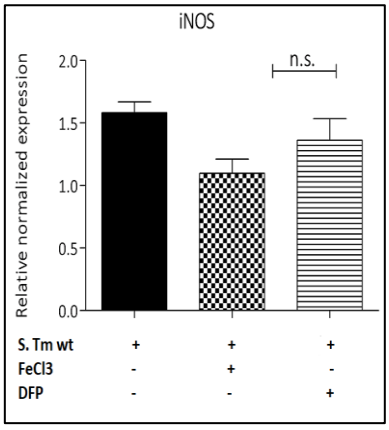

Fig. 3D

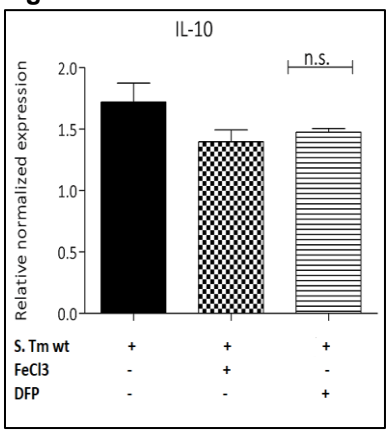

Fig. 3E

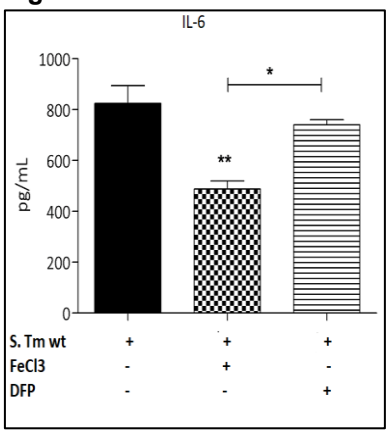

Fig. 3F

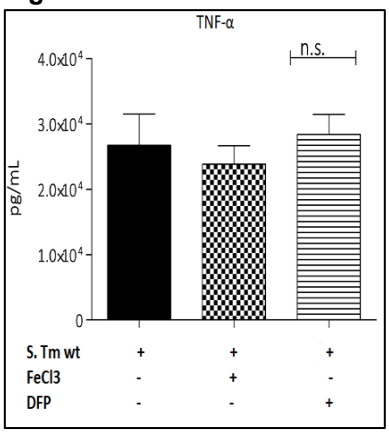

Fig. 3G

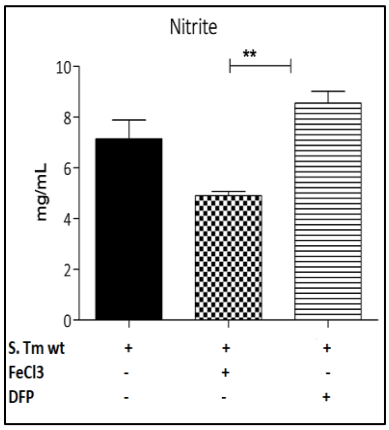

Fig. 3H

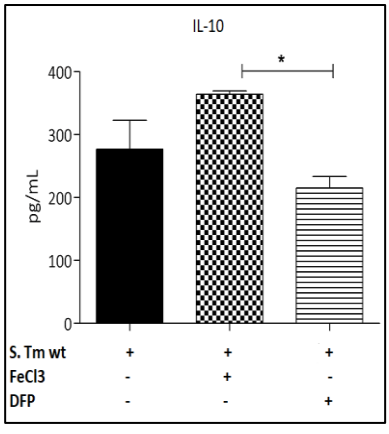

Figure 3 Expression of **(A)** IL-6, **(B)** TNF-α, **(C)** iNOS and **(D)** IL-10 mRNA was determined using qRT-PCR after treating RAW264.7 macrophages with either 50 µM of $FeCl_3$ or 50 µM of DFP for 6 h. Thereafter, cells were infected with *Salmonella* wt at a MOI of 10 for 1 h. After another incubation period for 23 h in presence of gentamycin and $FeCl_3$/DFP, cells were prepared for qRT-PCR. In addition, supernatants were collected and protein levels of **(E)** IL-6, **(F)** TNF-α, **(G)** iNOS and **(H)** IL-10 were determined using ELISA. Representative data from three independent experiments performed in triplicates are shown. Statistical analysis was performed using One-way ANOVA with Bonferroni

correction. The significance level was set at $p < 0.05$. Unless otherwise noted, * refers to the control group (shown in black).

Next, we were interested if this observed decrease in pro-inflammatory cytokine production as well as the impaired iNOS and nitrite production in iron loaded macrophages are the result of bacterial metabolic activity. Therefore, we treated RAW264.7 macrophages with the same conditions as in the prior experiment with the only difference, that heat-inactivated *Salmonella* were used instead of viable bacteria.

The results show similar effect on the immune response of macrophages when either infected with viable *Salmonella* or heat-inactivated bacteria **(Fig. 4A, 4B, 4C, 4D, 4E, 4F, 4G, 4H)**. These results ensure that the shown changes of the immune response during an infection are independent of bacterial metabolic activity and growth.

Fig. 4A

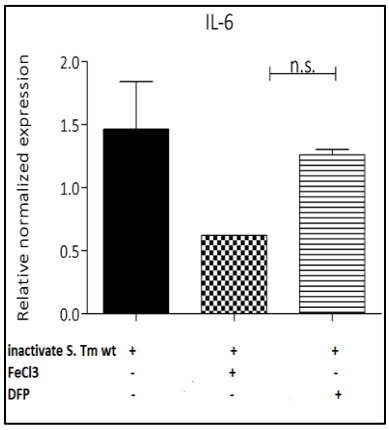

Fig. 4B

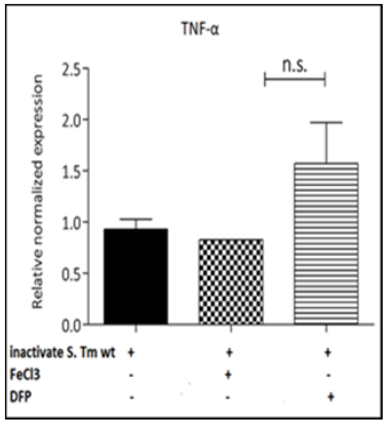

Fig. 4C

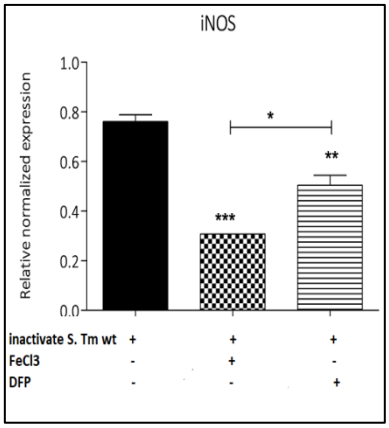

Fig. 4D

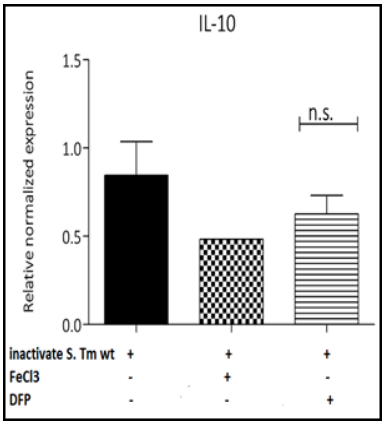

Fig. 4E

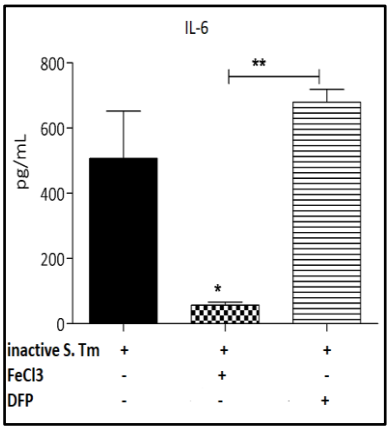

Fig. 4F

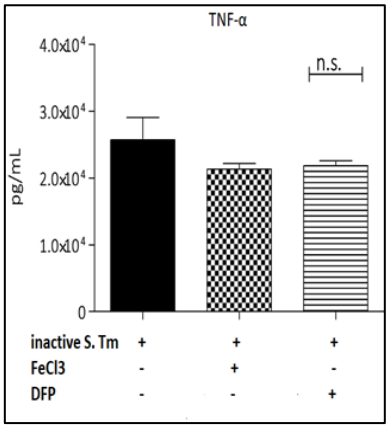

Fig. 4G **Fig. 4H**

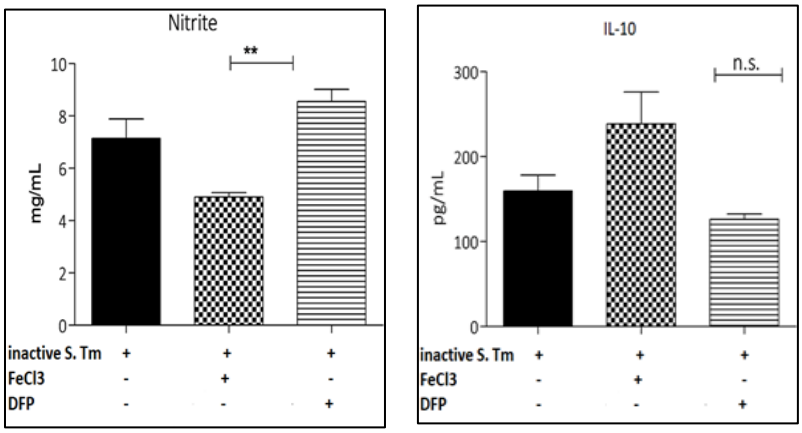

Figure 4 Expression of **(A)** IL-6, **(B)** TNF-α, **(C)** iNOS and **(D)** IL-10 mRNA was determined using qRT-PCR after treating RAW264.7 macrophages with either 50 µM of $FeCl_3$ or 50 µM of DFP for 6 h. Thereafter, cells were infected with heat-inactivated *Salmonella* wt at a MOI for 24 h in presence of $FeCl_3$ and DFP. In addition, supernatants were collected and protein levels of **(E)** IL-6, **(F)** TNF-α, **(G)** iNOS and **(H)** and IL-10 were determined using ELISA. Representative data from three independent experiments performed in triplicates are shown. Statistical analysis was performed using One-way ANOVA with Bonferroni correction. The significance level was set at $p < 0.05$. Unless otherwise noted, * refers to the control group (shown in black).

Since we now knew, that the decrease in the expression of pro-inflammatory cytokines as well as iNOS are not a result of the metabolic activity of bacteria, we were now interested if the observed effects above also persist after treatment of RAW264.7 cells with the *Salmonella* mutant strain, which is unable to acquire iron from the environment.

For the experimental procedure, RAW264.7 macrophages were treated as mentioned above with the only difference, that the *Salmonella* mutant strain was used instead of wildtype *Salmonella*.

The results show that the decrease in the pro-inflammatory cytokine levels, iNOS expression as well as nitrite production still persist **(Fig. 5A, 5B, 5C, 5E, 5F 5G)**. Additionally, also the levels of the anti-inflammatory cytokine IL-10 are not altered after infection of macrophages with the *Salmonella* mutant strain **(Fig. 5D, 5H)**, when compared to infections with wildtype *Salmonella*. In summary, the observed effects are due to the inhibitory effect of iron on macrophage immune function and are neither influenced by the bacterial metabolic activity nor bacterial proliferation, since it was

shown earlier that iron does not increase the proliferation of the *Salmonella* mutant strain within macrophages.

Fig. 5A

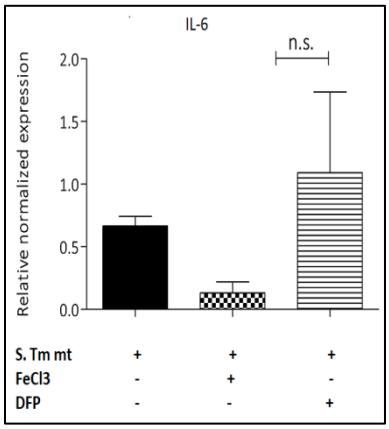

Fig. 5B

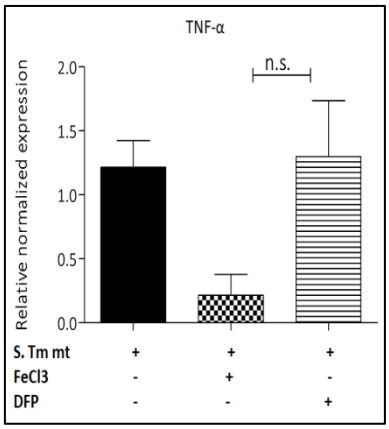

Fig. 5C

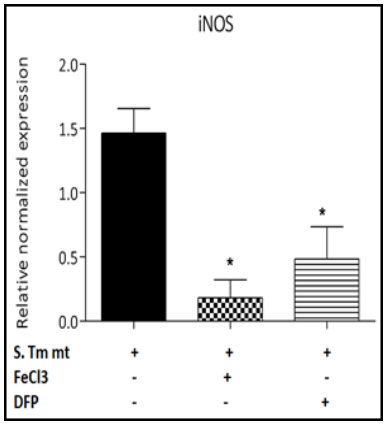

Fig. 5D

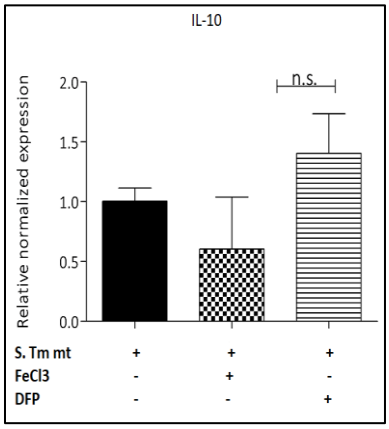

Fig. 5E

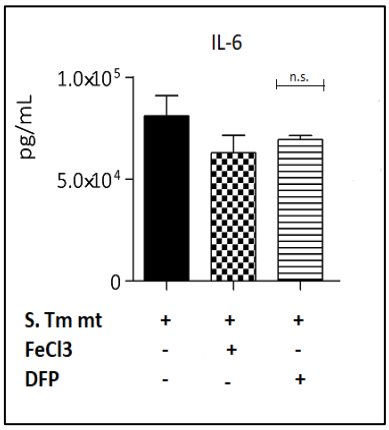

Fig. 5F

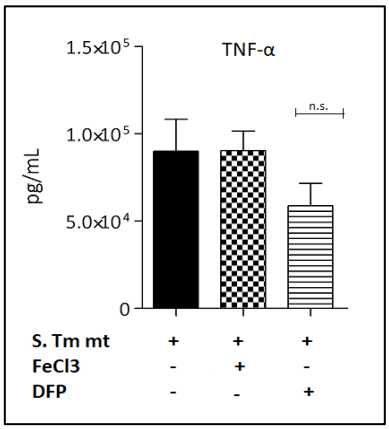

Fig. 5G

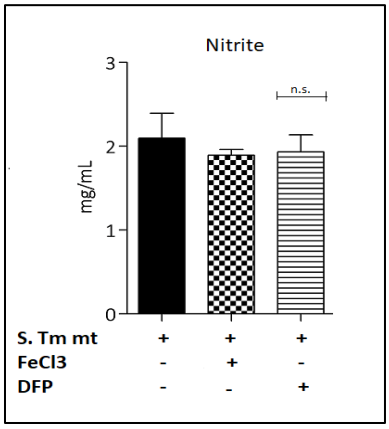

Fig. 5H

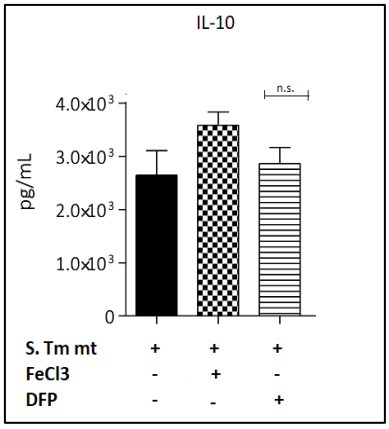

Figure 5 Expression of **(A)** IL-6, **(B)** TNF-α, **(C)** iNOS and **(D)** IL-10 mRNA was determined using qRT-PCR after treating RAW264.7 macrophages with either 50 μM of FeC_{l3} or 50 μM of DFP for 6 h. Thereafter, cells were infected with *Salmonella* mt at a MOI for 24 h in presence of $FeCl_3$ and DFP. In addition, supernatants were collected and protein levels of **(E)** IL-6, **(F)** TNF-α, **(G)** iNOS and **(H)** and IL-10 were determined using ELISA. Representative data from three independent experiments performed in triplicates are shown. Statistical analysis was performed using One-way ANOVA with

Bonferroni correction. The significance level was set at $p < 0.05$. Unless otherwise noted, * refers to the control group (shown in black).

4.4 Iron deficiency and infection states modulate the metabolic reprogramming in RAW264.7 cells

Since studies revealed that important enzymes of the citric acid cycle, such as aconitase and succinate dehydrogenase (SDH) are subjected to iron-mediated regulation, we were interested in the activity of these enzymes under iron-deprived and iron loaded states. In addition, it was reported that under critical environmental conditions, such as iron-deprived states or infections, immune cells reprogram their energy metabolism, shifting from oxidative phosphorylation towards aerobic glycolysis to provide both, ATP and building blocks needed for their activation (Cheng et al., 2016).

To investigate the influence of iron-deprived states and/or infections in the cellular energy metabolism of RAW264.7 cells, we simulated an iron-deficient state by treatment of this cell line with the iron-chelating agent DFP (50 µM) for 30 hours. To induce an infection, we stimulated the cells for 1 hour with *Salmonella* at a MOI of 10 and incubated it for another 23 hours in the presence of gentamycin (50 µM). Additionally, we were also interested if the results change after treating RAW264.7 cells with DFP and *Salmonella*, instead of each agent alone. To simulate this last condition, we pre-treated RAW264.7 macrophages with DFP (50 µM) for 6 hours and infected the cells afterwards for 1 hour with *Salmonella* at a MOI of 10 and incubated for another 23 hours in the presence of gentamycin (50 µM) as well as DFP (50 µM).

Thereafter, we investigated the expression rate of succinate dehydrogenase (SDH), aconitase (Aco) and isocitrate dehydrogenase (IDH) which are known to be major enzymes involved in the TCA cycle using qRT-PCR. Additionally, the supernatant was collected and protein levels of isocitrate, lactate, pyruvate and free fatty acids were determined using specific colorimetric assay kits.

In accordance with other reports (Oexle et al., 1999; Cheng et al., 2016), our findings show a significant decrease in the expression of succinate dehydrogenase (SDH), aconitase (Aco) and isocitrate dehydrogenase (IDH) during cellular iron restriction upon addition of DFP as well as during infections **(Fig. 6A, 6B, 6C)**, which leads to the

assumption, that the citric acid cycle is down-regulated during these critical environmental conditions. Contrary, under high iron levels within the cells, these effects are elevated **(Fig. 6B, 6C)** or reduced **(Fig. 6A)**. Since iron depletion and infections led to a reduction in aconitase activity, we assumed that also the isocitrate levels will decrease under such conditions. Our findings are in accordance with that, since a significant decrease in the isocitrate levels can be observed under both conditions **(Fig. 6D).** Interestingly, the decrease is significantly elevated during infections when compared to iron-deficient states. Upon simulation of both, an iron-deficient state and an infection in macrophages, the decrease in isocitrate levels are similar to those of an infection alone **(Fig. 6D)**. Additionally, a decrease in the pyruvate levels can be observed upon treatment of cells with DFP or infection with bacteria **(Fig. 6E)**.

Furthermore, it was reported in other studies (Oexle et al., 1999), that most of the pyruvate produced during glycolysis will be converted to lactate in iron-deprived states as well as during infections. In accordance with these studies, also in our experiment, an increase in lactate levels can be observed under both conditions, infections and iron chelator treatment, respectively **(Fig. 6F).** Lastly, we investigated the production of free fatty acids upon treatment of cells with DFP and/or infection of cells with *Salmonella*. The results show a significant increase in the formation of free fatty acids after the infection. In addition, also under iron-deprived states, an increase can be observed, even if being not significantly.

Fig. 6A

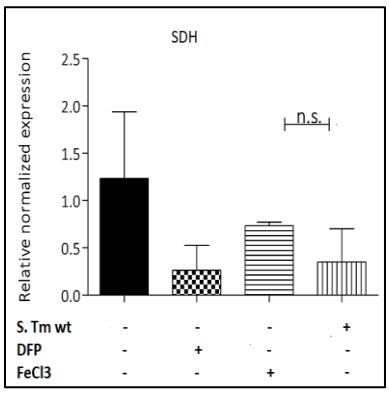

Fig. 6B

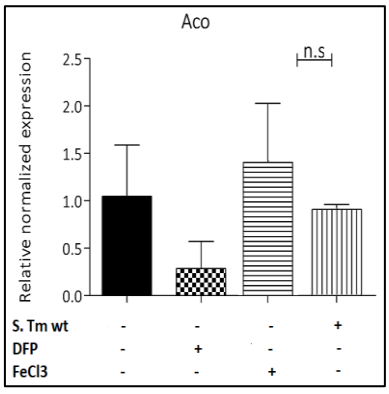

Fig. 6C

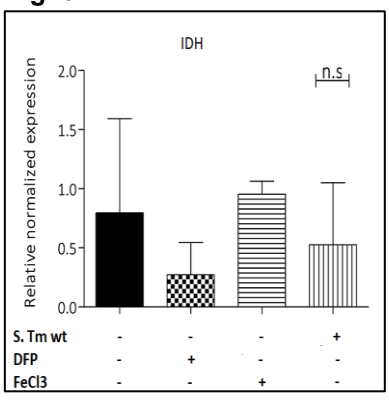

Fig. 6D

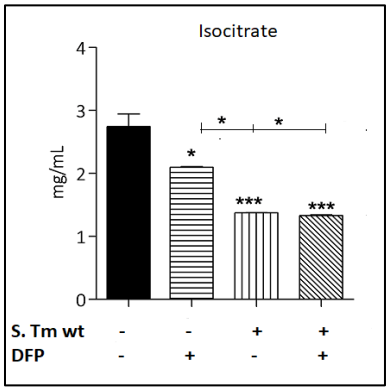

Fig. 6E

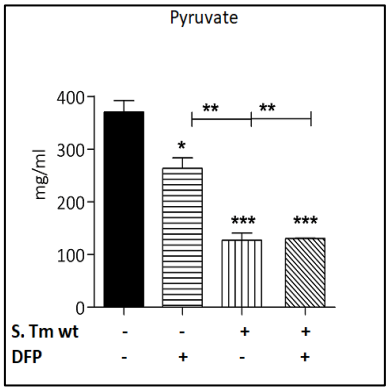

Fig. 6F

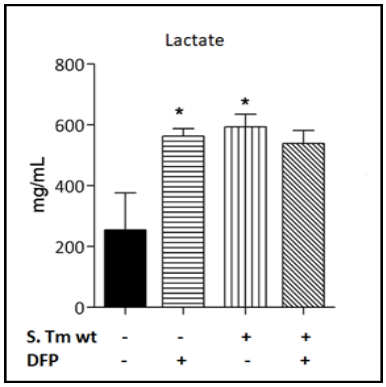

Fig. 6G

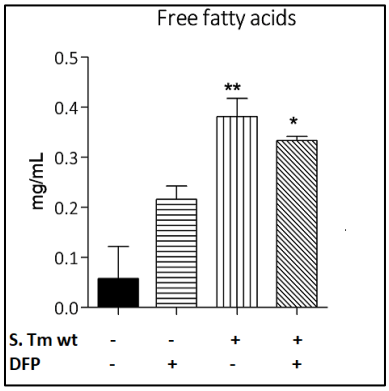

Figure 6 Expression of SDH **(Fig. 6A),** Aco **(Fig. 6B)** and IDH **(Fig. 6C)** mRNA was determined using qRT-PCR after treating RAW264.7 cells with either DFP (50 µM) for 30 h or infecting it with *Salmonella* at a MOI of 10 for 1 h and incubating it in presence of gentamycin (50 µM) for another 23 h. In addition, cells were also treated with both, DFP and *Salmonella*. Therefore, we pre-treated RAW264.7 macrophages with DFP (50 µM) for 6 h and infected the cells afterwards for 1 h with *Salmonella* at a MOI of 10 and incubated it for another 23 h in the presence of gentamycin (50 µM) as well as DFP (50 µM). Supernatants of all samples were collected, and proteins levels determined using specific colorimetric assay kits **(Fig. 6D, Fig. 6E, Fig. 6F, Fig. 6G).**

Statistical analysis was performed using One-way ANOVA with Bonferroni correction. The significance level was set at * = $p < 0.05$. Unless otherwise noted, * refers to the control group (shown in black).

In addition, we were also interested if these changes in the cellular energy metabolism of macrophages during infections requires the metabolic activity of the bacteria. Therefore, we treated RAW264.7 macrophages under the same conditions as in the prior experiment with the only difference, that heat-inactivated *Salmonella* were used instead of viable bacteria.

Upon treatment of cells with heat-inactivated bacteria, metabolic reprogramming can be observed **(Fig. 7A, 7B, 7C, 7D)**. However, the magnitude of metabolic alterations

within macrophages upon an infection with inactive bacteria are reduced when compared to the data using viable *Salmonella* **(Fig. 6)**.

In summary, the metabolic activity of microbes is required to induce a strong metabolic reprogramming of macrophages.

Fig. 7A

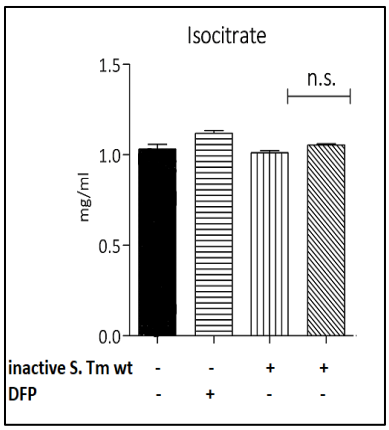

Fig. 7B

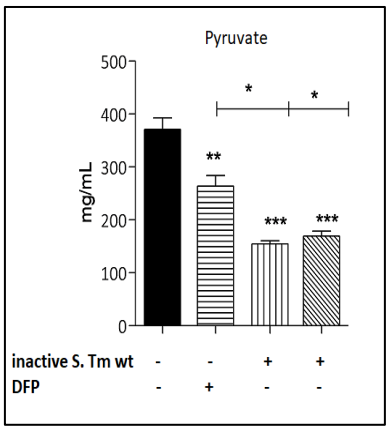

Fig. 7C

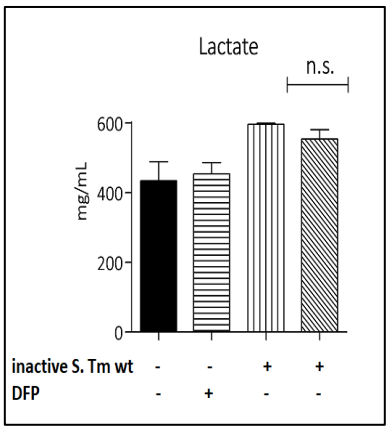

Fig.7D

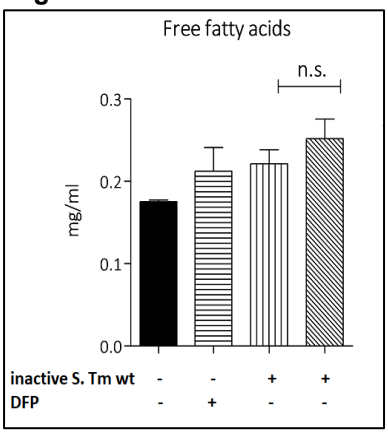

Figure 7 Levels of isocitrate **(Fig 7A),** pyruvate **(Fig. 7B),** lactate **(Fig. 7C)** and free fatty acids **(Fig. 7D)** were determined after treating of RAW264.7 cells with either DFP (50 µM) for 30 h or infecting it with heat-inactivated *Salmonella* at a MOI of 10 for 1 h. In addition, cells were also treated with both, DFP and inactivated *Salmonella*. Therefore, we pre-treated RAW264.7 macrophages with DFP (50 µM) for 6 h and infected the cells afterwards for 1 h with inactive *Salmonella* at a MOI of 10 and incubated it for another 23 h in the presence of DFP (50 µM). Supernatants of all samples were collected, and proteins levels determined using specific colorimetric assay kits. Representative data from three independent experiments performed in triplicates are shown. Statistical analysis was performed using One-way ANOVA with Bonferroni correction. The significance level was set at $p < 0.05$. Unless otherwise noted, * refers to the control group (shown in black).

4.5 mTOR mediates the shift towards aerobic glycolysis during infections

Mammalian target of rapamycin (mTOR) has been shown to be activated by carbon sources, such as glucose. Glucose thereby stimulates the phosphorylation of the two downstream targets of mTORC1, 4 E binding protein 1 (4E-BP1) and S6 kinase (S6K) in an mTOR-dependent manner. Since our prior studies have shown a shift towards aerobic glycolysis during infections, we were interested if this shift can be mediated by mTOR, since this complex is known to be an intracellular sensor of glucose.

For the experimental procedure, we therefore infected RAW264.7 macrophages with either viable *Salmonella* or heat-inactivated *Salmonella* at a MOI of 10 for 1 hour. Thereafter, cells were incubated for another 23 hours, either in the presence of gentamycin (50 µM) (viable bacteria) or without gentamycin (heat-inactivated bacteria) and protein levels of the two downstream targets of mTORC1 were determined using Western Blot analysis.

The results show an induced phosphorylation of both, S6K and 4E-BP1 upon treatment of macrophages with bacteria. However, treatment of cells with viable *Salmonella* led to a stronger phosphorylation 4E-BP1 when compared to S6K phosphorylation. Controversially, treatment of cells with heat-inactivated *Salmonella* led to a more pronounced phosphorylation of S6K, whereas 4E-BP1 phosphorylation was not altered when compared to the control group **(Fig. 8)**. This indicates, that the bacterial proliferation may be important for strong induction of the mTOR signaling pathway.

Moreover, we were also interested if iron perturbations within macrophages influence the activity of mTOR, since we showed earlier that iron deprivation also mediates the shift toward aerobic glycolysis.

Therefore, we treated RAW264.7 cells with either $FeCl_3$ or DFP for 30 hours and prepared the cells thereafter for Western blot analysis. Interestingly, treatment of cells with DFP decreases the phosphorylation of 4E-BP1 and S6K when compared to the control group, whereas only a moderate increase in phosphorylation of the molecules can be observed after $FeCl_3$ treatment **(Fig. 8).** These data suggest that during infections, especially with viable *Salmonella*, the metabolic reprogramming of macrophages may be driven by the activation of mTOR. These results are in

accordance with the prior data that show a stronger induction of the Warburg effect when cells were stimulated with viable bacteria than inactivated bacteria.

Fig. 8

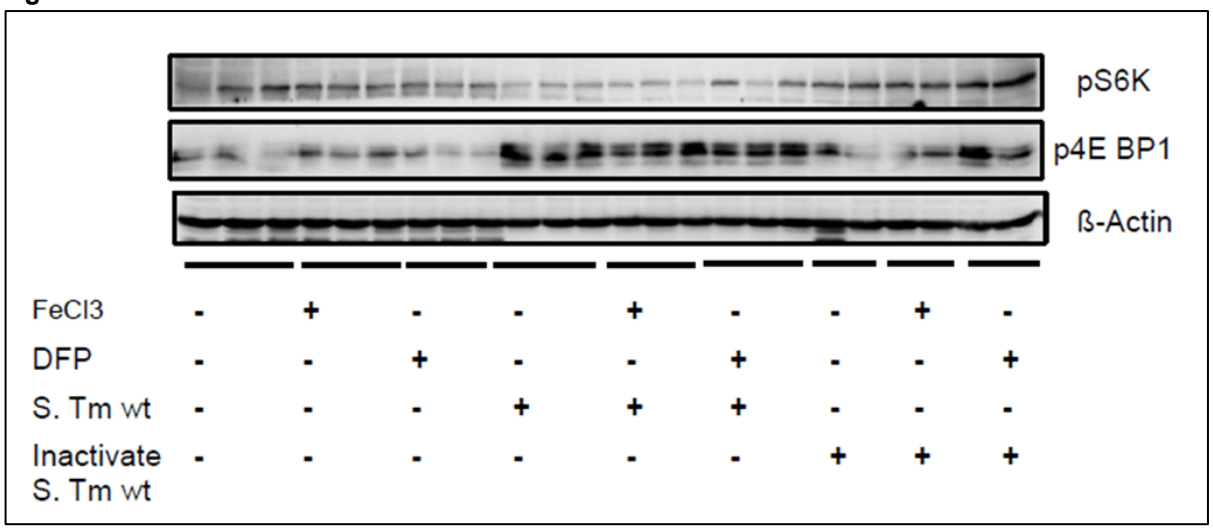

Figure 8 Protein levels of mTOR downstream targets pS6K and p4E-BP1 were determined after treating RAW264.7 cells with either viable *Salmonella* or heat-inactivated *Salmonella* at a MOI of 10 for 1 h. Thereafter, cells were incubated for another 23 h, either in the presence of gentamycin (50 µM) (viable bacteria) or without gentamycin (heat-inactivated bacteria). Additionally, cells were treated with $FeCl_3$ (50 µM) or DFP (50 µM) and protein levels of the two downstream targets of mTORC1 were determined using Western Blot analysis.

To ensure that the shift towards aerobic glycolysis in macrophages is determined by the mTOR pathway, we examined in our next experiment if this effect gets reversed after treatment of macrophages with the mTORC1 inhibitor rapamycin.

Therefore, we pre-treated RAW264.7 cells with rapamycin (200 nM) for 1 hour. Thereafter, cells were infected with *Salmonella* for 1 hour in presence of rapamycin (20 nM) and incubated afterwards for another 23 hours in presence of gentamycin (50 µM) and rapamycin (20 nM). SDH, Aco, IDH and LDH expression was determined using qRT-PCR. Additionally, supernatants were collected for metabolite measurement.

The results indicate that upon an infection and inhibition of the mTOR signaling pathway by rapamycin, the expression of the citric acid enzymes SDH **(Fig. 9A),** Aco **(Fig. 9B)** and IDH **(Fig. 9)** is increased when compared to the data showing an infection only. Moreover, the expression level of the lactate dehydrogenase (LDH) which is required for the conversion of pyruvate into lactate and NAD^+, is increased

after stimulation of RAW264.7 cells with *Salmonella*, but decreases after treatment of the cells with both, *Salmonella* and the mTORC1 inhibitor rapamycin **(Fig. 9D)**. Additionally, when we look at the lactic acid production, the same effect can be observed, showing that the expression rate of lactate dehydrogenase correlates with the amount of lactic acid produced **(Fig. 9E)**. Moreover, also an increase in the glucose production can be observed during an infection and contrary, there is a tendency of a decrease in the glucose level after inhibition of the mTOR pathway **(Fig. 9 F)**.

Furthermore, when we now looked at the succinic acid production and the cis-aconitic acid production, the data show an increase in succinic acid as well as aconitic acid production during an infection with *Salmonella*, whereas these effect is reduced after treatment of macrophages with rapamycin **(Fig. 9G, Fig. 9H)**. These data are in accordance with prior reports (Cordes et al., 2016; Geeraerts et al., 2017), showing that the increase in succinate levels during an infection is the result of the truncated TCA cycle at the level of SDH. Moreover, it was shown that the reduced IDH expression results in accumulation of citrate, which is needed to produce itaconic acid, a macrophage-specific metabolite. Thereby, the immunoresponsive gene 1 (irg1) plays an important role since it codes for the enzyme cis-aconitate decarboxylase, which converts aconitate to itaconic acid (Cordes et al., 2016; Geeraerts er al., 2017).

In summary, these data are in line with our assumption that during an infection and inhibition of the mTOR signaling pathway, the metabolic reprogramming gets reversed and indicate that mTOR is responsible for the shift towards aerobic glycolysis during infections.

Fig. 9A

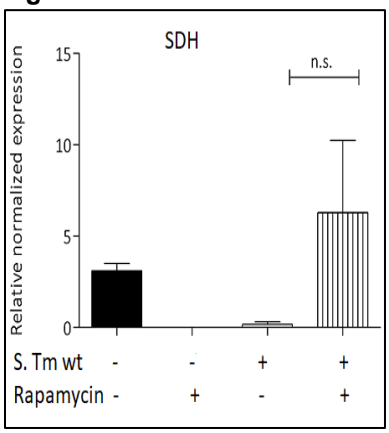

Fig. 9B

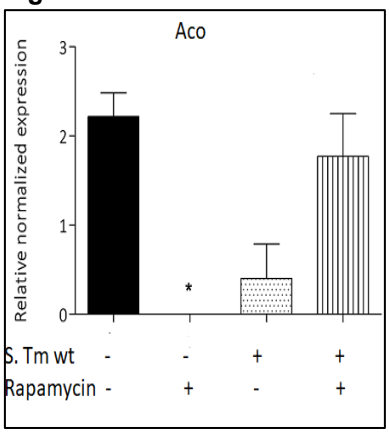

Fig. 9C

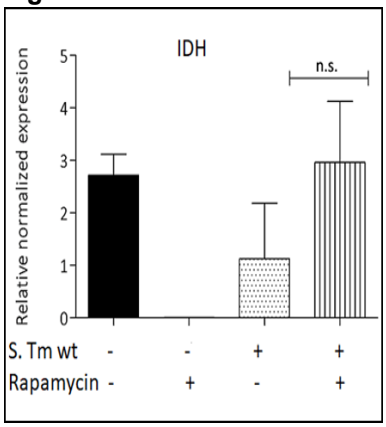

Fig. 9D

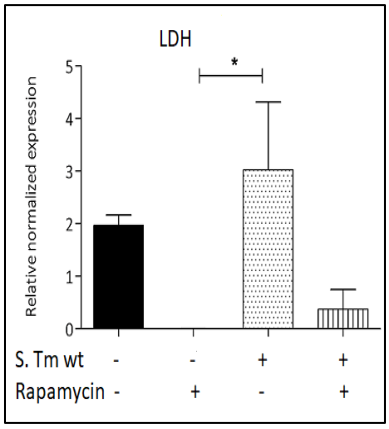

Fig. 9E

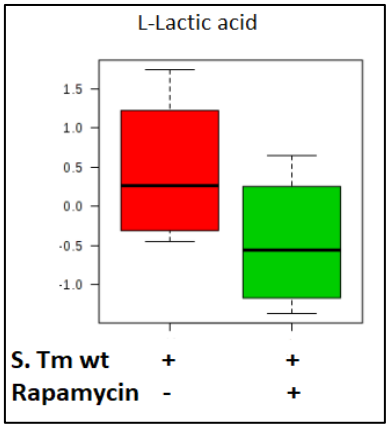

Fig. 9F

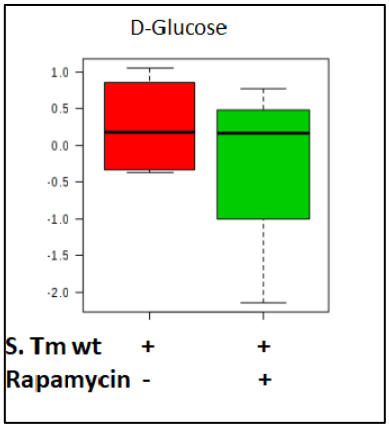

Fig. 9G

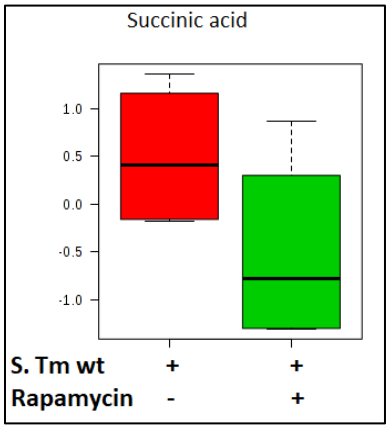

Fig. 9H

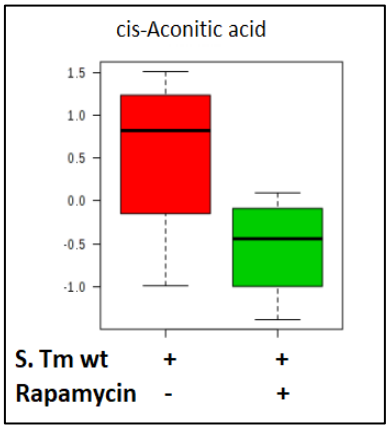

Figure 9 mRNA expression of SDH **(Fig. 9A)**, Aco **(Fig. 9B)**, IDH **(Fig. 9C)** and LDH **(Fig. 9D)** was determined after treating cells with 200 nM of rapamycin for 1 h and infecting it with *Salmonella* at a MOI of 10 for 1 h in the presence of rapamycin (20 nM) After another incubation period of 23 h in presence of gentamycin (50 µM) and rapamycin (20 nM) cells were prepared for qRT-PCR. Additionally, supernatants were collected and Lactic acid **(Fig. 9E),** D-Glucose **(Fig. 9F)**, Succinic acid **(Fig. 9G)** and cis-Aconitic acid **(Fig. 9H)** production was determined. Statistical analysis was performed using One-way ANOVA with Bonferroni correction. The significance level was set at $p < 0.05$. Unless otherwise noted, * refers to the control group (shown in black).

4.6 Blockage of mTOR negatively affects macrophages immune functions

Since our data indicate that the shift towards aerobic glycolysis, which is required for controlling an infection, is mediated by mTOR and gets abolished after treatment of macrophages with rapamycin, we were interested if rapamycin also affects other immune cells functions upon an infection.

For the experimental procedure we pre-treated RAW264.7 cells with 200 nM of rapamycin for 1 hour. Thereafter, cells were infected with viable *Salmonella* at a MOI

of 10 for 1 hour in presence of rapamycin (20 nM). Afterwards, cells were incubated for another 23 hours in the presence of gentamycin (50 µM) as well as rapamycin (20 nM) and the expression of IL-6, TNF-α, iNOS and IL-10 mRNA was determined using qRT-PCR. Additionally, supernatants were collected and the formation of the products in macrophage culture supernatants were determined using the ELISA kits and the Griess test.

The results show that the expression of pro-inflammatory cytokines IL-6 **(Fig. 10A)** and TNF-α **(Fig. 10B)** is decreased upon treatment of cells with rapamycin. Moreover, also the iNOS **(Fig. 10C)** expression is reduced **(Fig. 10D)**, whereas the expression rate of the anti-inflammatory cytokine IL-10 **(Fig. 10D)** is increased upon inhibition of mTOR. If we looked at the protein level of IL-6 **(Fig. 10E),** TNF-α **(Fig. 10F)** and IL-10 **(Fig. 10H)** the same results as shown at mRNA level can be observed. Additionally, also the nitrite formation decreases upon treatment of macrophages with rapamycin **(Fig. 10G).**

Fig. 10A

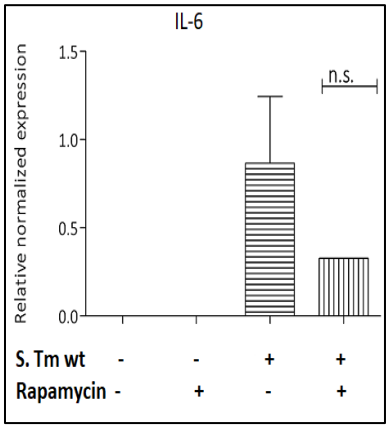

Fig. 10B

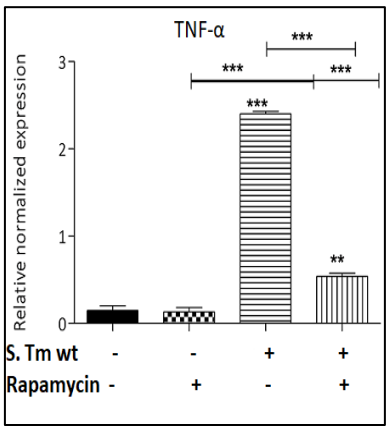

Fig. 10C

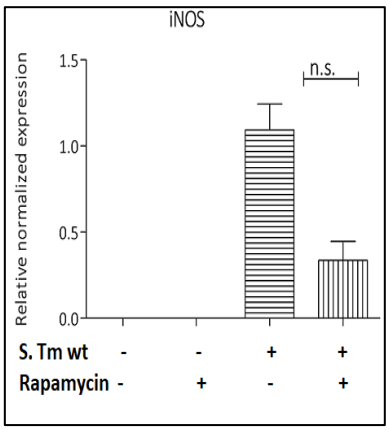

Fig. 10D

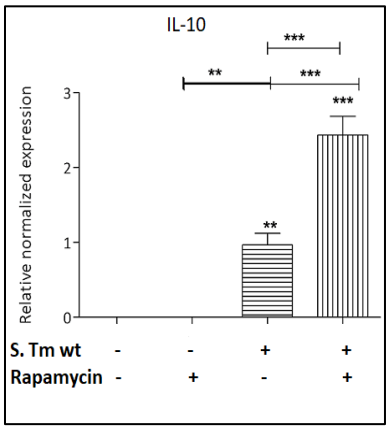

Fig. 10E

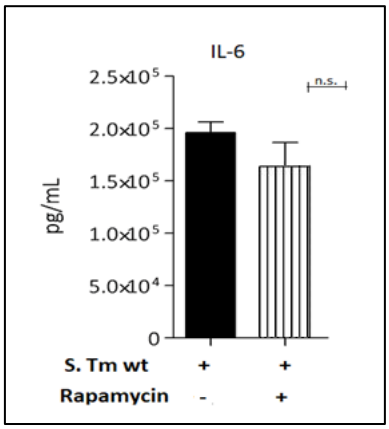

Fig. 10F

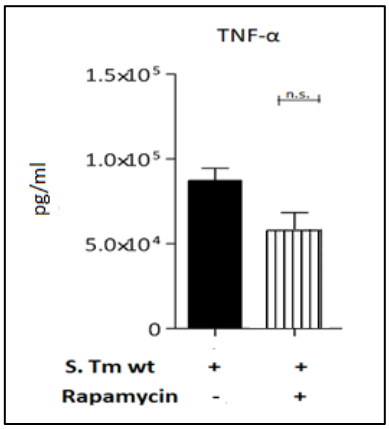

Fig. 10G **Fig. 10H**

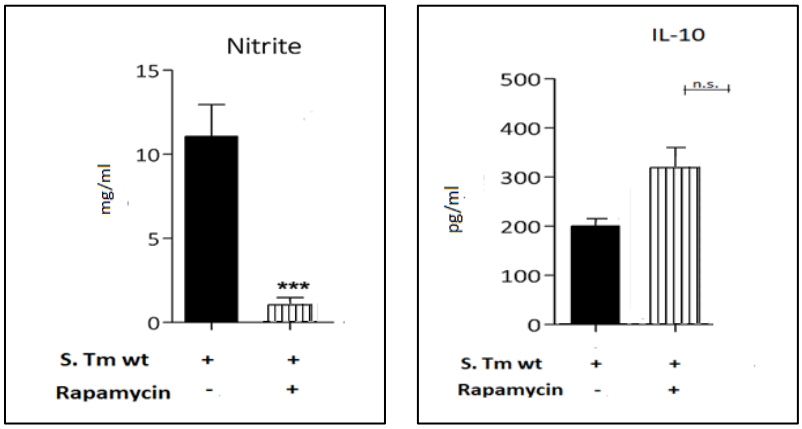

Figure 10 IL-6 **(Fig. 10A)**, TNF-α **(Fig. 10B)**, iNOS **(Fig.10C)** and IL-10 **(Fig.10D)** mRNA expression of RAW264.7 cells was determined after treating cells with 200 nM of rapamycin for 1 h. Thereafter cells were infected with *Salmonella* at a MOI of 10 for 1 h in presence of rapamycin (20 nM). After another incubation period of 23 h in presence of gentamycin (50 µM) and rapamycin (20 nM) cells were qRT-PCR. Additionally, the collected supernatant was used for IL-6 **(Fig. 10E),** TNF-α **(Fig. 10F),** IL-10 **(Fig. 10H)** and nitrite measurement **(Fig. 10G)** using the ELISA test and Griess test. Representative data from three independent experiments performed in triplicates are shown. Statistical analysis was performed using One-way ANOVA with Bonferroni correction. The significance level was set at $p < 0.05$. Unless otherwise noted, * refers to the control group (shown in black).

Further we were interested, if the diminished immune response after inhibition of mTOR is also accompanied with an increase in the bacterial load within macrophages. Therefore, we pre-treated RAW264.7 macrophages with 200 nM of rapamycin for 1 hour. Thereafter, cells were infected with *Salmonella* at a MOI of 10 for 1 hour in the presence of 20 nM of rapamycin. After another incubation period of 23 hours in in presence of gentamycin (50 µM) and rapamycin (20 nM) cells were subsequently lysed using natrium-deoxicolate. The number of *Salmonella* colony forming units (CFU) recovered from macrophages infection was determined by plating *Salmonella* on agar-plates and incubation for 24 h at 37°C.

The results show a significant higher bacterial load within macrophages after inhibition of the mTOR pathway **(Fig. 11).**

In summary, inhibition of mTOR results in lower pro-inflammatory cytokine production, iNOS and nitrite production and abolishes the metabolic reprogramming of macrophages during an infection, indicating a reduced first line response to pathogens and diminished outcome for the host, which in turn provides opportunities for pathogens to proliferate within macrophages. These data therefore attest the

importance of the mTOR pathway in robust immune response and effective host defense.

Fig. 11

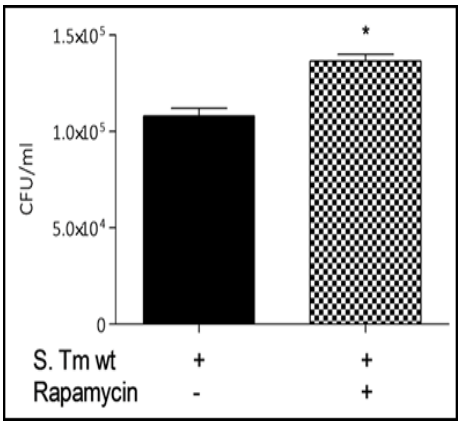

Figure 11 RAW264.7 were treated with 200 nM of rapamycin for 1 h. Thereafter, cells were infected with *Salmonella* at a MOI of 10 for 1 h in the presence of 20 nM of rapamycin. After another incubation period of 23 h in in presence of gentamycin (50 µM) and rapamycin (20 nM) cells were subsequently lysed using natrium-deoxicolate. The number of *Salmonella* colony forming units (CFU) recovered from macrophages infection was determined by plating *Salmonella* on agar-plates and incubation for 24 h at 37°C. Representative data from three independent experiments performed in duplicates are shown. Statistical analysis was performed using the Student's t-test. The significance level was set at $p < 0.05$. Unless otherwise noted, * refers to the control group (shown in black).

4.7 mTOR coordinates iron homeostasis within RAW264.7 cells

Recently, a study revealed that there is a link between mTOR and iron homeostasis. It was shown that cellular iron uptake by TfR1 is modulated by mTOR activity (Bayeva et al., 2012). This study identified tristetraprolin (TTP) as a downstream target of mTOR, that binds to and enhances degradation of TfR mRNA, leading to reduced iron import. TTP is recognized as an early response gene that is induced by inflammatory stimuli as well as rapamycin. Moreover, it was shown that under iron-deficient states, the binding affinity of IRPs to IREs is enhanced to prevent further iron loss. IRP/IRE complexes formed within the 5' UTR of an mRNA, for example ferritin, inhibit its translation, whereas IRP binding to IREs within the 3' UTR of TfR1 mRNA prevents its degradation.

Because of these reports, we investigated the influence of rapamycin as well as iron perturbation states on iron homeostasis in RAW264.7 macrophages. Therefore, we pre-treated RAW264.7 cells with 200 nM rapamycin for 1 hour and then with 20 nM for

another 23 hours. Furthermore, we treated RAW264.7 cells with 50 µM of $FeCl_3$ or 50 µM of DFP for 24 hours and investigated the protein levels of TfR1 and ferritin using Western blot analysis.

Our findings show that a blockage of mTOR by rapamycin led to a decrease in protein levels of TfR1 and an increase in the protein content of the iron storage protein ferritin **(Fig. 12).** These results show an accumulation of cellular iron, despite the reduced iron uptake after inhibition of mTOR and are in accordance with the study that demonstrated an induction of TTP by rapamycin and thereby altered cellular iron flux (Bayeva et al., 2012).

Interestingly, the same results can be observed when cells were treated with the iron source $FeCl_3$, which resemble a stage of iron overload **(Fig.12)**. Studies showed that during this process, the affinity of IRPs within the 5' untranslated region of the mRNA coding for ferritin to IREs is reduced, which results in increased ferritin translation. Moreover, the low affinity of IRPs within the 3' UTR of the TfR mRNA results in degradation of this mRNA (Muckenthaler et al., 2017).

When cells were treated with the iron-chelator DFP, the opposite effect can be observed **(Fig.12)**. These results are in in line with the well- established effect that low iron levels result in activation of IRPs to prevent further iron loss and therefore cause blockage of ferritin translation by high binding affinity of IRPs to IREs within the ferritin mRNA. Additionally, the protein levels of TfR are increased in iron deprived stages due to the binding of IRPs to the IREs within the 3' untranslated region of the mRNA which results in increased expression of the TfR protein by prolonging the mRNA half-life.

Interestingly, when treating cells with both, rapamycin and the iron source $FeCl_3$ or the iron-chelating agent DFP, the observed effects are elevated, showing an additive effect of the two components with low TfR1 protein level and high ferritin protein level **(Fig.12).** However, when cells are treated with rapamycin and the iron chelating agent DFP, the protein level of TfR1 and ferritin decline when compared to treatment with DFP alone **(Fig.12)**.

Fig. 12

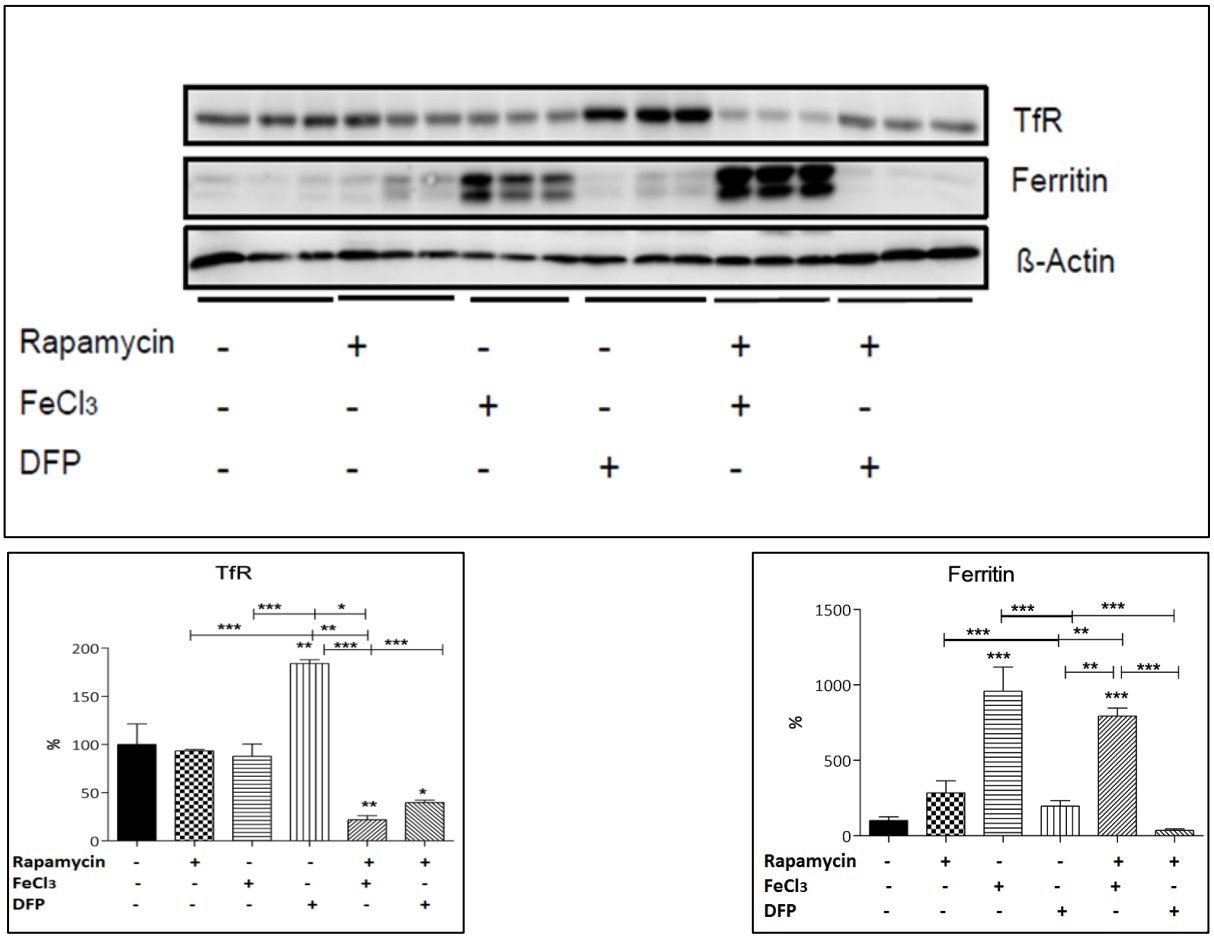

Figure 12 Protein levels of TfR and ferritin were determined in RAW264.7 cell extracts using Western blot analysis, after 24 h stimulation with DFP (50 µM) and $FeCl_3$ (50 µM) or 1 h stimulation with 200 nM rapamycin and another 23 h with 20 nM rapamycin. Statistical analysis was performed using One-way ANOVA with Bonferroni correction. The significance level was set at $p < 0.05$. Unless otherwise noted, * refers to the control group (shown in black).

The prior results show that, rapamycin combined with iron-overload states result in a down-regulation of the iron importer TfR1 and upregulation of the iron storage protein ferritin, whereas iron-deficient conditions combined with blockage of mTOR results in the opposite effect, meaning higher protein level of TfR1 and lower protein level of ferritin. Now we were interested in the impact of mTOR inhibition together with iron perturbation states on intramacrophage survival of *Salmonella*.

Therefore, we pre-treated RAW264.7 cells with DFP/$FeCl_3$ (50 µM) for 5 hours and supplied rapamycin (200 nM) for 1 hour prior to stimulating the cells with *Salmonella* at a MOI of 10 for 1 hour. Thereafter, cells were incubated for another 23 hours in presence of gentamycin (50 µM), rapamycin (20 nM) and $FeCl_3$/DFP (50 µM), followed

by subsequent lysing of the cells using Na-deoxycolate. The number of *Salmonella* colony forming units (CFU) recovered from macrophages after 24 hours of infection was determined by plating *Salmonella* on agar-plates and incubation for 24 hours at 37°C.

The results show that iron-overload states as well as mTOR blockage positively influence the bacterial load within macrophages. Additionally, the colony forming units after treatment with both, rapamycin and $FeCl_3$ are not altered when compared by treatment of macrophages with each component only. However, like observed in the prior experiment, iron-deficient conditions reduced the intramacrophage survival of *Salmonella*. Interestingly, in iron-deficient states, combined with inhibition of mTOR, the bacterial growth within macrophages is enhanced when compared to treatment with the iron-chelating agent only **(Fig.13A).**

Since the prior data showed that storage of iron within macrophages positively influenced the bacterial growth within macrophages, we were now interested, if the higher proliferation rate of *Salmonella* is abolished when macrophages were treated with the *Salmonella* mutant strain, which is unable to acquire iron from the environment.

For the experimental procedure, we therefore treated RAW264.7 cells with the same conditions as in the prior experiment, with the only difference, that the *Salmonella* mutant strain was used for infecting macrophages instead of *Salmonella* wt.

The results show that the bacterial load is not affected either by iron-overload conditions nor by iron-deficient states. However, rapamycin results in an increase in bacterial growth which is in accordance the data that show the importance of mTOR in controlling infections. Treatment of cells with both, rapamycin and either $FeCl_3$ or DFP did not alter the bacterial growth when compared to treatment with each component only **(Fig. 13B).**

In summary, the increased iron availability for bacteria within macrophages in iron-overload states and blockage of the mTOR, positively affects the intracellular survival of *Salmonella*. Contrary, iron-deficient states, negatively affects the bacterial load within macrophages. However, in iron-deficient states and after treatment of the cells with rapamycin, which is known to enhance bacterial proliferation, the bacterial survival improves somewhat.

Fig. 13A

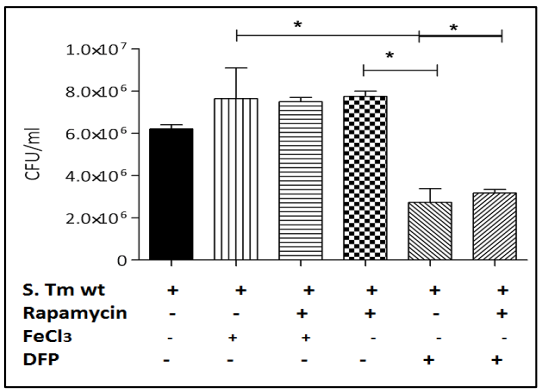

Fig. 13B

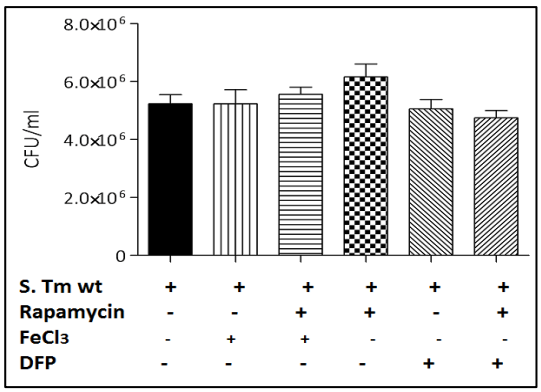

Figure 13 Impact of exogenous iron perturbations and mTOR blockage on intramacrophage survival of *Salmonella* was determined by gentamycin protection assay. Therefore, RAW264.7 macrophages were either treated with 50 µM of $FeCl_3$ or 50 µM of DFP for 5 h and rapamycin for 1 h. Thereafter, cells were infected with *Salmonella* wt **(Fig.13A)** or *Salmonella* mt **(Fig. 13B)** at a MOI of 10 for 1 h. After another incubation period for 23 h in presence of gentamycin and $FeCl_3$/DFP, and rapamycin cells were subsequently lysed using natrium-deoxicolate and CFU/ml were determined. Experiment was performed in duplicates for each condition. Statistical analysis was performed using One-way ANOVA with Bonferroni correction. The significance level was set at $p < 0.05$. Unless otherwise noted, * refers to the control group (shown in black).

5. Discussion

Iron overload of macrophages exerts multiple effects on immune cells. These effects are associated with impaired cellular mediated immune functions, since iron inhibits the transcription of the pro-inflammatory cytokines IL-6 and TNF-α and has suppressive effects on iNOS expression as well as nitrite formation (Weiss et al., 1994; Oexle et al., 2003). This alterations in the cellular immune functions in iron loaded macrophages are neither influenced by bacterial metabolic activity nor by bacterial proliferation, since the effects still persist after stimulation of macrophages with heat-inactivated *Salmonella* as well as the *Salmonella* mutant strain, which shows unaltered proliferation rates within iron-treated and untreated macrophages. These data are in accordance with the well-established data showing that iron influences the binding affinity of transcription factors such as NF-IL-6, IRF-1 or HIF-1α to target gene promoters. Moreover, reports show that the nuclear transcription of iNOS mRNA is decreased after iron supplementation (Weiss et al., 1994), which is in accordance with our data, showing a decrease in iNOS expression in iron-overload macrophages.

Additionally, iron improves the growth of wildtype *Salmonella* outside -, as well as inside of macrophages. This enhanced bacterial growth within iron loaded macrophages is related to the positive effect of the metal for bacteria proliferation and not a result of the suppressed immune response, since after stimulation of macrophages with the *Salmonella* mutant strain, which is unable to acquire iron for the environment, no increase in intramacrophage bacterial growth can be observed in iron-loaded macrophages, despite the suppressed immune functions. As a fact, we can therefore say, that iron negatively affects macrophages immune functions whereas it positively affects bacterial proliferation.

Additionally, it was shown that iron perturbations within macrophages influences the cellular metabolic activity. Our results show that the expression of the citric acid enzymes aconitase (Aco), isocitrate dehydrogenase (IDH) and succinate dehydrogenase (SDH) is reduced upon treatment of macrophages with the iron-chelating agent DFP.

This is in accordance with prior reports that show that mitochondrial aconitase is regulated via the interaction of iron regulatory proteins (IRP) with a RNA stem loop structure (IRE) within the 5’ untranslated region of mitochondrial aconitase mRNA

(Oexle et al., 1999). Such interactions of IRPs with IREs occur under iron deprived states as well as during infections. This data is in accordance with our experimental data, demonstrating that the aconitase activity is also reduced after stimulating of RAW264.7 macrophages with *Salmonella*. Moreover, the enzymes active center contains a relatively unstable iron-sulfur cluster. Therefore, it cannot be ruled out that the decrease in the aconitase activity could be a result of changes in the catalytic center of the enzyme.

Moreover, the reduction in aconitase activity led to a reduced isocitrate formation, the product of the enzymatic activity of aconitase. Since isocitrate is the substrate for IDH and IDH is not regulated via the IRP/IRE system, the limited IDH activity in iron-deficient cells as well as during infections could be explained by the reduced availability of isocitrate.

Similar to aconitase, also SDH was shown to be regulated via the IRP/IRE system and in analogy to aconitase, the catalytic center contains an iron-sulfur cluster (Oexle et al., 1999). Therefore, iron-perturbations as well as infections may regulate SDH activity similar as discussed for aconitase.

This modulation of the citric acid cycle also affects glycolysis. Studies reported that under such critical environmental conditions, a shift from oxidative phosphorylation towards aerobic glycolysis occurs, to generate ATP and to promote the activation of immune cells, thereby ensuring their enhanced proliferation (Geeraerts et al., 2017). Pyruvate, the end product of the glycolytic pathway is thereby converted to lactate and NAD^+, instead of entering the mitochondria to undergo oxidation. These data are in accordance with our experiments, showing an increased in lactate levels under iron-deficient conditions as well as during infections. Moreover, it has been reported that LPS activation of TRL induces lipid accumulation through enhanced fatty acid uptake. Also, our experiments show an increase in free fatty acid (FFA) levels upon stimulation of macrophages with *Salmonella*. Additionally, the increase in the FFA levels can also be observed upon treatment of cells with DFP. Moreover, a decrease in pyruvate levels can be observed upon treatment of cells with DFP as well as during infection, which may be the result of the repressed citric acid cycle due to blockage of aconitase activity.

It becomes clear that the switch during iron-deficient states in macrophages results via the interaction of IREs and IRPs. However, this doesn't explain the change in the metabolic activity of macrophages during infections.

To understand these metabolic alterations of macrophages during infections, we looked at the activity of the mammalian target of rapamycin (mTOR) signalling pathway since prior studies reveal that mTOR may drives the shift towards aerobic glycolysis in acute inflammation (Cheng et al., 2016). Our results are in line with that, since an increased phosphorylation of the two downstream targets of mTOR, S6K and 4E-BP1 can be observed during infections, but not in iron perturbation states. Moreover, this increased activity of mTOR is enhanced during infections with viable *Salmonella* when compared to infections with inactivated *Salmonella*, which leads to the assumption that the metabolic activity of bacteria is required to activate this signalling pathway and thereby induce a strong metabolic reprogramming of immune cells. Interestingly, inhibition of the mTOR complex mTORC1 by rapamycin results in the opposite effect, namely an increase in the activity of the citric acid cycle enzymes IDH, SDH and Aco and a decrease in the lactate dehydrogenase (LDH) activity as well as lactic acid formation. Moreover, an accumulation of succinic acid and cis-aconitic acid can be observed during infections, whereas this effect gets lowered after treatment of cells with rapamycin. This accumulation of succinate results from the truncated TCA cycle at the SDH level. Moreover, the reduced IDH expression results in accumulation of citrate, which is needed to produce itaconic acid, a macrophage-specific metabolite. Thereby, the immunoresponsive gene 1 (irg1) plays an important role since it codes for the enzyme cis-aconitate decarboxylase, which converts aconitate to itaconic acid (Cordes et al., 2016; Geeraerts et al., 2017).

Additionally, reports show that the increased succinate concentrations within cells leads to the stabilization of HIF-1α and therefore increased glycolytic flux (Geeraerts et al., 2017). This is in accordance with our data, showing an increase in D-glucose production during an infection, which reassembles an enhanced glycolytic flux within cells. Contrary, this effect gets reduced after inhibiting the mTOR pathway, indicating the requirement of mTOR for the metabolic alterations during infections and the influence of mTORC1 in the activation of HIF-1α.

Moreover, accumulation of citric acid due to the truncated TCA cycle is shuttled into the cytosol, which results in enhanced fatty acid biosynthesis and thereby FFA

accumulation (Stienstra et al., 2017; Kim et al., 2015)., which is also reflected in our data.

In summary, these data ensure that during an infection, the shift towards aerobic glycolysis is mediated by mTOR. Moreover, our data show that inhibition of mTOR results in a reduction of anti-microbial properties and cytokine production, indicating that there is a link between metabolic adaptions and immune cell functions. The reduced first line response to pathogens after blockage of mTOR signalling pathway correlates with a diminished outcome for the host and this in turn provides opportunities for pathogens to proliferate within macrophages. These data therefore attest the importance of the mTOR pathway in robust immune response and effective host defence.

Interestingly a study revealed that there is a link between mTOR and iron homeostasis. The tandem zinc finger protein tristetraprolin (TTP) is a downstream target of mTOR and gets activated in response to rapamycin and iron-deficient states. Thereby, TTP negatively regulates the expression of TfR1, leading to reduced iron import (Bayeva et al., 2012). Our data are in accordance with this report, since they show a reduced TfR1 protein level upon inhibition of mTOR with rapamycin, but also an increase in the protein content of the iron storage protein ferritin, which has not been reported before. Moreover, it was shown in reports, that under iron-deficient conditions, iron consuming processes are down-regulated to preserve intracellular iron by a posttranscriptional mechanism via the RNA-binding protein TTP, which is up-regulated in iron-deficient conditions (Bayeva et al., 2012).

Moreover, IRPs gets activated during iron-deficiency to ensure a sufficient cellular iron supply. IRPs thereby form a complex with IREs in the 5’ UTR of ferritin mRNA, which results in the inhibition of the translation and reduced ferritin production. Additionally, IRP binding to IREs in the 3’ UTR of TfR mRNA prevents its degradation which leads to an increased iron uptake (Oexle et al., 1999). In accordance with these observations, our data show a decrease in ferritin formation and an increase in TfR formation upon treatment of cells with DFP, which resembles a stage of iron deficiency. Moreover, in other reports was shown that also NOS controls iron homeostasis in macrophages by activating IRP1, which binds to IREs and prolongs the mRNA half-life of TfR and at the same time blocks the mRNA translation of ferritin (Nairz et al., 2013). These data are in accordance with our results, showing an increased iNOS expression and therefore

NO production during iron-deprived states, which results in an increase in free intracellular iron concentrations and indicates, that parts of the high intracellular iron levels during iron limited states can be traced back to the increased iNOS expression.

Interestingly, when cells were treated with $FeCl_3$, the opposite effect can be observed, meaning a reduced TfR1 expression and an increased ferritin production. Therefore, during this process, which resembles an iron overload stage, the affinity of IRPs within the 5' untranslated region of the mRNA coding for ferritin to IREs is reduced, which results in increased ferritin translation, whereas the low affinity of IRPs within the 3' UTR of the TfR mRNA results in degradation of this mRNA.

Furthermore, we showed that when cells were treated with both, rapamycin and $FeCl_3$, the observed effects are synergistically elevated which leads to the assumption, that there is an additive effect and a link between mTOR pathway and iron homeostasis.

Taken together, the results show a reduced iron uptake and an increased level of the iron storage protein ferritin, when mTOR gets inactivated as well as under iron overload states, which is a result of the downstream target of mTOR, TTP.

Reports show that TTP gets also activated in iron-deprived states (Bayeva et al., 2012), but under such circumstances, our results show an increase in TfR formation and decrease in ferritin. This upregulation of the TfR and decrease in ferritin is mediated by the interaction between IRPs and IREs and is necessary to prevent further iron shortage within macrophages. IRPs are shown to act independently of TTP and this leads to the assumption, that under iron-limited conditions, IRPs act to enhance cellular ion uptake, while TTP regulates iron proteins within the cell and hence, both mechanisms together enhance an effective preservation of cell viability under iron deficient states.

Moreover, the increased iron storage within ferritin under iron-overload states and mTOR inhibition, increases the availability of the metal for intracellular bacteria which positively affects the intracellular survival of *Salmonella* and enhances the bacterial load within macrophages. Contrary, if iron resources are low within macrophages, the bacterial number within macrophages decrease. However, in iron-deficient states and additionally treatment of cells with rapamycin, what is known to enhance bacterial proliferation, the bacterial survival improves somewhat. These results are in accordance with other reports, showing that accumulation of iron within cells has

advantage effects for bacteria which have an intracellular lifestyle, such as *Salmonella* (Nairz et al., 2010).

6. Summary

Taken together, under iron-rich conditions, microbes have better access to iron within macrophages, which positively influences the bacterial number within macrophages and negatively affects the immune response. This results in limited control over infections and a diminished outcome for the host.

Contrary, iron-limited conditions and therefore low concentrations of iron within macrophages reduces the number of intracellular bacteria and positively influences the immune response, providing opportunities for the host.

Moreover, during infections and iron-limited states, a metabolic shift towards aerobic glycolysis can be observed, resulting in stronger proliferation of immune cells and hence elevated control over infections. During infections, this shift is mediated by the mTOR signalling pathway, since inhibition of mTOR using rapamycin abolishes the metabolic reprogramming. Next to the role in altering the metabolism of macrophages, mTOR is important for an effective immune response, since rapamycin treatment negatively affects the production of immune mediators, such as pro-inflammatory cytokines and therefore facilitate bacterial expansion within macrophages. mTOR inhibition not only affects metabolic reprogramming but also increases the availably of iron for bacteria within cells. Of note, the increase of iron and mTOR inhibition have similar effects on metabolic reprogramming thus affecting infection control. Subsequent studies will have to clarify in more detail to which extend alterations of the mTOR pathways and iron homeostasis are inter-connected and how their modulations affect disease outcomes in infection in vitro and in vivo.

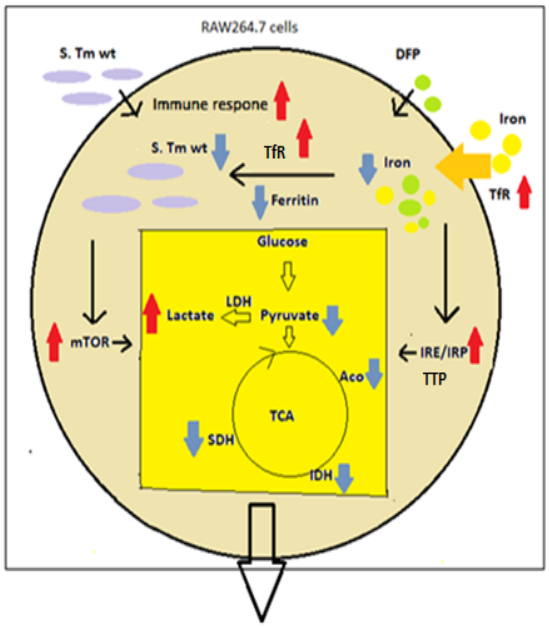

higher proliferation of immune cells, enhanced immune response and reduced number of intracellular bacteria results in stronger control over infections

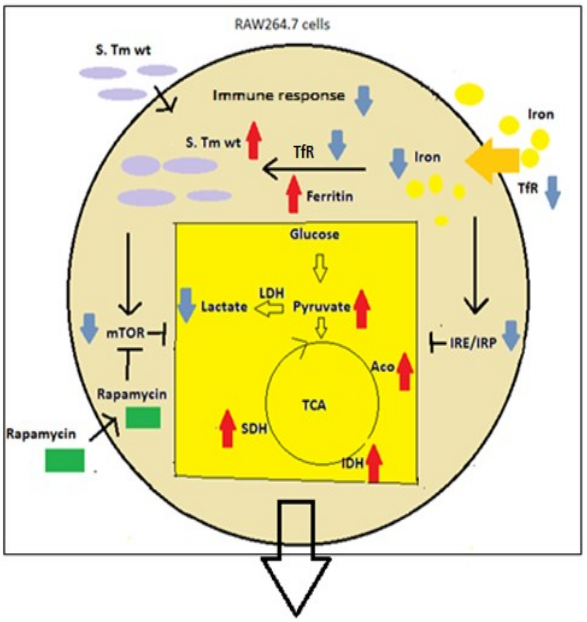

limited proliferation of immune cells, reduced immune response and higher number of intracellular bacteria results in dimished control over infections

7. References

1. Abbaspour N, Hurrell R, Kelishadi R. Review on iron and is importance for human health. J Res Med Sci. 2014 Feb; 19(2):164-174.
2. Arango Duque G1, Descoteaux A1. Macrophage Cytokines: Involvement in Immunity and Infectious Diseases. Front Immunol. 2014 Oct 7; 5:491.
3. Arsenault RJ, Napper S, Kogut MH. Salmonella enterica Typhimurium infection causes metabolic changes in chicken muscle involving AMPK, fatty acid and insulin/mTOR signalling. Vet Res. 2013 May 17; 44:35
4. Bayeva M, Khechaduri A, Puig S, Chang HC, Patial S, Blackshear PJ, Ardehali H. mTOR Regulates Cellular Iron Homeostasis through Tristetraprolin. Cell Metab. 2012 Nov 7; 16(5):645-57.
5. Cassat JE, Skaar EP. Iron in infection and immunity. Cell Host Microbe. 2013 May 15; 13(5):509-19.
6. Chaban Y, Boekema EJ, Dudkina NV. Structures of mitochondrial oxidative phosphorylation supercomplexes and mechanisms for their stabilisation. Biochim Biophys Acta. 2014 Apr;1837(4):418-26.
7. Cheng SC, Scicluna BP, Arts RJ, Gresnigt MS, Lachmandas E, Giamarellos-Bourboulis EJ, Kox M, Manjeri GR, Wagenaars JA, Cremer OL, Leentjens J, van der Meer AJ, van de Veerdonk FL, Bonten MJ, Schultz MJ, Willems PH, Pickkers P, Joosten LA, van der Poll T, Netea MG. Broad defects in the energy metabolism of leucocytes underlie immunoparalysis in sepsis. Nat Immunol. 2016 Apr; 17(4):406-13.
8. Cheng SC, Quintin J, Cramer RA, Shepardson KM, Saeed S, Kumar V, Giamarellos-Bourboulis EJ, Martens JH, Rao NA, Aghajanirefah A, Manjeri GR, Li Y, Ifrim DC, Arts RJ, van der Veer BM, Deen PM, Logie C, O'Neill LA, Willems P, van de Veerdonk FL, van der Meer JW, Ng A, Joosten LA, Wijmenga C, Stunnenberg HG, Xavier RJ, Netea MG. mTOR- and HIF-1α-mediated aerobic glycolysis as metabolic basis for trained immunity. Science. 2014 Sep 26; 345(6204):1250684.
9. Cherayil BJ. The role of iron in the immune response to bacterial infection. Immunol Res. 2011 May; 50(1):1-9.
10. Cooper GM. The Cell: A molecular approach. 2nd edition. Suderland (MA): Sinauer Associates; 2000. ISBN-10: 0-87893-106-6.

11. Cordes T, Wallace M, Michelucci A, Divakaruni AS, Sapcariu SC, Sousa C, Koseki H, Cabrales P, Murphy AN, Hiller K, Metallo CM. Immunoresponsive gene 1 and itaconate inhibit succinate dehydrogenase to modulate intracellular succinate levels. J Biol Chem. 2016 Jul 1;291(27):14274-84.
12. Dandekar T, Astrid F, Jasmin P, Hensel M. Salmonella enterica: a surprisingly well-adapted intracellular lifestyle. Front Microbiol. 2012 May 3; 3:164.
13. Dean W, MD, English J. Krebs cycle intermediates. Nutrition Review, April 22, 2013, 61552.
14. Dulak J, Deshane J, Jozkowicz A, Agarwal A. Heme Oxygenase-1 and Carbon Monoxide in Vascular Pathobiology. Circulation. 2008 Jan 15; 117(2):231-41.
15. Eiden AM, Zhang S, Gary JM, Simmons JK, Mock BA. Molecular Pathways: Increased Susceptibility to Infection Is a Complication of mTOR Inhibitor Use in Cancer Therapy. Clin Cancer Res. 2016 Jan 15; 22(2):277-83.
16. Elhelu Mohamed A. The role of macrophages in Immunology. J Natl Med Assoc. 1983 Mar; 75(3):314–317.
17. Fleming RE, Ponka P. Iron Overload in Human Disease. N Engl J Med. 2012 Jan 26; 366(4):348-59.
18. Gabay C. Interleukin-6 and chronic inflammation. Arthritis Res Ther. 2006;8 Suppl 2:S3.
19. Gammella E, Buratti P, Cairo G, Recalcati S. Macrophages: central regulators of iron balance. Metallomics. 2014 Aug; 6(8):1336-45.
20. Gan Zhen-Shun, Wang Qian-Qian, Li Jia-Hui, Wang Xu-Liang, Wang Yi-Zhen, Du Hua-Hua. Iron reduces M1 macrophage polarization in RAW264.7 Macrophages associated with inhibition of STAT1. Hindawi. 2017 Feb 13, 2017:8570818.
21. Ganesan R, Hos NJ, Gutierrez S, Fischer J, Stepek JM, Daglidu E, Krönke M, Robinson N1. Salmonella Typhimurium disrupts Sirt1/AMPK checkpoint control of mTOR to impair autophagy. PLoS Pathog. 2017 Feb 13; 13(2):e1006227.
22. Ganz T. Systemic iron homeostasis. Physiol Rev. 2013 Oct; 93(4):1721-41.
23. Ganz T. Macrophages and Systemic Iron Homeostasis. J Innate Immun. 2012; 4(5-6):446-53.
24. Garai P, Gnanadhas DP, Chakravortty D. Salmonella enterica serovars Typhimurium and Typhi as model organisms. Virulence. 2012 Jul 1; 3(4):377-88.

25. Geeraerts X, Bolli E, Fendt SM, Van Ginderachter JA. Macrophage Metabolism as Therapeutic Target for Cancer, Atherosclerosis, and Obesity. Front Immunol. 2017 Mar 15;8:289.
26. Geeraerts Xenia, Bolli Evangelia, Fendt Sarah-Maria Fendt, Van Ginderachter Jo A. Front. Immunol.,March, 15, 2017,8:289.
27. Ginhoux F, Jung S. Monocytes and macrophages: developmental pathways and tissue homeostasis. Nat Rev Immunol. 2014 Jun; 14(6):392-404.
28. Goh C, Knight JC. Enhanced understanding of the host-pathogen interaction in sepsis: new opportunities for omic approaches. Lancet Respir Med. 2017 Mar; 5(3):212-223.
29. Guan P, Wang N. Mammalian target of rapamycin coordinates iron metabolism with iron-sulfur cluster assembly enzyme and tristetraprolin. Nutrition. 2014 Sep; 30(9):968-74.
30. Henson SM. CD8+ T-cell senescence: no role for mTOR. Biochem Soc Trans. 2015 Aug; 43(4):734-9.
31. Hvidberg V, Maniecki MB, Jacobsen C, Højrup P, Møller HJ, Moestrup SK. Identification of the receptor scavenging hemopexin-heme complexes. Blood. 2005 Oct 1; 106(7):2572-9.
32. Husain M, Bourret TJ, McCollister BD, Jones-Carson J, Laughlin J, Vázquez-Torres A. Nitric oxide evokes an adaptive response to oxidative stress by arresting respiration. J Biol Chem. 2008 Mar 21; 283(12):7682-9.
33. Janeway CA, Jr, Travers P, Walport M. Shlomchik MJ. Immunobiology: The Immune System in Health and Disease. 5th edition. New York: Garland Science; 2001. ISBN-10: 0-8153-3642-X.
34. Kim DK, Jeong JH, Lee JM, Kim KS, Park SH, Kim YD, Koh M, Shin M, Jung YS, Kim HS, Lee TH, Oh BC, Kim JI, Park HT, Jeong WI, Lee CH, Park SB, Min JJ, Jung SI, Choi SY, Choy HE, Choi HS. Inverse agonist of estrogen-related receptor γ controls Salmonella typhimurium infection by modulating host iron homeostasis. Nat Med. 2014 Apr; 20(4):419-24.
35. Kim S, Joe Y, Kim HJ, Kim YS, Jeong SO, Pae HO, Ryter SW, Surh YJ, Chung HT. Endoplasmic Reticulum Stress–Induced IRE1α Activation Mediates Cross-Talk of GSK-3β and XBP-1 To Regulate Inflammatory Cytokine Production. J Immunol. 2015 May 1; 194(9):4498-506.

36. Knutson MD, Oukka M, Koss LM, Aydemir F, Wessling-Resnick M. Iron release from macrophages after erythrophagocytosis is up-regulated by ferroportin 1 overexpression and down-regulated by hepcidin. Proc Natl Acad Sci USA. 2005 Feb 1; 102(5):1324-8.
37. Laplante M and Sabatini DM. mTOR signaling in growth control and disease. Cell. 2012 Apr 13; 149(2): 274–293.
38. Leung KY, Finlay BB. Intracellular replication is essential for the virulence of Salmonella Typhimurium. Proc Natl Acad Sci USA. 1991 Dec 15;88(24):11470-4.
39. Li XB, Gu JD, Zhou QH.Review of aerobic glycolysis and its key enzmyes- new targets for lung cancer therapy. Thorac Cancer. 2015 Jan; 6(1):17-24.
40. Lo JH, Kulp SK, Chen CS, Chiu HC. Sensitization of Intracellular Salmonella enterica Serovar Typhimurium to Aminoglycosides in Vitro and in Vivo by a Host-Targeted Antimicrobial Agent. Antimicrob Agents Chemother. 2014 Dec; 58(12):7375-82.
41. Lu SC. Regulation of Hepatic Glutathione Synthesis: Current Concepts and Controversies. FASEB J. 1999 Jul; 13(10):1169-83.
42. Lu SC. Regulation of glutathione synthesis. Mol Aspects Med. 2009 Feb-Apr; 30(1-2):42-59.
43. Mancio-Silva L, Slavic K, Grilo Ruivo MT, Grosso AR, Modrzynska KK, Vera IM, Sales-Dias J, Gomes AR, MacPherson CR, Crozet P, Adamo M, Baena-Gonzalez E, Tewari R, Llinás M, Billker O, Mota MM.Nutrient sensing modulates malaria parasite virulence.Nature. 2017 Jul 13; 547(7662):213-216.
44. Mathieu J, Ruohola-Baker H. Metabolic remodeling during the loss and acquisition of pluripotency. Development. 2017 Feb 15; 144(4):541-551.
45. Mitterstiller AM, Haschka D, Dichtl S, Nairz M, Demetz E, Talasz H, Soares MP, Einwallner E, Esterbauer H, Fang FC, Geley S, Weiss G. Heme oxygenase 1 controls early innate immune response of macrophages to Salmonella Typhimurium infection. Cell Microbiol. 2016 Oct; 18(10):1374-89.
46. Moné Y, Monnin D, Kremer N. The oxidative environment: a mediator of interspecies communication that drives symbiosis evolution. Proc Biol Sci. 2014 May 7; 281(1785):20133112.
47. Muckenthaler MU, Rivella S, Hentze MW, Galy B. A red carpet for iron metabolism. Cell. 2017 Jan 26; 168(3):344-361.

48. Murshid A, Gong J, Prince T, Borges TJ, Calderwood SK. Scavenger Receptor SREC-I Mediated Entry of TLR4 into Lipid Microdomains and Triggered Inflammatory Cytokine Release in RAW 264.7 Cells upon LPS Activation. PLoS One. 2015; 10(4): e0122529.
49. Nairz M, Schroll A, Demetz E, Tancevski I, Theurl I, Weiss G. Ride on the ferrous wheel'--the cycle of iron in macrophages in health and disease. Immunobiology. 2015 Feb; 220(2):280-94.
50. Nairz M, Schroll A, Sonnweber T, Weiss G. The struggle of iron- a metal at the host-pathogen interface. Cell Microbiol. 2010 Dec; 12(12):1691-702.
51. Nairz M, Theurl I, Ludwiczek S, Theurl M, Mair SM, Fritsche G, Weiss G. The co-ordinated regulation of iron homeostasis in murine macrophages limits the availability of iron for intracellular *Salmonella* Typhimurium. Cell Microbiol. 2007 Sep; 9(9):2126-40.
52. Nairz M, Schleicher U, Schroll, Sonnweber T, Theurl I, Ludwiczek S, Talasz H, Brandacher G, Moser PL., Muckenthaler MU., Fang FC., Bogdan C, Weiss G. Nitric oxide-mediated regulation of ferroportin-1 controls macrophage iron homeostasis and immune function in Salmonella infection. J Exp Med. 2013 May 6; 210(5):855-73.
53. Nemeth E, Tuttle MS, Powelson J, Vaughn MB, Donovan A, Ward DM, Ganz T, Kaplan J. Hepcidin regulates cellular iron efflux by binding to ferroportin and inducing its internalization. Science. 2004 Dec 17; 306(5704):2090-3.
54. Oexle H, Kaser A, Möst J, Bellmann-Weiler R, Werner ER, Werner-Felmayer G, Weiss G. Pathways for the regulation of interferon-gamma-inducible genes by iron in human monocytic cells. J Leukoc Biol. 2003 Aug; 74(2):287-94.
55. Oexle H, Gnaiger E, Weiss G. Iron-dependent changes in cellular energy metabolism: influence of citric acid cycle and oxidative phosphorylation. Biochim Biophys Acta. 1999 Nov 10; 1413(3):99-107.
56. Ong PS, Wang LZ, Dai X, Tseng SH, Loo SJ, Sethi G.Judicious Toggling of mTOR Activity to Combat Insulin Resistance and Cancer: Current Evidence and Perspectives. Front Pharmacol. 2016 Oct 25; 7:395.
57. Patra KC, Hay N. The pentose phosphate pathway and cancer. Trends Biochem Sci. 2014 Aug; 39(8):347-54.
58. Paiva CN, Bozza MT. Are Reactive Oxygen Species Always Detrimental to Pathogens? Antioxid Redox Signal. 2014 Feb 20; 20(6):1000-37.

59. Pan X, Tamilselvam B, Hansen EJ, Daefler S. Modulation of iron homeostasis in macrophages by bacterial intracellular pathogens. BMC Microbiol. 2010 Feb 25; 10:64.
60. Pietrangelo A. Hereditary hemochromatosis--a new look at an old disease. N Engl J Med. 2004 Jun 3; 350(23):2383-97.
61. Raval FM, Nikolajczyk BS. The Bidirectional Relationship between Metabolism and Immune Responses. Discoveries (Craiova). 2013; 1(1):e6.
62. Ramanathan A, Schreiber SL. Direct control of mitochondrial function by mTOR. Proc Natl Acad Sci USA. 2009 Dec 29; 106(52):22229-32.
63. Rouault TA, Maio N. Biogenesis and functions of mammalian iron-sulfur proteins in the regulation of iron homeostasis and pivotal metabolic pathways. J Biol Chem. 2017 Aug 4; 292(31):12744-12753.
64. Schaer DJ, Vinchi F, Ingoglia G, Tolosano E, Buehler PW. Haptoglobin, hemopexin, and related defense pathways—basic science, clinical perspectives, and drug development. Front Physiol. 2014 Oct 28; 5:415.
65. Scheller J, Chalaris A, Schmidt-Arras D, Rose-John S. The pro- and anti-inflammatory properties of the cytokine interleukin-6. Biochim Biophys Acta. 2011 May;1813(5):878-88.
66. Sharp P, Srai SK. Molecular mechanisms involved in intestinal iron absorption. World J Gastroenterol. 2007 Sep 21;13(35):4716-24.
67. Shi H, Bencze KZ, Stemmler TL, Philpott CC. A cytosolic iron chaperone that delivers iron to ferritin. Science. 2008 May 30; 320(5880):1207-10.
68. Silvestri L, Colucci S, Pagani A, Artuso I, Pettinato M, Nai A, Camaschella C. A noval crosstalk between iron hoemostasis and mTOR mediated by the immunophilin FKBP12. Blood. 2016; 128:261.
69. Soares MP, Weiss G. The Iron age of host-microbe interactions. EMBO Rep. 2015 Nov; 16(11):1482-500.
70. Soe-Lin S, Apte SS, Andriopoulos B Jr, Andrews MC, Schranzhofer M, Kahawita T, Garcia-Santos D, Ponka P. Nramp1 promotes efficient macrophage recycling of iron following erythrophagocytosis in vivo. Proc Natl Acad Sci USA. 2009 Apr 7; 106(14):5960-5.
71. Spooner R, Yilmaz O. The Role of Reactive-Oxygen-Species in Microbial Persistence and Inflammation. Int J Mol Sci. 2011 Jan 13; 12(1):334-52.

72. Stienstra R, Netea-Maier RT, Riksen NP, Joosten LAB, Netea MG. Specific and complex reprogramming of cellular metabolism in myeloid cells during innate immune responses. Cell Metab. 2017 Jul 5; 26(1):142-156.
73. Sun Q, Chen X, Ma J, Peng H, Wang F, Zha X, Wang Y, Jing Y, Yang H, Chen R, Chang L, Zhang Y, Goto J, Onda H, Chen T, Wang MR, Lu Y, You H, Kwiatkowski D, Zhang H. Mammalian target of rapamycin up-regulation of pyruvate kinase isoenzyme type M2 is critical for aerobic glycolysis and tumor growth. Proc Natl Acad Sci U S A. 2011 Mar 8; 108(10):4129-34.
74. Theurl I, Theurl M, Seifert M, Mair S, Nairz M, Rumpold H, Zoller H, Bellmann-Weiler R, Niederegger H, Talasz H, Weiss G. Autocrine formation of hepcidin induces iron retention in human monocytes. Blood. 2008 Feb 15; 111(4):2392-9.
75. Theurl I, Hilgendorf I, Nairz M, Tymoszuk P, Haschka D, Asshoff M, He S, Gerhardt L, Holderried TA, Seifert M, Sopper S, Fenn AM, Anzai A, Rattik S, McAlpine C, Theurl M, Wieghofer P, Iwamoto Y, Weber GF, Harder NK, Chousterman BG, Arvedson TL, McKee M, Wang F, Lutz OM, Rezoagli E, Babitt JL, Berra L, Prinz M, Nahrendorf M, Weiss G, Weissleder R, Lin HY, Swirski FK. On-demand erythrocyte disposal and iron recycling requires transient macrophages in the liver. Nat Med. 2016 Aug; 22(8):945-51.
76. Ullah MS, Davies AJ, Halestrap AP. The plasma membrane lactate transporter MCT4, but not MCT1, is up-regulated by hypoxia through a HIF-1α-dependent mechanism. J Biol Chem. 2006; 281(14):9030–7.
77. Vander Heiden MG, Cantley LC, Thompson CB. Understanding the Warburg Effect: The metabolic requirements of cell proliferation. Science. 2009 May 22;324(5930):1029-33.
78. Weis S, Carlos AR, Moita MR, Singh S, Blankenhaus B, Cardoso S, Larsen R, Rebelo S, Schäuble S, Del Barrio L, Mithieux G, Rajas F, Lindig S, Bauer M, Soares MP. Metabolic adaption establishes disease tolerance to sepsis. Cell. 2017 Jun 15; 169(7):1263-1275.e14.
79. Weiss G. Iron and immunity: a double-edged sword. Eur J Clin Invest. 2002 Mar; 32 Suppl 1:70-8.
80. Weiss G, Goodnough LT. Anemia of chronic disease. N Engl J Med. 2005 Mar 10; 352(10):1011-23.

81. Weiss G, Goossen B, Doppler W, Fuchs D, Pantopoulos K, Werner-Felmayer G, Wachter H, Hentze MW. Translational regulation via iron-responsive elements by the nitric oxide/NO-synthase pathway. EMBO J. 1993 Sep; 12(9):3651-7.
82. Weiss G, Meusburger E, Radacher G, Garimorth K, Neyer U, Mayer G. Effect of iron treatment on circulating cytokine levels in ESRD patients receiving recombinant human erythropoietin. Kidney Int. 2003 Aug; 64(2):572-8.
83. Weiss G, Schaible UE. Macrophage defense mechanisms against intracellular bacteria. Immunol Rev. 2015 Mar; 264(1):182-203.
84. Weiss G, Werner-Felmayer G, Werner ER, Grünewald K, Wachter H, Hentze MW. Iron regulates nitric oxide synthase activity by controlling nuclear transcription. J Exp Med. 1994 Sep 1;180(3):969-76.
85. Weyand CM, Zeisbrich M, Goronzy JJ. Metabolic signatures of T-cells and macrophages in rheumatoid arthritis. Curr Opin Immunol. 2017 Jun; 46:112-120.
86. Xing Z, Gauldie J, Cox G, Baumann H, Jordana M, Lei X F, Achong M K. IL-6 is an antiinflammatory cytokine required for controlling local or systemic acute inflammatory responses. J Clin Invest. 1998 Jan 15; 101(2):311-20.

8. Abstract

Iron is an essential nutrient for both, the immune cells and microbes. During infections, the control over iron homeostasis is therefore essential for counteracting bacterial expansion.

Within the current master thesis, we show that iron-overload results in an increased storage of the metal within the iron storage protein ferritin, whereas iron-deprivation results in an enhanced iron import through TfR.

This increased iron levels within macrophages in iron-overloaded conditions not only enhance the bacterial number within the cells, but also reduce cytokine expression, which results in limited control over infections and have therefore negative effects on the host immune cells. Contrary, iron- limitation results in the opposite effect, since it lowers the bacterial number within macrophages and ensures a strong immune response and therefore, provides opportunities for the host.

In addition, we show that the metabolic activity of macrophages alters during an infection as well as iron-deprived states, resulting in sift towards aerobic glycolysis and hence higher proliferation of immune cells and elevated control over infections. We show that under infection conditions, the mTOR signalling pathway plays an essential role for the metabolic reprogramming within macrophages, since inhibition of mTOR using rapamycin results in abolishment of this metabolic alterations. Moreover, we show that mTOR is important for an effective immune response, since rapamycin treatment of macrophages enhances the bacterial number within the cells and reduces the production of effective immune mediators, such as pro-inflammatory cytokines, and therefore impede a strong and effective elimination of the pathogens.

9. Zusammenfassung

Eisen ist ein wichtiger Nährstoff – sowohl für Immunzellen als auch für Mikroben. Daher ist die Regulation des Eisenstoffwechsels während einer Infektion unerlässlich.

Während der Durchführung der Masterarbeit konnte gezeigt werden, dass Eisenüberladung in Makrophagen zu einer Speicherung dieses Metalls innerhalb der Zellen führt, in einem sogenannten Speicherprotein Ferritin. Im Gegensatz dazu führt Eisenarmut zu einer erhöhten Aufnahme von Eisen durch den TfR.

Eisenüberladung und somit eine erhöhte Eisenverfügbarkeit innerhalb von Makrophagen erschwert die Kontrolle über eine Infektion mit intrazellulären Pathogenen. Es konnte gezeigt werden, dass nicht nur die Anzahl von *Salmonellen* innerhalb der Zellen ansteigt, sondern auch eine Reduktion der Zytokin-Expression und somit eine Reduktion der Immunantwort stattfindet.

Limitierung von Eisen innerhalb von Makrophagen führt hingegen zum gegenteiligen Effekt. Eine starke Immunantwort und eine bessere Bekämpfung von intrazellulären Bakterien ist somit gewährleistet.

Zusätzlich konnte gezeigt werden, dass sich die metabolische Aktivität von Makrophagen durch Umwelteinflüsse verändert. Eine Verschiebung der metabolischen Aktivität hin zur aeroben Glykolyse konnte sowohl bei einer Infektion als auch bei Eisenarmut beobachtet werden. Die Änderung des Metabolismus während einer *Salmonellen*-Infektion konnte auf die Aktivität von mTOR zurückgeführt werden, da Inhibierung von mTOR durch Rapamycin zu einer Aufhebung des Effekts führt.

Zudem konnte herausgefunden werden, dass durch eine Behandlung von Makrophagen mit Rapamycin die Anzahl intrazellulärer Bakterien erhöht und die Expression von Immunmediatoren reduziert wird, was wiederum eine starke und effektive Eliminierung von Bakterien verschlechtert.

Zusammengefasst kann gesagt werden, dass Eisenüberladung die Kontrolle über eine Infektion erschwert, wohingegen sich eine Limitierung von Eisen positiv auf die Wirtszelle auswirkt und somit eine starke Immunantwort gewährleistet wird.